

Alma Mater Studiorum – Università di Bologna

**DOTTORATO DI RICERCA IN
SCIENZE BIOTECNOLOGICHE E FARMACEUTICHE**

Ciclo XXXII

Settore Concorsuale: 03/D1

Settore Scientifico Disciplinare: CHIM/08

INNOVATIVE APPROACHES TO CANCER THERAPY

Presentata da: Noelia Montel De La Roche

Coordinatore Dottorato

Prof. Maria Laura Bolognesi

Supervisore

Prof. Andrea Cavalli

Co-supervisor

José A. Ortega Martínez

Rita M. C. Di Martino

Esame finale anno 2020

Table of Contents

List of acronyms and abbreviations.....	1
I. Introduction.....	6
1. Cancer disease	7
2. Current cancer treatment	8
3. Innovative approaches to cancer treatment	8
4. Epigenetic therapy.....	9
5. New technologies in drug discovery and development of high-throughput X-ray crystallography	11
6. Fragment-based screening.....	11
7. Research project	14
II. Part 1: Targeting Chromodomains (ChDs): a promising epigenetic approach for cancer treatment.	15
1. Introduction	16
1.1. Epigenetic regulation of gene expression	17
1.2. Acetyl and methyl epigenetic marks.....	17
1.2.1. Acetyl readers: bromodomain (BRD)-containing proteins	19
1.2.2. Methyl readers and methyl-Lys recognition motifs	19
1.2.2.1. Chromodomain (ChD)-containing proteins.....	20
1.3. Epi-drugs in cancer treatment	21
1.4. Targeting ChDs as a promising epigenetic approach for cancer treatment	24
2. PhD project background.....	25
2.1. Starting point of the project	26
3. PhD project.....	32
3.1. Compounds design	33
3.1.1. Design of analogs of compound 2	33
3.1.2. Design of analogs of compound 3	34
3.2. Synthetic strategies	35
3.2.1. Synthesis of compound 2.....	35
3.2.2. Synthesis of compounds of series 1.....	36
3.2.3. Synthesis of compound of series 2	36
3.2.4. Synthesis of compound of series 3	36
3.2.5. Synthesis of compounds of series 4.....	37
3.2.6. Synthesis of compound of series 5	38
3.2.7. Synthesis of compounds of series 6.....	38
3.2.8. Synthesis of compound of series 7	39
4. Results and Discussion.....	41

4.1. ChD binding assay results and discussion	42
5. Conclusions	46
III. Part 2: Development of small-molecules as Tubulin Colchicine-site binders for cancer therapy....	49
1. Introduction	50
1.1. Microtubules roles and dynamics	51
1.2. Altering microtubule dynamics and cancer therapy	51
1.3. Colchicine-binding site.....	53
1.4. Nocodazole	56
2. PhD project background.....	57
2.1. High-throughput X-ray crystallography for fragment screening in the identification of new tubulin binders	58
2.2. Identification of compound 29.....	58
3. PhD project.....	60
3.1. Design of compounds	61
3.1.1. Design of series 1	61
3.1.2. Design of series 2	63
3.2. Synthesis of compounds	64
3.2.1. Nucleophilic aromatic substitution reaction (S _N Ar) approach	65
3.2.2. 2-amino benzimidazole formation approach.....	66
4. Results and Discussion.....	69
4.1. Preliminary results.....	70
5. Conclusions	72
IV. Experimental section.....	74
1. Section 1. Targeting Chromodomains (ChDs): a promising epigenetic approach for cancer treatment.....	76
1.1. Synthesis.....	76
1.2. ChD-competition FP assay	91
1.3. Fluorescence measurements	91
2. Section 2. Development of small-molecules as Tubulin Colchicine-site binders for cancer therapy	92
2.1. Synthesis.....	92
2.2. Docking studies	102
2.3. Resazurin assay.....	103
V. Appendix	104
VI. References.....	113

List of acronyms and abbreviations

A alanine

Ac acetyl

ADC antibody drug conjugates

Ala alanine

AML acute myeloid leukemia

Arg arginine

Asn asparagine

ATP adenosine triphosphate

BBI Double Resonance Broadband

BEH Ethylene Bridged Hybrid

Bn benzyl

Boc *tert*-butyloxycarbonyl

BOP benzotriazol-1-yloxytris(dimethylamino)phosphonium hexafluorophosphate

53BP1 p53-binding protein 1

BRD bromodomain

°C degree Celsius

CADD computational-aided drug design

Cbx Chromobox Homolog

ChD chromodomain

CHD 1 Chromodomain helicase DNA-binding protein 1

¹³C-NMR carbon nuclear magnetic resonance

COSY homonuclear correlation spectroscopy

CTCL cutaneous T cell lymphoma

Da dalton

DBU 1,8-diazabicyclo[5.4.0]undec-7-ene

DCM dichloromethane

DIBAL-H diisobutylaluminium hydride

DIPEA *N,N*-diisopropylethylamine

DMA dimethylacetamide

DMA-DMF *N,N*-dimethylformamide dimethyl acetal

4-DMAP 4-dimethylaminopyridine

DMEM Dulbecco's Modified Eagle Medium

DMF dimethylformamide
DMSO dimethyl sulfoxide
DNA deoxyribonucleic acid
DOT1L Disruptor of telomeric silencing 1-like
DPPA Diphenylphosphoryl azide
E entgegen (opposite)
E glutamate
EDC 1-ethyl-3-(3-dimethylaminopropyl)carbodiimide
equiv. equivalent
ESI electron spray ionization
EZH2 Enhancer of zeste homolog 2
F phenylalanine
FBDD fragment-based drug discovery
FCS fetal calf serum
FDA Food and Drug Administration
FITC Fluorescein isothiocyanate
FP fluorescence polarization
FT Fourier Transform
g gram
GDP guanosine diphosphate
Gln glutamine
Glu glutamate
GTP guanosine triphosphate
h hour
HAT histone acetyltransferase
HBA hydrogen bond acceptor
HBD hydrogen bond donor
HDAC histone deacetylase
¹H-NMR proton nuclear magnetic resonance
HOBt 1-hydroxybenzotriazole
HP1 heterochromatin protein 1
HPLC high performance liquid chromatography
HSS High Strength Silica
HTS High-Throughput Screening

Hz hertz
ID internal diameter
iHDAC histone deacetylase inhibitor
iDNMT DNA methylation inhibitor
IEO Istituto Europeo di Oncologia
iit Istituto Italiano di Tecnologia
inh inhibition
J coupling constant
K Kelvin
K lysine
L leucine
 λ_{em} wavelength of emission
 λ_{exc} wavelength of excitation
L3MBTL Lethal (3) malignant brain tumor-like protein
LSD1 Lysine-specific histone demethylase 1A
Lys lysine
M molar
MBT Malignant Brain Tumor
MDS myelodysplastic syndrome
mg milligram
[M-H]⁺ protonated pseudo-molecular ion
[M-H]⁻ deprotonated pseudo-molecular ion
MHz Megahertz
min. minutes
ml milliliter
mm millimeter
mM millimolar
 μ m micrometer
mmol millimole
MD molecular dynamics
MDA microtubule-destabilizing agent
MS mass spectrometry
MSA microtubule-stabilizing agent
MTA microtubule-targeting agent

m/z mass/charge
N normal
NMR Nuclear Magnetic Resonance
OBD Optimum Bed Density
PDA photodiode array detector
PDB protein data bank
PHD plant homeodomain
Phe phenylalanine
PPW Protein Preparation Wizard
Pro proline
PSI Paul Scherrer Institute
PTM post-translational modification
PWWP Pro-Trp-Trp-Pro
Pygo2 Pygopus homolog 2
RMSD root-mean-square deviation
RNA ribonucleic acid
rt room temperature
Rt retention time
S serine
SAHA suberanilohydroxamic acid
SAM S-adenosylmethionine
SAR structure-activity relationship
SN2 bi-molecular nucleophilic substitution
SNAr Nucleophilic aromatic substitution
SP standard precision
SPR surface plasmon resonance
SQD single quadrupole detector
STAB Sodium triacetoxyborohydride
tBuXPhos 2-di-tert-butylphosphino-2',4',6'-triisopropylbiphenyl
Trp tryptophan
TSA thermal shift assay
TTL Tubulin-tyrosine ligase
UPLC Ultra performance liquid chromatography
Val valine

VLS virtual ligand screening

W watt

WD40 tryptophan-Aspartic acid 40

I. Introduction

1. Cancer disease

Cancer is a major health concern in the current society and is the second cause of death worldwide. It is a broad term used to define a very large group of diseases characterized by abnormal cell-proliferation due to the alteration of biological processes that normally regulate cell-cycle, like cell growth or cell-division.¹ As a consequence, old or damaged cells are not replaced, new cells form when they are not necessary and these latter proliferate in an uncontrolled manner and, after exponential increase in their number, form tumours. In some specific conditions, cancer cells can detach from the original primary tumour and invade nearby tissues through the blood or the lymph system and proliferate, determining the formation of new masses defined as “metastases”. Metastases development is very common and it accounts for almost 90 % of cancer deaths.²

In order to become tumorigenic and eventually metastatic, cancer cells highly differ from normal ones. Specifically, according to Hanahan and Weinberg, there are a few traits that cancer cells progressively acquire: the capability to sustain continuous proliferation through deregulated production and release of growth-signals, abnormalities in downstream pathways and altered responsiveness to growth-inhibitory signals, acquired resistance to programmed cell death (apoptosis), unlimited replicative potential, sustained angiogenesis to provide more nutrients and oxygen through newly-formed blood vessels, tissue invasion and metastasis, metabolic reprogramming to support continuous growth, evasion of immune system.

Inflammation and genomic instability are at the origin of these characteristics. On one hand, immune-system cells that cause inflammation contribute to cancer development through the release of tumour-promoting molecules in the microenvironment. On the other hand, genomic instability accounts for the progressive acquisition of genetic alterations that promote the development of the previously described characteristics in a subset of cells and confer them selective advantage over the remaining cells. Outgrowth of such cell subpopulation determines the acquisition of tumour phenotype.³ Interestingly, the genetic alterations that drive cancer do not involve the whole genome, but tend to affect specific types of genes: proto-oncogenes, tumour suppressor genes, and DNA repair genes. Proto-oncogenes are involved in normal cell growth and division. However, when these genes are somehow altered, they may become oncogenes, allowing cells to proliferate out of control. Tumour suppressor genes are involved in the protection of normal cells from uncontrolled proliferation and their inactivation can promote tumour development.⁴ DNA repair genes are involved in fixing damaged DNA and

their inactivation can lead to higher sensitivity to mutagenic agents and accumulation of additional mutations.³

Together, the described characteristics of tumour cells provide a framework for understanding the complexity of cancer disease and the consequent difficulty to treat such disorder in a specific and efficient manner.

2. Current cancer treatment

There are many types of cancer treatment. Conventional treatments include both local therapies, such as surgery and radiation therapy, and the use of drugs that act systemically. These latter comprise mainly conventional cytotoxic chemotherapeutics (such as alkylating agents, anti-metabolites, topoisomerases inhibitors and tubulin-targeting agents) and hormonal agents. Although being very successful in clinics, conventional treatments show some specific and common drawbacks. While hormonal therapies tend to be useful only for specific types of cancer (e.g., breast, prostate cancer) and surgery tends to be suitable only during a specific stage of the tumour development, cytotoxic conventional therapies and radiation therapy mainly suffer from adverse side-effects development, that can lead also to therapy dismissal (e.g., myelosuppression, nausea and hair-loss). This toxicity is mainly due to the lack of specificity of such therapies, since radiations act indistinctly on normal and cancer cells and chemotherapeutics affect common biological processes that are shared by both normal and cancer cells.⁵

A drawback that seems to be common of all conventional treatments is inherent or induced drug resistance. Underlying this characteristic is the ability of cancer cells to develop molecular mechanisms to sustain stressors, like drug exposure, through genetic and epigenetic changes. From a molecular viewpoint, resistance development involves, for example, drug target modification, acquisition of new drug elimination systems and increased drug metabolism through overexpression of enzymes involved in drug metabolism.⁶

3. Innovative approaches to cancer treatment

In the last few years, several research efforts have been addressed to find innovative approaches in cancer treatment to overcome toxicity and drug resistance that characterize current therapies.

Among these, nanoparticles have emerged as interesting delivery systems to increase cancer-specificity and bioavailability of conventional chemotherapeutics, thus reducing their side-effects. In some cases, new formulations consisting in nanosystems have even allowed time- and space-control of drug release, while highly limiting toxicity.⁷

Another more specific treatment of cancer consists in targeted-therapy that implies acting on pathways or proteins that are specific or show aberrant expression in cancer cells. In this context, to treat certain types of cancer the Food and Drug Administration (FDA) approved Imatinib, a small-molecule targeting BCR-ABL kinase, which represents the most common example of successful targeted therapy.⁸

Besides nanomedicine and targeted-therapy, recently, increased research efforts have been devoted to the development of so-called immunotherapy agents to mobilize the immune system against the cancer cells instead of directly attacking the tumour. Immunotherapeutic approaches use adaptive or innate immunity and encompass a broad range of compounds. Among the most recently studied approaches, modulation of check-points through antibodies seems very promising.⁹

Another interesting therapeutic approach in cancer is epigenetic therapy. In fact, recent technological developments have allowed to better study the epigenome of several cancers, evidencing a clear link between epigenetic alterations and cancer development and progression.¹⁰

4. Epigenetic therapy

Epigenetics is defined as the phenomenon of heritable phenotypic features that do not imply any alteration of the DNA sequence.¹⁰ DNA is wrapped around an octamer composed by basic, and hence positively charged, histone proteins, forming the so-called nucleosome that is the basal unit of chromatin.¹¹ Chromatin represents the compacted state of the genome and locally is present in two conformational states: euchromatin, the more accessible structure to transcription factors and enzymes, and heterochromatin, the less accessible form. Regulating transcription of the genetic code underlies epigenetic regulation mechanisms and among the major epigenetic control mechanisms there are DNA methylation, and a set of specific post-translational modifications (PTMs) on histone proteins such as addition or removal of methyl and acetyl groups on lysine (Lys) residues of the histone tails.¹² The dynamic mechanisms that regulate chromatin structure through PTMs involve the balanced activity of a vast number of protein families. In particular, PTMs on histones are controlled by three different groups of proteins namely: writers, erasers and readers. The two former are enzymes that add or remove chemical marks from histones, respectively, whereas the readers are proteins encompassing specific domains to recognize and interpret distinct PTMs leading to recruitment of protein complexes and regulation of gene expression.¹³

As previously mentioned, since deregulation of the epigenetic control of gene expression has been associated to cancer disease and histone marks are globally and locally altered within cancer epigenomes,¹⁴ epigenetic therapies are gaining ever increasing attention as promising and innovative strategies to reverse the aberrations and restore the physiological conditions. In this context, several research has been recently focused on the development of “epi-drugs”, chemical entities able to target specific epigenetic actors.¹¹

Nowadays, several epi-drugs are under clinical and pre-clinical studies, but only two classes have been approved by the FDA: DNA methylation inhibitors (iDNMTs) including 5-azacitidine to treat acute myeloid leukemia (AML) and myelodysplastic syndrome (MDS), and histone deacetylase inhibitors (iHDACs), like Vorinostat or suberanilohydroxamic acid (SAHA), approved for the treatment of cutaneous T cell lymphoma (CTCL). Even if such drug classes resulted efficacious for some specific cancer subtypes, consistent clinical results are lacking, most probably due to their use in a poorly targeted approach, in consideration of the limited knowledge of the epigenetic alterations present in cancer cells.^{11,14,15} Notwithstanding the caveats expressed above, the potential to act on new epigenetic proteins is supported by recent studies on cancer genome and epigenome that have revealed mutations or altered expression levels of specific proteins involved in epigenetic regulation of transcription.¹⁰ This information has encouraged the application of epigenetic approaches for the development of more specific cancer therapies aimed at reducing the side-effects of conventional treatments.

Among the most interesting targets in the epigenetics field, proteins involved in Lys histone methylation have been extensively studied,¹⁶ since aberrant histone methylation is a common feature of several cancer subtypes, such as haematological tumours.¹⁵ These proteins can be classified into three classes depending on their role:

- Histone methyltransferases, that add methyl marks to histone tails and are, therefore, defined as “writers”
- Demethylases, enzymes that remove methyl groups, acting as “erasers”¹⁶
- Chromatin “methyl-readers” that recognize methylated residues through protein-protein interaction and recruit multiprotein complexes, leading to regulation of gene expression.¹⁷

This last class includes a small group of proteins encompassing a conserved methyl-Lys recognition motif defined Chromodomain (ChD). ChD-containing proteins are involved in gene silencing and chromatin remodelling and show altered expression or mutations in human related diseases, in particular in cancer, leading to abnormal gene transcription.¹⁸ Recently,

small-molecule inhibitors of ChDs have been developed, thus providing evidence of the druggability of such targets¹⁹ and are emerging as innovative and promising tools to treat cancer.

5. New technologies in drug discovery and development of high-throughput X-ray crystallography

Current cancer research has not only considered new delivery systems and targets but it has also taken advantage of emerging technologies in gene-sequencing, automation technology or bioinformatics to improve the drug discovery process.²⁰ Specifically, advances in technology and automation of almost all stages in the process of protein crystallization have fastened and reduced the cost of crystal structure determination, allowing X-ray crystallography to be used in a high-throughput way.²¹

Nowadays, thanks to new technologies, DNA-sequencing and construct-expression can be automatically performed using very small amounts of sample, thereby making protein expression faster and simpler. Moreover, protein purification became a less challenging step after the introduction of affinity tags on constructs, allowing the wide application of standard purification protocols, the development of automated chromatography systems and, thus reducing the time required to purify the target proteins.²² In fact, thanks to robotics and automation, parallel expression and purification of large-scale of more than 100 proteins per day is currently possible.²³ For the simplification of the crystallization step, over the last few years, research has focused on automated liquid handling development and fast data collection during X-ray experiments, the last ones being assured by potent X-ray sources as third-generation synchrotrons or by the incorporation of high technology-devices on in-house systems.²¹

6. Fragment-based screening

Fragment-based drug discovery (FBDD) approach consists in screening libraries of low molecular weight compounds so-called fragments, which are selected following the “rule of 3”: no more than 300 Da weight, fewer than three H-bond donors and acceptors, fewer than three rotatable bonds and a cLogP lower than three. This screening allows the identification of hit compounds that, after subsequent cycles of elaboration, can eventually evolve into drug candidates (Figure 1).²⁵

Fragment-based screening is considered as an alternative to high-throughput screening (HTS) and a very promising strategy for the hit identification phase in drug discovery.²⁴ Indeed, fragment-like compounds increase the likelihood to identify genuine hits in comparison with

larger compounds of much bigger HTS libraries. In fact, fragments can explore more efficiently the chemical space, since they have increased chemical diversity relative to the volume of chemical space and show higher-quality interactions. The latter characteristic is conserved during compounds' development, leading to reduced time to obtain drug candidates.²⁶

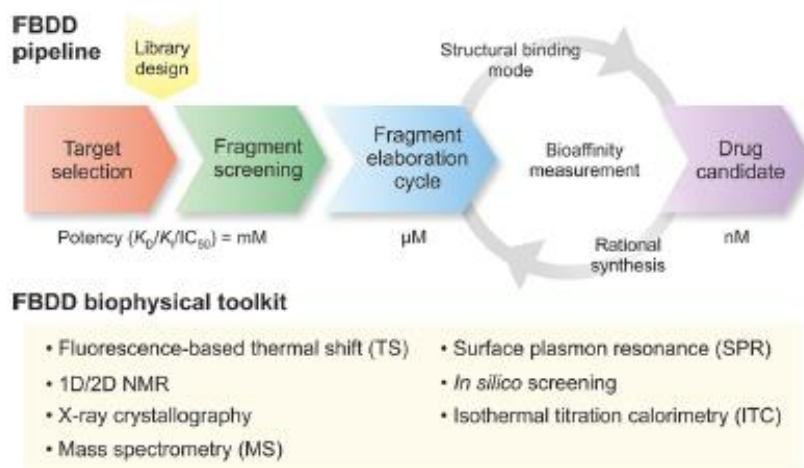


Figure 1. Workflow of FBDD approach.²⁵

Considering that fragment-like compounds show a lower affinity to the target in comparison with higher-weight-compounds of HTS, the techniques used for fragment screening are different and much more sensitive than those applied in HTS. Indeed, only biophysical methods are used. NMR, X-ray crystallography and SPR are considered “classical” methods, but also microscale thermophoresis, thermal shift assay (TSA), weak affinity chromatography and mass spectrometry (MS) are currently applied.²⁴

After hit identification, the elaboration process consists of interactive cycles of rational design and synthesis of compounds, guided by structural binding data and affinity or activity information. The strategies of fragment elaboration include: fragment merging, linking and growing (Figure 2).²⁵

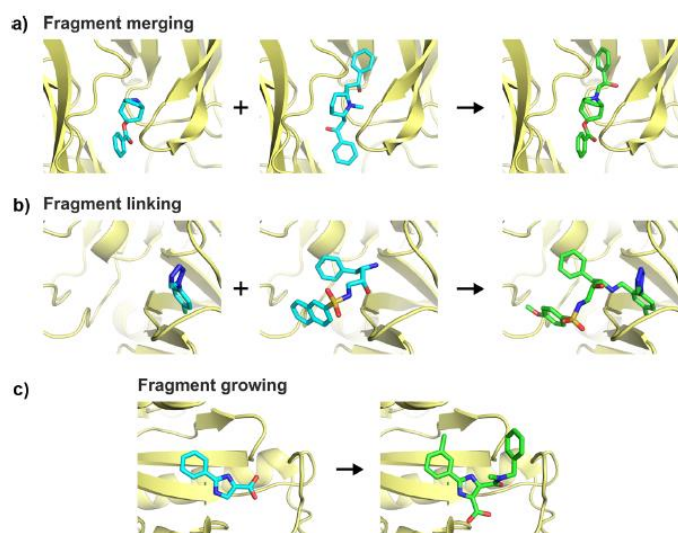


Figure 2. Fragment elaboration strategies. a) Fragment merging. b) Fragment linking c) Fragment growing.²⁵

On one hand, “merging” is a term used to define the combination of overlapping portions of different molecules into a new fragment, and “linking” consists of joining molecules binding different sites. On the other hand, “growing”, that is the most common used approach, consists of adding chemical groups to a fragment to identify new interactions²⁴ with the selected target.

Structural information is fundamental for fragment elaboration²⁵ and, for this reason, the drug discovery field has taken advantage of such innovations applying high-throughput X-ray crystallography for fragment-based screening.²¹ This application allowed to expand the use of X-ray crystallography beyond the lead optimization step in drug discovery, where it had an established role, into the hit-identification step.²⁰ The application of X-ray crystallography in the screening phase, providing knowledge of binding properties of compounds and information of protein-ligand interacting features in only one step, offers the opportunity to reduce the time required to develop drug candidates, making the drug discovery process more efficient.

Fragment screening by high-throughput X-ray follows a specific procedure that consists in soaking target protein crystals with high-concentration DMSO solutions of single compounds or cocktails of molecules. The soaked crystals are allowed to stand for a specified timeframe in order to favour compounds interaction with the target binding site, and then crystallographic data are collected and interpreted.²³ Several approaches based on this strategy had been developed by research groups leading in some cases to the screen of up to 1000 compounds in two or three days.²¹ Considering that fragment libraries are composed of 1000-5000 compounds,²⁴ this technology confirms its suitability to screen fragment libraries and contemporary guide the elaboration of binding fragments.

7. Research project

In conclusion, cancer research is moving remarkable steps towards more effective and less toxic therapies through the application of novel approaches and thanks to the development of new technologies that improve the drug discovery process. The present work reports some examples; in fact, this thesis includes two research projects (Part 1 and Part 2, respectively) having in common the application of innovative approaches and technologies in cancer drug discovery. On one hand, the first part of the work focused on ChD-containing proteins, as new epigenetic targets. The aim was to identify, design and synthesize small-molecules able to bind ChDs and interfere with their biological function. On the other hand, the objective of the second part was, firstly, the identification of new potential antitumour fragments able to bind tubulin, a validated target in cancer therapy; to achieve this aim high-throughput X-ray crystallography in a fragment-based screening was applied. Secondly, taking advantage from X-ray obtained structural information; the identified fragments were developed into new chemical entities through a computational-aided drug design (CADD) strategy to obtain novel anticancer small-molecules.

II. Part 1: Targeting Chromodomains (ChDs): a promising epigenetic approach for cancer treatment

1. Introduction

1.1. Epigenetic regulation of gene expression

Epigenetic regulation of gene expression is a dynamic and reversible process by which cells showing the same genotype can express different phenotypes in response to a stimulus due to different transcriptional programmes defined by specific post-translational modifications (PTMs).

Since epigenetic mechanisms influence the cellular response to the environment cues, they play a key role in diseases related to lifestyle, diet or exposure to toxins (e.g., cancer, inflammatory disorders or neurological diseases).

At the molecular level, such mechanisms include covalent modifications of DNA, chromatin remodelling, regulation by non-coding RNAs, exchange of histones and PTMs on histones such as acetylation, methylation, phosphorylation or ubiquitylation^{14,27} that are regulated by different proteins and enzymes determining a specific “epigenetic code” that expands the information beyond the DNA sequence as summarized in Figure 3.²⁸

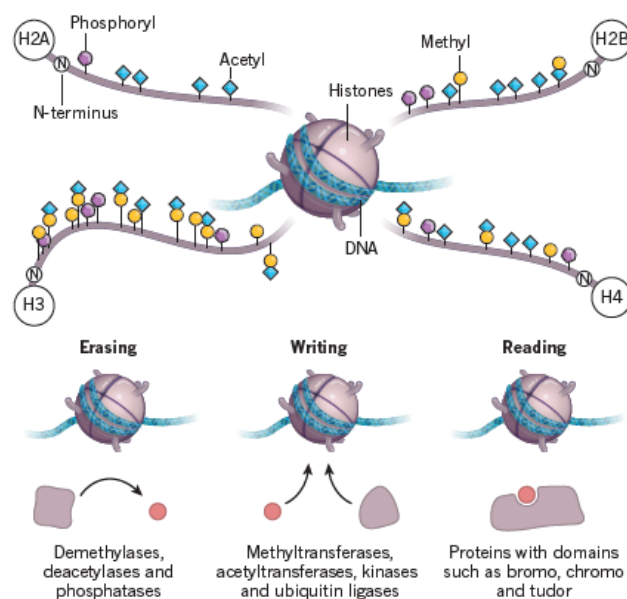


Figure 3. Histone PTMs and proteins regulating the “histone code”.²⁹

1.2. Acetyl and methyl epigenetic marks

From a therapeutic point of view, acetyl and methyl marks are among the most important PTMs of histones.

Histone acetylation can occur on the ϵ -amino group of Lys side chains or within the core of the histone proteins and it is regulated by two different families of enzymes: histone acetyltransferases (HATs), which are the workhorses of the epigenome and act as writer proteins, and histone deacetylases (HDACs) that play the role of erasers. Acetylation has the

effect of changing the overall charge of the histone tail from positive to neutral; therefore, chromatin structure becomes more relaxed, and DNA is more accessible to multi-protein complexes interaction leading to transcriptional activation.¹⁴

On the other hand, histone methylation represents a more complex PTM. Indeed, it is possible to methylate both Lys and arginine (Arg) residues on histones; each Lys residue can be mono-, di- or trimethylated, while Arg can exist as either mono- or dimethylated, the latter in asymmetric or symmetric manner (Figure 4).²⁷

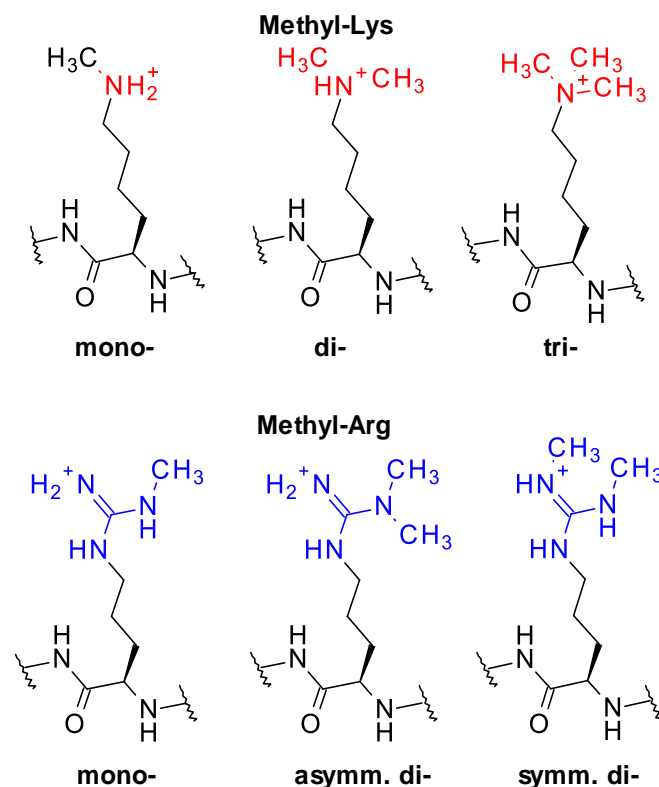


Figure 4. Different methylation states of Lys and Arg residues on histones.

S-Adenosylmethionine (SAM)-dependent methyl transferases act as writer proteins, while either Jumonji family of 2-oxoglutarate-dependent demethylases or the Flavin dependent enzymes Lys-specific histone demethylase 1 and 2 are responsible of erasing methyl marks.

Differently from what happens after histone acetylation, methylated residues do not change the charged state of the protein.¹⁴ According to the effector-mediated paradigm, each methyl mark is recognized by specific modules of reader proteins and such interaction determines protein complexes recruitment or stabilization, activation of downstream effects and gene expression regulation, either transcriptional repression or activation.³⁰

1.2.1. Acetyl readers: bromodomain (BRD)-containing proteins

Three protein modules are able to recognize acetylated residues on histones: double PHD (plant homeodomain) fingers, bromodomains (BRDs) and pleckstrin homology domain.

Among them, Bromodomains (BRDs) have been widely investigated. They consist of 110 amino acids and define a deep hydrophobic pocket shared by 61 different proteins that is highly conserved.³² BRDs' proved to be involved in cancer, inflammation, cardiovascular disease and other disorders³¹ encouraging the development of BRD binders to both gain deeper insight into their roles and eventually identify new therapeutic agents.

1.2.2. Methyl readers and methyl-Lys recognition motifs

Methyl reader proteins, in particular the methyl-Lys readers, are gaining ever-increased interest among the scientific community and significant research has been focused on the elucidation of histone methylation in general.^{33,34}

These proteins are classified into three families: the PHD zinc finger proteins, the WD40 (tryptophan-aspartic acid 40) repeat domain-containing proteins, and the Royal family of reader proteins. The latter include Tudor, chromodomain (ChD), Pro (proline)-Trp (tryptophan)-Trp-Pro (PWWP), and malignant brain tumor (MBT) domain containing proteins.¹²

These reader proteins bind to methylated residues through a conserved motif, including multiple aromatic residues, called “aromatic cage”, that is involved in cation- π interactions with the methylammonium group on histone chains.³³ Differences in the physicochemical and steric properties of methylated residues and in the close residues explain why reader proteins have developed selective pockets for a specific methylation mark (mono-, di- or trimethylated Lys residues) on a specific histone.³⁴ Generally, lower Lys methylated states (mono- and dimethyl) are engaged via a “cavity insertion recognition mode”. In this case, steric exclusion and H-bond interactions play important roles in the binding event (Figure 5).³⁰ On the other hand, a “surface groove recognition mode” has been associated to readers that recognize trimethyl-Lys residues. Indeed, the binding site of these latter consists in a shallow hydrophobic recognition surface rather than a pocket (Figure 5).³⁴

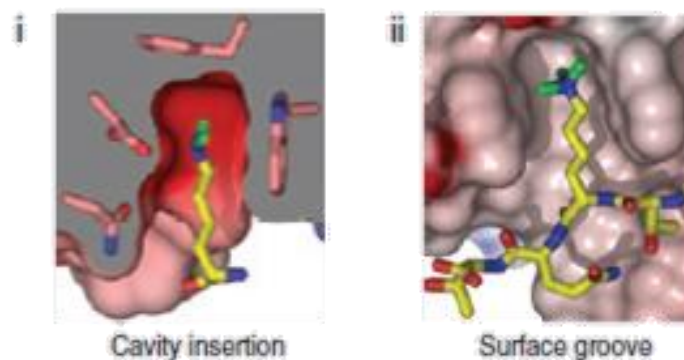


Figure 5. Recognition modes of methyl-Lys readers i) cavity insertion, ii) surface groove.³⁰

Inhibition of methyl-Lys readers is a much less explored field in drug discovery compared to other epigenetic targets³⁴ and targeting the aromatic cage is challenging, especially if it involves the surface groove recognition mode. However, since multiple lines of evidence link these readers to cancer and other diseases, there is an increasing interest in studying deeper these proteins and their roles.²⁷

1.2.2.1. Chromodomain (ChD)-containing proteins

Among the methyl-Lys readers mentioned above, chromodomain-(ChD) containing proteins have been associated to different aggressive cancers, like prostate and lymphoma ones.³⁴

The chromatin-organization-modifier domain (chromodomain, ChD) is a conserved binding module that consists of 40-60 amino acids shared by 34 proteins.^{27,33} Among these latter, the heterochromatin (HP1) Cbx 1/3/5 and the chromobox homolog (Cbx) 2/4/6/7/8¹² are the most studied and are able to recognize the trimethyl-Lys 9 on histone 3 (H3K9me3) and the trimethylated Lys 27 on histone 3 (H3K27me3), respectively, being involved in transcriptional repression.³⁴

The aromatic cage of ChDs consists of 3-4 aromatic residues (Figure 6) able to bind the trimethylated-Lys residues and, having been defined as a shallower recognition surface, it has been considered as a difficult module to target.²⁷ However, since mutations in some aromatic residues of the aromatic cage drastically reduce ChDs' partner affinity, there is a great interest for developing new molecular entities able to block their biological activity.³³

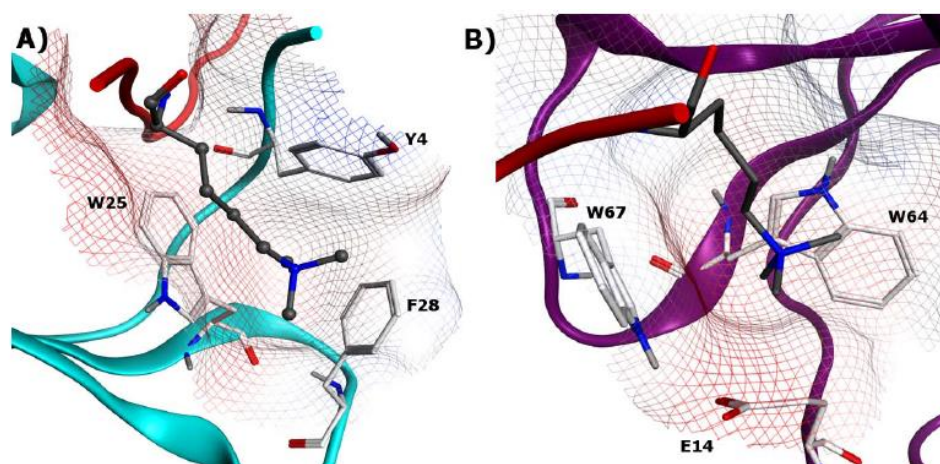


Figure 6. Examples of ChD-containing proteins. A) Aromatic cage of CBX5 bound to trimethylated peptide (PDB (Protein Data Bank): 3FDT). B) ChD CHD1 (Chromodomain helicase DNA-binding protein 1) binding pocket with trimethylated peptide (PDB: 2B2W).³³

1.3. Epi-drugs in cancer treatment

Initially, epi-drugs were limited to inhibitors of few epigenetic enzymes as HATs, HDACs and DNA demethylases (e.g., Vorinostat, 5-azacitidine and decitabine).¹¹ Over the last few years, the reversible processes involving histones' PTMs were deeply studied, leading to the identification of new epigenetic targets with potential therapeutic application.³⁵ As a consequence of the increased breath of the epigenetic target space, the amount of small-molecules under clinical trials targeting epigenetics grew, as confirmed by the studies regarding Disruptor of telomeric silencing 1-like (DOT1L) inhibitors, Lysine-specific histone demethylase 1A (LSD1) inhibitors and Enhancer of zeste homolog 2 (EZH2) inhibitors, among others.³⁶

In particular, the epigenetic medicinal chemistry started to focus broadly on reader proteins in 2010 with the identification of **JQ1** and **I-BET762** (Figure 7) as potent inhibitors of BRD-containing proteins.^{31,37,38} If until that time reader proteins were an unexplored territory for drug discovery, the confirmed druggability of BRDs, promoted the searching of new on agents targeting methyl-Lys reader proteins.³³

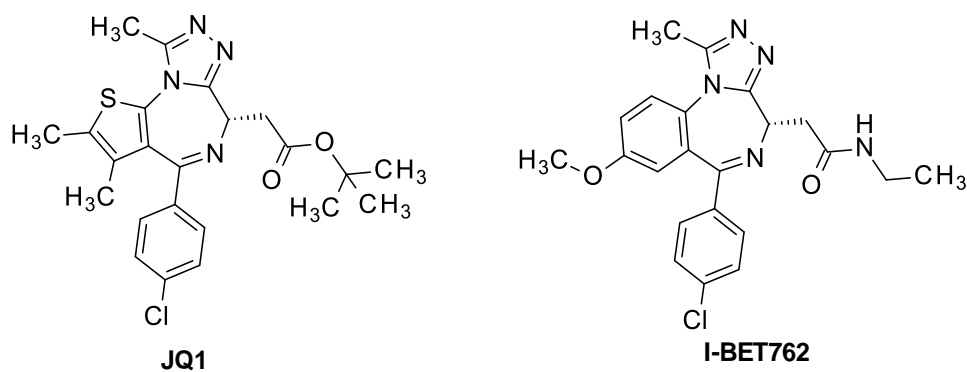


Figure 7. Chemical structures of the first identified BRDs inhibitors.

Compared to BRD-containing proteins and epigenetic enzymes, readers of methyl marks are considered more challenging targets for two main reasons: low-affinity for their natural ligand, that complicated the development of high-throughput assays, and their lack of enzymatic activity that hampered target validation.³³ Nevertheless, some methyl-Lys reader proteins have been successfully targeted by chemical entities. MBT domain was the first methyl-Lys binding domain studied and a nicotinamide antagonist (Figure 8) was the first small-molecule co-crystallized with Lethal (3) malignant brain tumor-like protein 1 (L3MBTL1) at its MBT domain. Nicotinamide antagonist (PDB code: 3P8H)³⁹ paved the road to the identification of inhibitors of other methyl-Lys readers, belonging to ChD, MBT, PHD finger and Tudor domain families.³⁴ Some examples of such ligands and their corresponding epigenetic target proteins are reported in Table 1.

The field of methyl-Lys reader proteins has just started to be uncovered and there is much to do to develop potent and selective small-molecules as potential epi-drugs for cancer treatment.

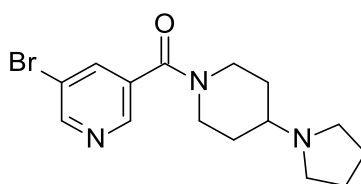
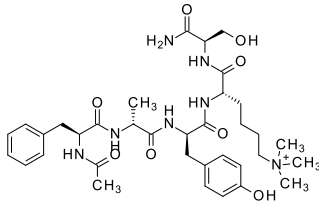
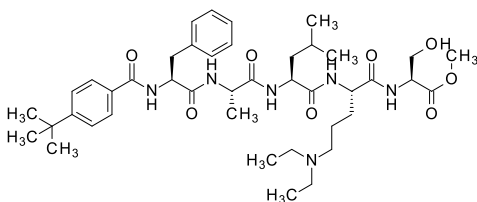
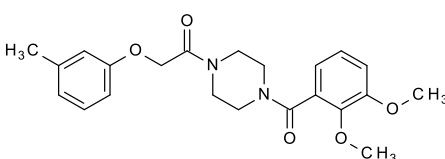
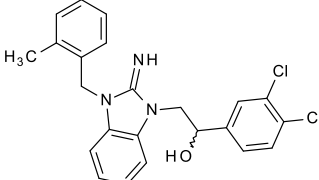
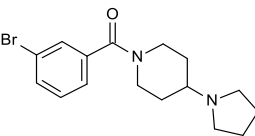
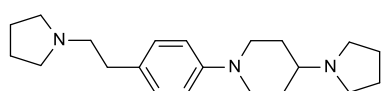
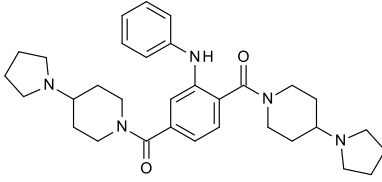
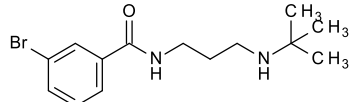
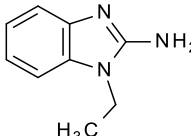


Figure 8. Chemical structure of a nicotinamide antagonist: the first small-molecule ligand co-crystallized with L3MBTL1 (PDB: 3P8H).³⁹

Table 1. Examples of inhibitors of methyl-Lys recognition motifs.³⁴

Inhibitors	Structure	Target protein
Ac-FAYKme3S		CBX7 ChD
UNC3866		CBX7 ChD
MS37452		CBX7 ChD
MS351		CBX7 ChD
UNC926		L3MBTL1 MBT domain
UNC2533		Lethal (3) malignant brain tumor-like 3 protein (L3MBTL3) MBT domain

UNC1215		L3MBTL3 MBT domain
UNC2170		p53-binding protein 1 (53BP1) Tandem Tudor domain
CF16		Pygopus homolog 2 (Pygo2) PHD finger

1.4. Targeting ChDs as a promising epigenetic approach for cancer treatment

Aberrant expression of ChD-containing proteins has been observed in a large variety of cancer types, as prostate, breast, thyroid, colon and brain tumours.^{12,34} Moreover, increased literature links ChD-containing proteins to the regulation of the balance between haematopoietic stem-cell self-renewal and differentiation, implying a pivotal role of such proteins in hematopoietic neoplasms development.⁴⁰ Therefore, ChD-containing proteins have been recognised as promising targets to fight cancer.

The druggability of several ChD-containing proteins was evaluated in the past and was proved in the first decade of the 2000s by the development of peptidic antagonists of CBX7 ChD (e. g., Ac-FAYKme3S, Table 1).⁴¹ Subsequent optimization of the physicochemical properties of such compounds led to the identification of the first cell permeable peptide chemical probe for CBX7 ChD with antiproliferative properties against PC3 prostate cancer cells (UNC3866, Table 1).^{34,42} Moreover, MS37452⁴³ and MS351 (Table 1)⁴⁴ proved that also cell-active small-molecules with modest potency could be developed as interesting inhibitors of ChDs and encouraged the searching of new ChD-containing proteins inhibitors.

Overall, this scenario suggests that the development of small-molecules binding ChDs as potential epi-drugs is a goal that could be achieved.

2. PhD project background

2.1. Starting point of the project

With the aim to identify new small-molecules able to inhibit ChD-containing proteins as potential anticancer agents, a Virtual Ligand Screening (VLS) campaign was carried out at the University of Bologna. Specifically, four structures of ChDs were selected on the basis of the PDB quality and RMSD (root-mean-square deviation) (maximum structural diversity). Each selected structure was prepared with the PPW (protein preparation wizard) (hydrogen treatment, protonation and minimization) and was used for a high throughput docking of the LifeChemicals database (about 500 K molecules) with the software Glide (SP). For each structure, the 1K top-scoring compounds were stored. The final selection of 120 compounds to test was performed by the elimination of duplicates, clustering with Tanimoto on the basis of a description of each molecule in terms of 2D fingerprints (Molprint2D), visual inspection of the binding mode and finally on the basis of the commercial availability. The compounds were tested at 100 μ M concentration from the research group of Professor S. Minucci, at Istituto Europeo di Oncologia (IEO) in Milan, by employing a ChD-Competition Fluorescent Polarization (FP) assay (see VI. Experimental section, 1.2 ChD-competition FP assay).⁴⁵ This latter was chosen for screening the compounds' ability to inhibit, in a competitive way, the interaction between the recombinant ChD of our selected target and a FITC-labeled peptide H3K27me3, that mimicks the trimethylated Lys27 residue on histone 3. According with this assay, briefly depicted in Figure 9, the target protein binding to the FITC-labeled peptide forms a large complex, that rotating slowly in solution does not disrupt the light, that remains polarised (Figure 9). When a small molecule (or hit compound) displaces the fluorescent peptide, it begins to spin rapidly disrupting the light and forcing it to become depolarised (Figure 9). The depolarized fluorescence emission passes through parallel and perpendicular filters with respect to the plane of the excitation light. Intensity of parallel and perpendicular emission light are employed to calculate FP readout according to equation 1 (Figure 10)⁴⁵ and the wavelengths of excitation (λ_{exc}) and emission (λ_{em}) set in the assay, according to the specific FITC-labeled peptide employed, are 485 and 535 nm, respectively. The displacement of the fluorescent peptide from its binding site by a compound results in a decrease of the FP signal.

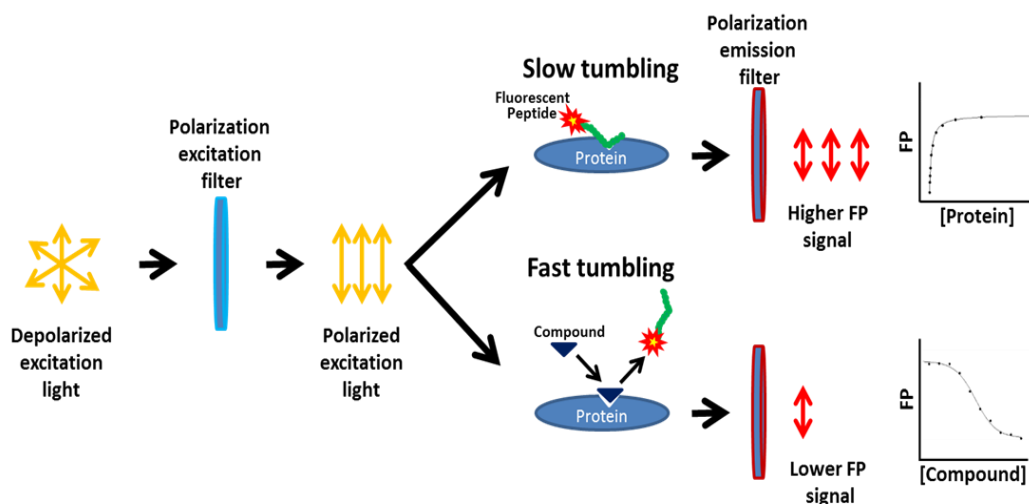


Figure 9. Schematic description of the ChD-competition FP assay principle.

Equation 1:

$$FP: \frac{I(\text{parallel}) - I(\text{perpendicular})}{I(\text{parallel}) + I(\text{perpendicular})}$$

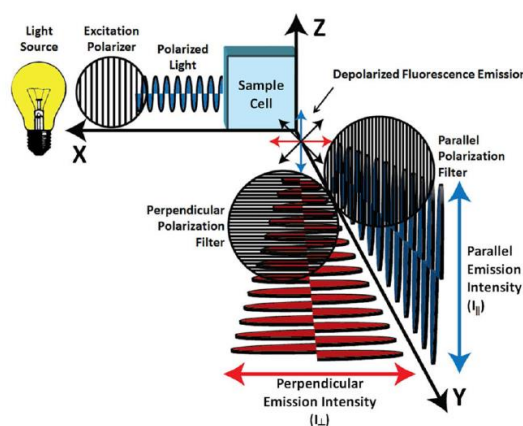


Figure 10. Schematic description of the ChD-competition FP assay principle. Equation 1 reports the calculation of the FP readout.⁴⁵

Interestingly, results from FP assay showed that only commercial compound **1** (Figure 11), was able to display 32 % of reference FITC-labeled peptide at 100 μM concentration.

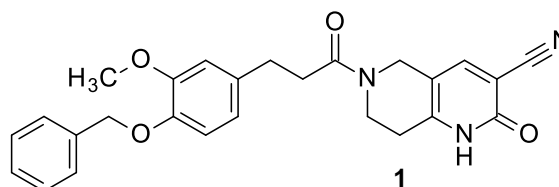
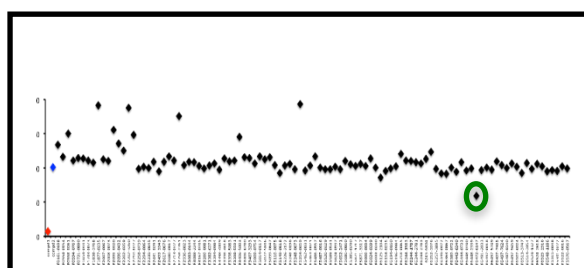


Figure 11. On the left, result of the initial screening of 102 selected compounds by FP assay at 100 μM (18 compounds were not tested due to low DMSO solubility). Green circle highlights compound **1** whose structure is reported on the right.

Compound **1** was resynthesized in iit's (Istituto Italiano di Tecnologia) laboratories in Genoa via a coupling reaction between commercial 3-(3-benzyloxy-4-

methoxyphenyl)propionic acid and commercial 2-oxo-5,6,7,8-tetrahydro-1*H*-1,6-naphthyridine-3-carbonitrile; hydrochloride, in a mixture of dichloromethane/*N,N*-dimethylformamide (9:1) by employing 1-ethyl-3-(3-dimethylaminopropyl)carbodiimide (EDC) and 1-hydroxybenzotriazole (HOBt) hydrate as coupling reagents and triethylamine as base. Then, re-synthesized **1** was tested in IEO in order to confirm the results obtained by testing the commercial one. In the ChD-competition FP assay, re-synthesized compound **1** was evaluated at three different concentrations (6.25, 25 and 100 μ M) but, unexpectedly, it did not show any effect at all tested concentrations. On the contrary, the commercial compound proved to inhibit the interaction between the recombinant ChD and FITC-labeled peptide at concentrations 25 μ M and 100 μ M, of 10 % and 32 %, respectively (Figure 12).

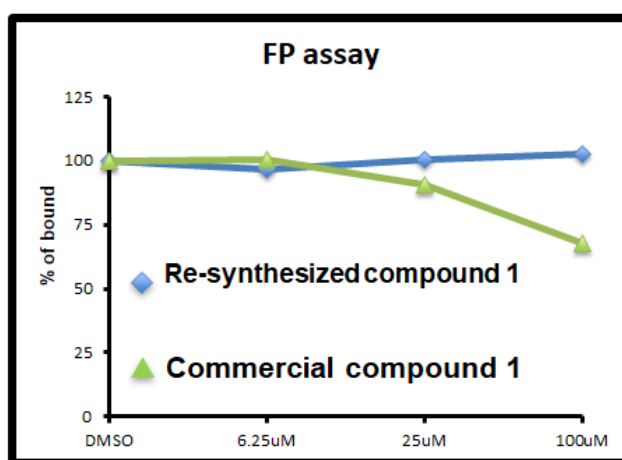


Figure 12. Results of ChD-competition FP assay of commercial and re-synthesized compound **1** at 6.25, 25 and 100 μ M concentrations. Data are reported as % of FITC-peptide bound relative to DMSO after compound addition.

UPLC-MS and $^1\text{H-NMR}$ analysis of commercial and re-synthesized compound **1** (see V. Appendix, Figures A1-A5) revealed a higher purity grade for resynthesized one, suggesting a possible role of the observed impurities of the commercial one in influencing its biological activity. Accurate analysis of proton NMR spectrum of commercial batch of compound **1** allowed us to identify as main impurity a small molecule with a structure similar to that the amine portion of amide derivative **1**. Therefore, we decided to test in the same FP assay also the commercial hydrochloride salt **2** (Figure 13), based on a 2-oxo-5,6,7,8-tetrahydro-1*H*-1,6-naphthyridine structure and employed to prepare **1**. Remarkably, **2** showed an interesting activity at 6.25 μ M concentration (20 % inhibition, see Figure 14).

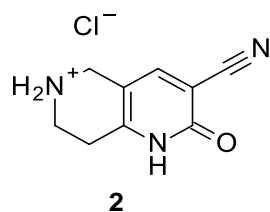


Figure 13. Structure of compound **2**.

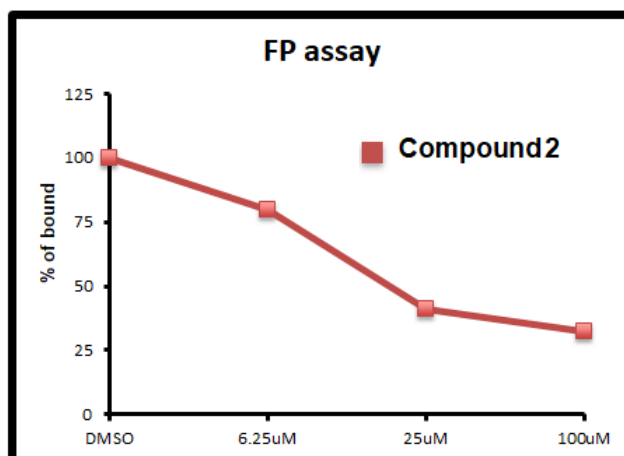


Figure 14. Results of ChD-competition FP assay of compound **2** tested at 6.25, 25 and 100 μM concentrations. Data are reported as % of FITC-peptide bound relative to DMSO after compound addition.

With this promising result in hand, compound **2** was subject to docking studies and molecular dynamics (MD) simulations (Figure 15).

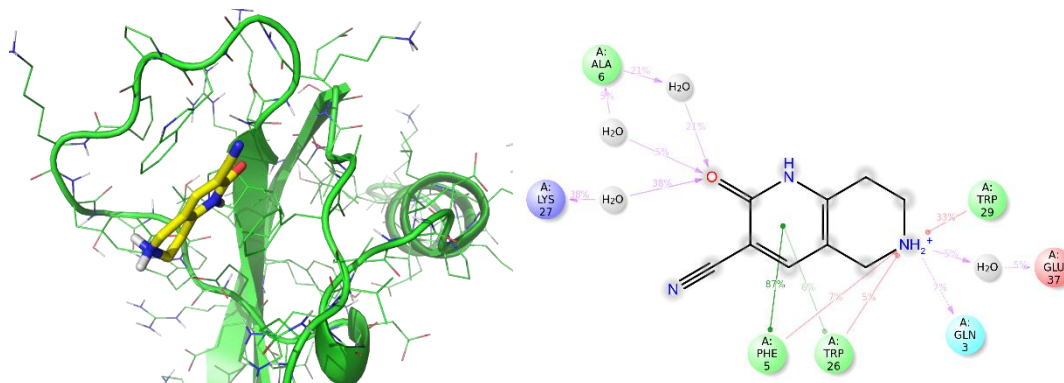


Figure 15. Predicted pose of compound **2** docked at the ChD (left) of the selected target protein. Main interactions of compound **2** with the target ChD according to computational studies (right).

Interestingly, docking studies revealed possible cation- π interactions between the protonated amine group of compound **2** and some aromatic residues in the aromatic cage of the selected ChD [Trp26, Trp29 and Phenylalanine (Phe) 5], and direct or water-mediated H-bonds between the same protonated secondary amine group of **2** and glutamine (Gln) 3 and Glutamate (Glu) 37, respectively (Figure 15). These results allowed us to hypothesize a key role of the

positive charged amine group in mimicking the methylammonium moiety of the Lys residues on histones. Furthermore, additional interactions were observed (Figure 15):

1. Water-mediated H-bonds between the carbonyl moiety of the 2-pyridone ring of compound **2** and alanine (Ala) 6 and Lys27 residues of ChD.
2. π - π interactions between the 2-pyridone ring of compound **2** and Trp26 and Phe5 of the ChD aromatic cage.

To better explore the binding role of the amine group of compound **2**, we looked for a commercially available analog without the presumed essential basic nitrogen atom. Thus, compound **3** (2-oxo-5,6,7,8-tetrahydro-1*H*-quinoline-3-carbonitrile) (Figure 16, top) was bought and was tested by using the FP assay. Surprisingly, compound **3** showed 36.8 % inhibition at 6.25 μ M and 100 % inhibition at 100 μ M (Figure 16), thus displaying even higher inhibitory properties in comparison to compound **2** (20 % inhibition at 6.25 μ M concentration and 70 % at 100 μ M concentration) (Figure 14).

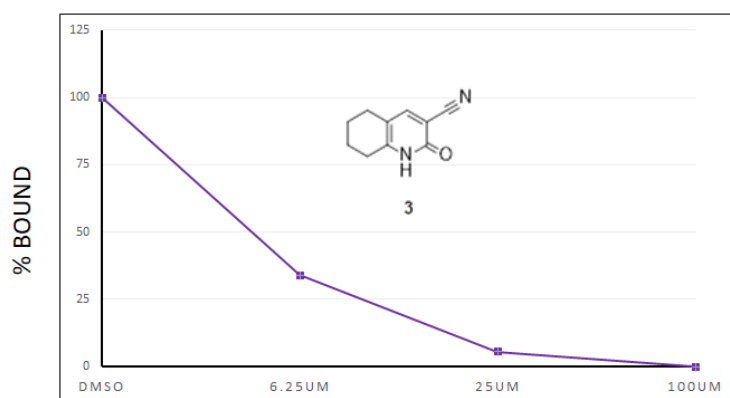


Figure 16. Results of ChD-competition FP assay of compound **3** at 6.25, 25 and 100 μ M concentrations. Data are reported as % of FITC-peptide bound relative to DMSO after compound addition.

To explain these unexpected data, computational investigations were also carried out on analog **3**. Docking studies suggested the compound capability to interact with the selected ChD in a different binding pose compared with compound **2** (Figure 17, left). In detail, π - π interactions were observed between Trp26 and Phe5 of ChD aromatic cage and the aromatic portion of the 2-oxo-5,6,7,8-tetrahydro-1*H*-quinoline framework of **3**; moreover, similarly to **2**, the carbonyl group of the 2-pyridone ring was able to establish a H-bond interaction with Lys27 of ChD (Figure 17, right).

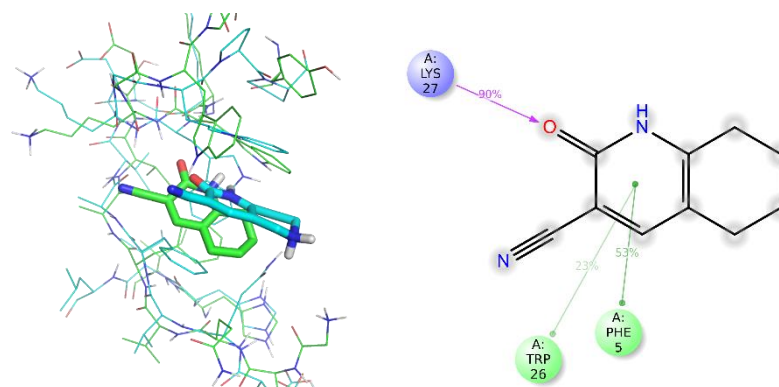


Figure 17. Superimposition of predicted poses of compound **2** (in light blue) and compound **3** (in green) docked at the ChD (left). Compound **3** main interactions with the target ChD according to computational studies (right).

Taken together, these data suggested the suitability of both compounds **2** and **3** as interesting scaffolds to develop potential new ChD-binding agents.

3. PhD project

3.1. Compounds design

The promising results of the competitive FP assay and the computational studies encouraged us to develop small libraries consisting in both compounds **2** and **3** analogs. The aim was to explore the chemical space of the selected target and perform structure-activity relationship (SAR) studies.

3.1.1. Design of analogs of compound **2**

Based on the binding interactions between compound **2** and the selected ChD, suggested by docking studies (Figure 18), and considering the synthetic feasibility of 5,6,7,8-tetrahydro-1,6-naphthyridine-based compounds, three different series of analogs were designed in order to gain deeper knowledge on the essential structural features for ChD binding (Figure 18).

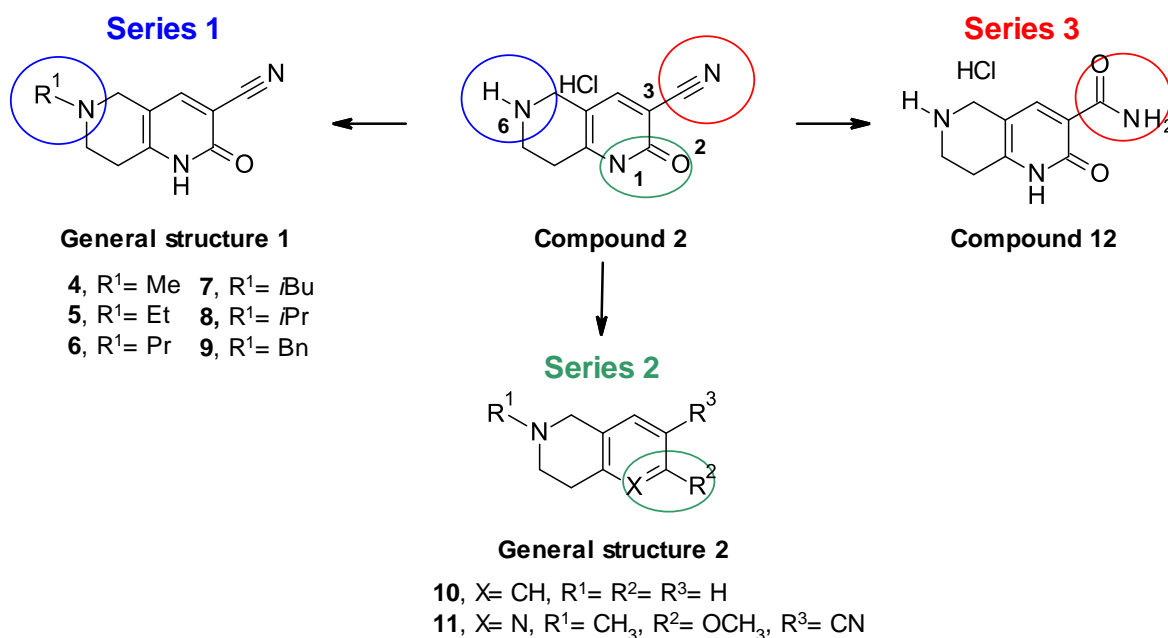


Figure 18. Design strategy for compound **2** analogs.

In series **1** the role of the NH₂⁺ present in 6-position of the main scaffold was explored. In detail, different alkyl groups and a benzyl (Bn) substituent were introduced in order to investigate their steric hindrance effect on ChD binding (derivatives **4-9**, Figure 18).

Then, in series **2** the role of the pyridone system (Figure 18) was investigated. Computational studies suggested the possibility of removing that moiety without detrimental effects for the binding, so novel scaffolds were explored based on that hypothesis. In this context, firstly it was decided to evaluate the commercially available 1,2,3,4-tetrahydroisoquinoline (compound **10**, Figure 18) where the pyridone system is completely removed. Secondly, it was decided to explore the effect of the 2-pyridone/2-hydroxypyridine

tautomerism. Therefore, compound **11** was synthesized in order to shift the tautomeric equilibrium towards the 2-hydroxypyridine isomer and study its binding properties (Figure 19).

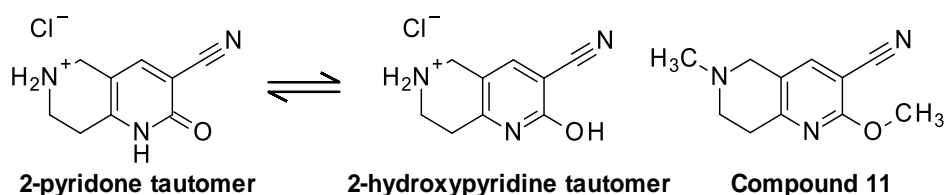


Figure 19. Tautomeric equilibrium of compound **2** (left) and compound **11** structure (right).

Finally, in series **3** the effect of substituents in position 3 of compound **2** was explored. Concerning this series, commercially available 2-oxo-5,6,7,8-tetrahydro-1*H*-1,6-naphthyridine-3-carboxamide free base, where the cyano group of **2** was replaced by a carboxamide function, was the only compound taking into consideration. Since this free base displayed a poor solubility in DMSO, its hydrochloride salt was prepared obtaining compound **12** (Figure 18).

3.1.2. Design of analogs of compound **3**

As previously discussed, MD simulations and docking studies suggested the unexpected suitability of 2-oxo-5,6,7,8-tetrahydro-1*H*-quinoline scaffold of compound **3** to engage the selected ChD. So, a computational-aided drug design (CADD) campaign was carried out to design four new scaffolds able to establish the same main interactions identified in compound **3** engagement (H-bond with Lys27 and π - π interactions with some residues of the aromatic cage) while increasing the chemical diversity (Figure 20).

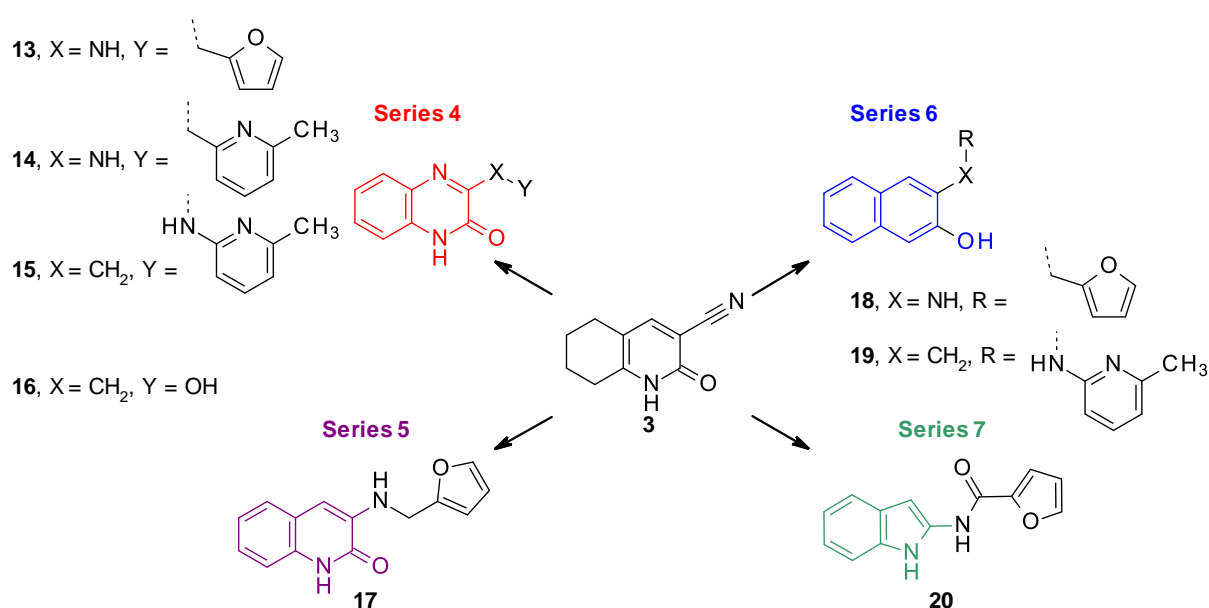


Figure 20. Design of different series of compound **3** analogs.

From the structural point of view, all compounds were designed to maintain the key structural features of compound **3**: an aromatic hydrophobic portion, an H-bond donor (HBD) and two H-bond acceptors (HBAs). All series of derivatives bear an aromatic bicyclic core (2-hydroxyquinoxaline for series **4**, 2-quinolone for series **5**, 2-naphtol for series **6** and indole for series **7**) connected to a pyridine ring, a furan ring or a hydroxyl group through linkers of different nature and length (Figure 20). The most drastic modification was proposed in series **7**. Although, the 5,6,7,8-tetrahydro-1*H*-quinolin-2-one central scaffold was replaced by a *N*-(1*H*-indol-2-yl)carboxamide system, superimposition of both structures confirmed an equivalent three dimensional space orientation for the functional groups involved in main hydrogen bond interactions (Figure 21).

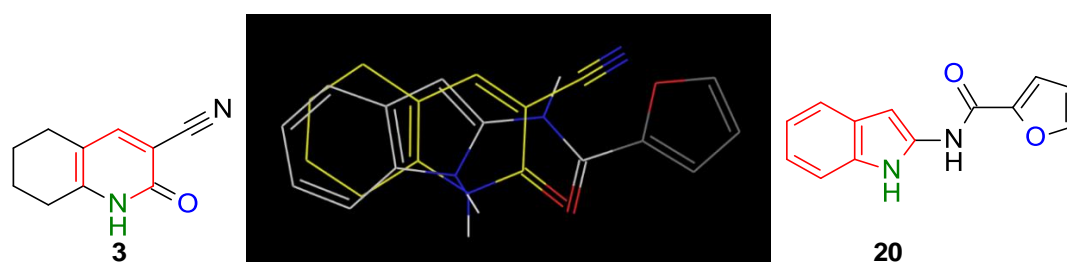
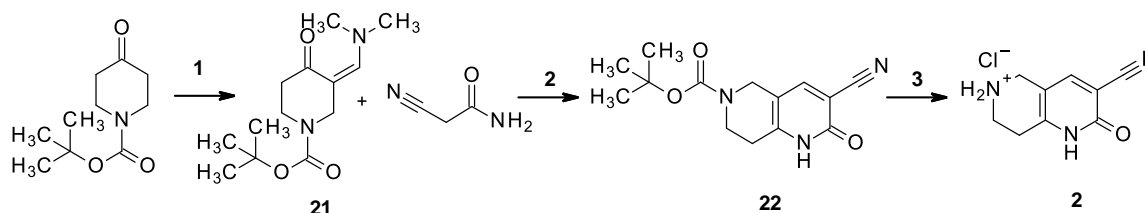


Figure 21. Superimposition of compound **3** (in yellow) and **20** structures (in white).

3.2. Synthetic strategies

3.2.1. Synthesis of compound **2**

Compound **2** was synthesized via a three-step synthetic procedure as shown in Scheme 1. In summary, treatment of commercial *N*-Boc protected 4-oxopiperidine with refluxing *N,N*-dimethylformamide dimethyl acetal (DMF-DMA) afforded enamine **21** that was isolated and cyclocondensed with 2-cyanoacetamide in the presence of sodium hydride (NaH) as base to afford intermediate **22**. Final acid treatment (HCl 4 M in 1,4-dioxane) allowed Boc elimination obtaining compound **2** as hydrochloride salt.^{46,47}

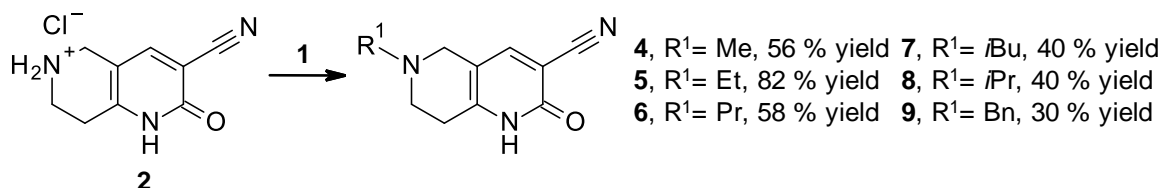


Scheme 1. Reagents and conditions: 1. DMF-DMA (10.8 mmol), N₂, 105 °C, 21 h, yield: 66 %. 2. 2-cyanoacetamide (1.05 equiv.), NaH (60 % dispersion in mineral oil, 2 equiv.), dry DMF, N₂, 0 °C to 80 °C, 15 h, yield: 10 %. 3. HCl (4 M) in 1,4-dioxane (30 equiv.), dry methanol, rt, 5 h, yield: 40 %.

3.2.2. Synthesis of compounds of series 1

Preparation of derivatives 4-9: reductive amination reaction

Reductive amination reaction between compound **2** and a selected ketone or aldehyde, using sodium triacetoxyborohydride (STAB) as a reducing agent, was performed to afford compounds **4-9** (Scheme 2). Depending on the starting aldehyde or ketone, the reaction was carried out at rt or at 55 °C.

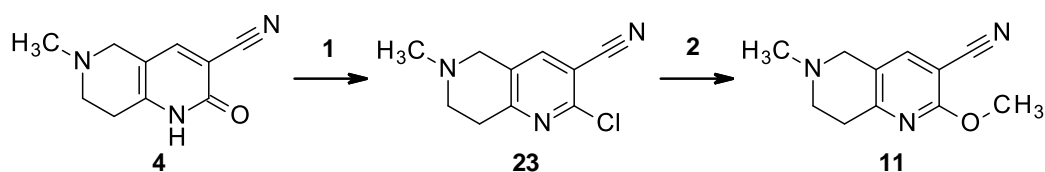


Scheme 2. Reagents and conditions: 1. Aldehyde or ketone (5.0-33.5 equiv.), STAB (2.4-4.88 equiv.), dry methanol, N₂, 55 °C or rt, 5-24 h.

3.2.3. Synthesis of compound of series 2

Two-step preparation of analog 11

Compound **11** was obtained via a two-step synthesis (Scheme 3). In the first step, a 2-chlorination reaction of compound **4**,⁴⁷ by employing phosphorous oxychloride (POCl₃) under reflux, gave intermediate **23**, that was converted in **11** through a palladium-catalyzed C-O cross coupling reaction with sodium methoxide.⁴⁸

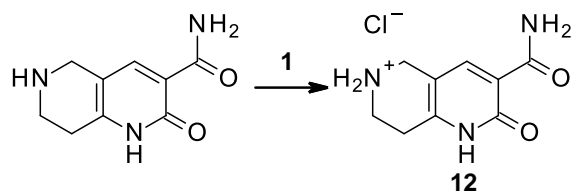


Scheme 3. Reagents and conditions: 1. POCl₃ (20 equiv.), Ar, 0 °C to 105 °C, 24 h. 2. Pd(OAc)₂ (3 mol %), tBuXPhos (6 mol %), CH₃ONa (5 equiv.), dry methanol/toluene (1:1), Ar, rt to 80 °C, 15 h, yield: 21%.

3.2.4. Synthesis of compound of series 3

Preparation of compound 12

The hydrochloride salt **12** was obtained via treatment of commercial 2-oxo-5,6,7,8-tetrahydro-1*H*-1,6-naphthyridine-3-carboxamide with HCl solution (1.25 M) in methanol (Scheme 4) and the salt formation was monitored by ¹H-NMR.



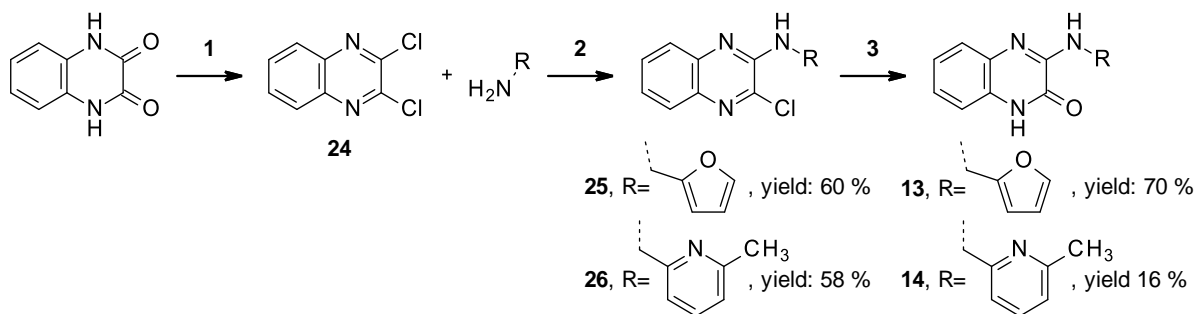
Scheme 4. Reagents and conditions: 1. HCl (1.25 M) in methanol (10 equiv.), rt, 3 h, yield: 93%.

3.2.5. Synthesis of compounds of series 4

Preparation of derivatives 13 and 14

The synthetic route for compounds **13** and **14** is outlined in Scheme 5. In particular, chlorination of 1,4-dihydroquinoxaline-2,3-dione with neat POCl_3 gave 2,3-dichloroquinoxaline **24** as a key intermediate.⁴⁹ Subsequent nucleophilic aromatic substitution ($\text{S}_{\text{N}}\text{Ar}$) with the appropriate amine followed by hydrolysis under basic conditions⁵⁰ afforded compound **13** and **14**.

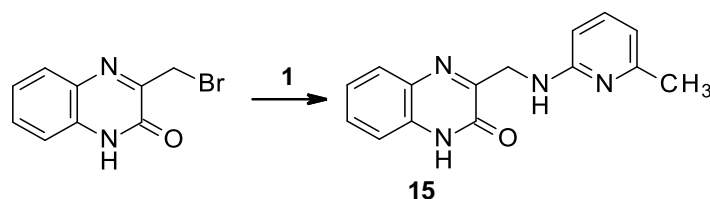
At the beginning, a two-step strategy consisting of monochlorination of 1,4-dihydroquinoxaline-2,3-dione followed by $\text{S}_{\text{N}}\text{Ar}$ of the obtained halogenated intermediate was attempted. Nevertheless, the low yield of monochlorination reaction and the high amount of compound **24** isolated prompted us to develop the procedure previously described.



Scheme 5. Reagents and conditions: 1. POCl_3 (10 equiv.), 100 °C, 4 h. 2. Triethylamine (4.5-6 equiv.), dry 1,4-dioxane, Ar, 100 °C, 24 h. 3. LiOH (4-5 equiv.), dry 1,4-dioxane/ H_2O , 60-70 °C, 48 h.

Synthesis of compound 15

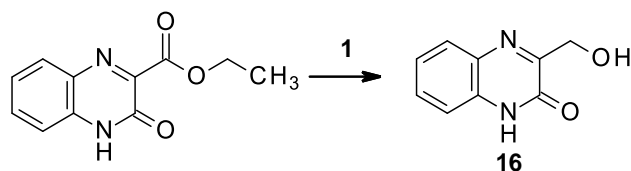
15 was prepared under $\text{S}_{\text{N}}2$ reaction conditions reacting 3-(bromomethyl)-1*H*-quinoxalin-2-one with 6-methylpyridin-2-amine (Scheme 6).⁵¹



Scheme 6. Reagents and conditions: 1. 2-amino-6-methylpyridine (2 equiv.), DMSO, rt, 14 h, yield: 8 %.

Synthesis of compound 16

The quinoxaline-based compound **16** was obtained through a reduction reaction of ethyl 3-oxo-4*H*-quinoxaline-2-carboxylate into its corresponding alcohol, using diisobutylaluminum hydride (DIBAL-H) as reducing agent (Scheme 7).⁵²

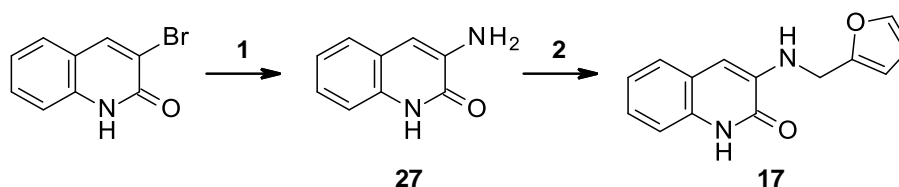


Scheme 7. Reagents and conditions: 1. DIBAL-H (1.0 M) in hexane (2 equiv.), diethyl ether, Ar, 0 °C to rt, 3 h, yield: 20 %

3.2.6. Synthesis of compound of series 5

Preparation of compound 17

Compound **17** was prepared through a two-step synthetic procedure. The first step consisted of a copper catalyzed C(sp²)-NH₂ bond formation between 3-bromo-1*H*-quinolin-2-one and sodium azide (NaN₃) in the presence of pipercolinic acid as a ligand, ascorbic acid as an additive and ethanol as a solvent at 100 °C.⁵³ The second step was a reductive amination reaction of the 3-amino-1*H*-quinolin-2-one intermediate **27** with furaldehyde using STAB as the reducing agent (Scheme 8).

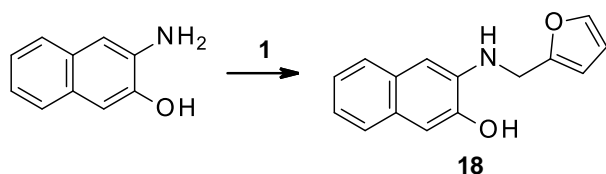


Scheme 8. Reagents and conditions: 1. NaN₃ (2 equiv.), Cu (0) powder (10 % mol. equiv.), pipercolinic acid (30 % mol. equiv.), L-ascorbic acid (20 % mol. equiv.), ethanol dry, Ar, rt to 100 °C, 4 days. 2. furaldehyde (2 equiv.), STAB (4.88 eq.), dry methanol, Ar, 60 °C to rt, 4 days, yield: 13 %.

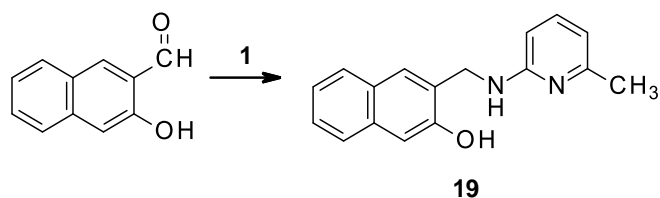
3.2.7. Synthesis of compounds of series 6

Synthesis of derivatives 18 and 19: reductive amination reaction

The synthesis of 2-naphthol derivatives **18** and **19** was performed by direct reductive amination reaction between the appropriate primary arylamine and aldehyde, as described in Schemes 9 and 10.



Scheme 9. Reagents and conditions: 1. Furaldehyde (2 equiv.), STAB (7.31 equiv.), dry methanol, Ar, 50 °C to rt, 21 h, yield: 22 %.

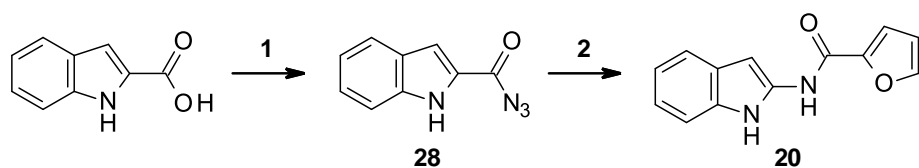


Scheme 10. Reagents and conditions: 1. 2-amino-3-methylpyridine (1 equiv.), NaBH₄ (2.44 equiv.), dry ethanol, N₂, 78 °C to rt, 5 h, yield: 46 %.

3.2.8. Synthesis of compound of series 7

Two-step preparation of compound 20

As described in scheme 11, commercial 1*H*-indole-2-carboxylic acid, treated with diphenylphosphoryl azide (DPPA), was first converted into its carboxazide derivative **28**. This acyl azide intermediate underwent a Curtius rearrangement followed by amide formation in presence of commercial 2-furoic acid and 4-dimethylaminopyridine (DMAP) to afford compound **20** in only one step.⁵⁴ A proposed reaction mechanism is reported in Figure 22. In detail, carboxazide **28** undergoes thermal decomposition to afford the corresponding isocyanate A that reacts with 2-furoic acid to obtain intermediate B. Final elimination of carbon dioxide (CO₂) gives compound **20**.



Scheme 11. Reagents and conditions 1. DPPA (0.9 equiv.), triethylamine (2 equiv.), dry dichloromethane, Ar, rt, 7 h, yield: 83 %. 2. 2-furoic acid (2 equiv.), 4-DMAP (10 mol equiv.%), dry toluene, Ar, 110 °C, 5 h, yield: 5 %

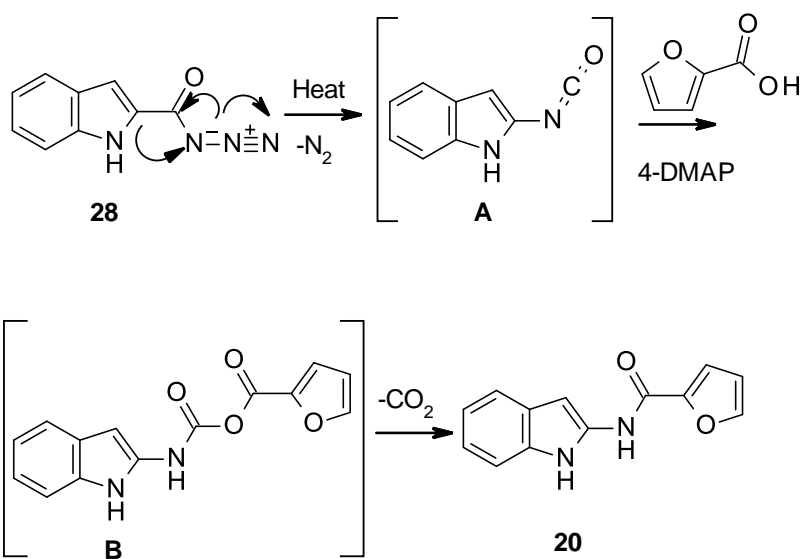


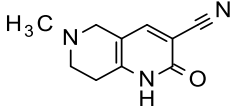
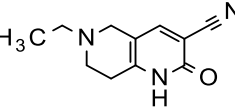
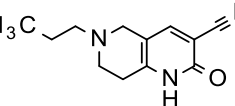
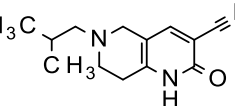
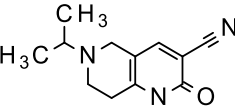
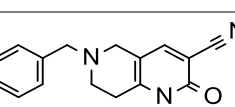
Figure 22. Proposed reaction mechanism of **20** synthesis starting from carboxazide **28** intermediate.

4. Results and Discussion

4.1. ChD binding assay results and discussion

The ChD-Competition FP assay,⁴⁵ described in paragraph 2.1, was employed at IEO to test compounds ability to inhibit, by displacement, the interaction between the selected ChD and FITC-labeled peptide H3K27me3. In particular, compounds **4-9** were tested at 6.25, 25 and 100 μM concentrations as shown in Table 2 (see VI. Experimental section, 1.2 ChD-competition FP assay).

Table 2. Inhibition data of compounds **4-9** tested in FP assay at 6.25, 25 and 100 μM . Data are reported as % of inhibition.

Cpd	Structure	% Inh (6.25 μM)	% Inh (25 μM)	% Inh (100 μM)
4		17.5	36.5	82
5		16	22.5	59.5
6		33.5	68.5	100.0
7		38.5	62.5	100.0
8		19	46.5	88.5
9		34	48	84

Remarkably, all evaluated compounds displayed inhibition even at the lowest tested concentration (6.25 μM) and dose-response effects. In detail, for compounds **4-9** the percentage of inhibition at 6.25 μM , ranging from 16 to 38.5 %, was comparable to the percentage of inhibition of both compound **2** and **3** (20 % inh and 36.8 % inh, respectively) (Table 2). At 100 μM concentration, all derivatives, except for compound **5**, displayed higher inhibition with respect to hit compound **2** (70 % inh at 100 μM) and two compounds (**6** and **7**) out of six showed full inhibition (100 % inh) as hit compound **3**. According to these encouraging FP data, a large variety of substituents were tolerated in 6-position of the 5,6,7,8-tetrahydro-1,6-

naphthyridine framework and even sterically hindered compounds (i.e., compound **9**, Table 2) showed inhibition.

Among the tested compounds, compound **6** and **7**, showing 100 % of inhibition at 100 μM , together with hit compound **3** (Paragraph 2.1) were selected for the determination of the IC_{50} value, that is considered the inhibitor concentration required to produce the 50 % dissociation of the complex between the selected ChD and FITC-labeled peptide.

Unexpectedly, in these FP experiments of IC_{50} values determination, reproducible data were obtained only for compound **3** that showed an IC_{50} value of 13.47 μM (Figure 23). Compounds **6** and **7** did not confirm the inhibition of previous FP tests. In detail, two different experiments were run testing the selected compounds at two different concentrations ranges (0.097-200 μM for experiment I and 0.0312-200 μM for experiment II) and, in both cases, the obtained results were not in agreement with those of initial experiments at three different concentrations (6.25, 25 and 100 μM) (Figure 23).

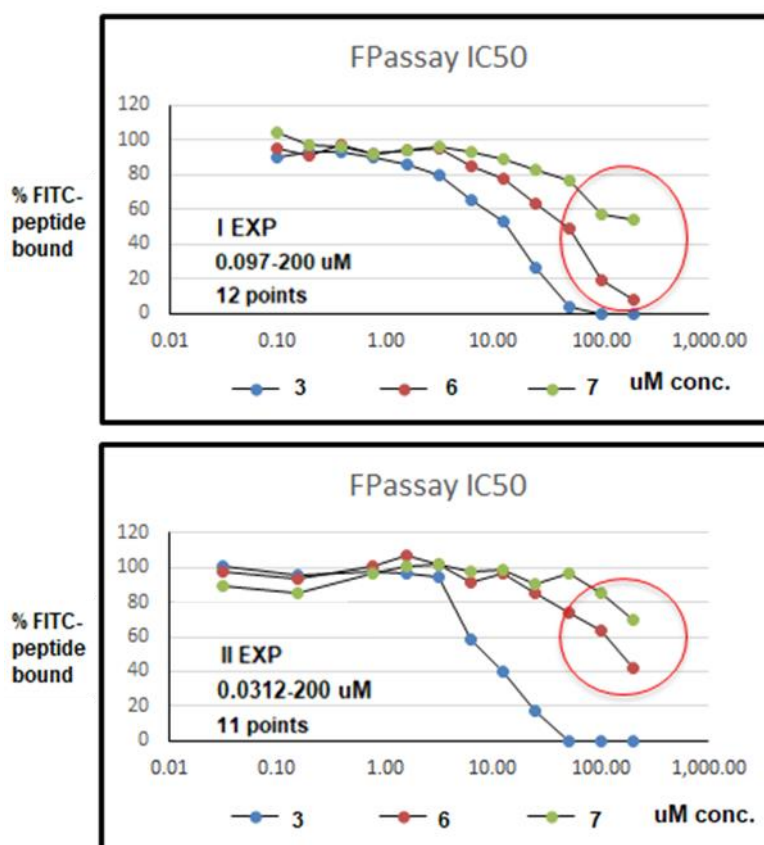


Figure 23. Experiments I (concentration range: 0.097-200 μM) and II (concentration range: 0.0312-200 μM) for IC_{50} determination of compounds **3**, **6** and **7**. Data are reported as % of FITC-peptide bound relative to DMSO after incubation with the compound.

The lack of reproducibility of the preliminary results of compounds **6** and **7** (Figure 23) suggested a possible compounds interference with the assay readout. Thus, the spectroscopic properties of re-synthesized compounds **1** and **2** and all derivative of series 1 were investigated.

In particular, the compounds capability to emit light around the emission wavelength used for assay readout (λ_{em} : 535 nm) after excitation at the same wavelength used in the assay (λ_{exc} : 485, see Paragraph 2.1) was studied. First, the absorption spectrum of each selected compound was registered from 200 to 800 nm; then, the fluorescence spectra of compounds **1-9** were recorded (some representative examples of fluorescence spectra are reported in Figure 24). The samples for analysis were prepared in line with the protocol of the ChD-competition FP assay (VI Experimental section, 1.2 ChD-competition FP assay), except for the buffer. Indeed, water Milli-Q was employed for samples preparation having proved that assay buffer (pH 8) did not affect the spectroscopic properties of the selected molecules. In detail, freshly prepared solution 20 mM in DMSO of each compound were diluted with water Milli-Q to 100 μ M, thus providing the appropriate percentage of DMSO in the final volume (0.5 %).

Fluorescence analysis revealed that except for re-synthesized compound **1** (Figure 24 a), all other tested compounds **2-9** were able to emit light around 535 nm upon excitation at 485 nm (Figure 24 b, c, d), thus interfering with the assay readout.

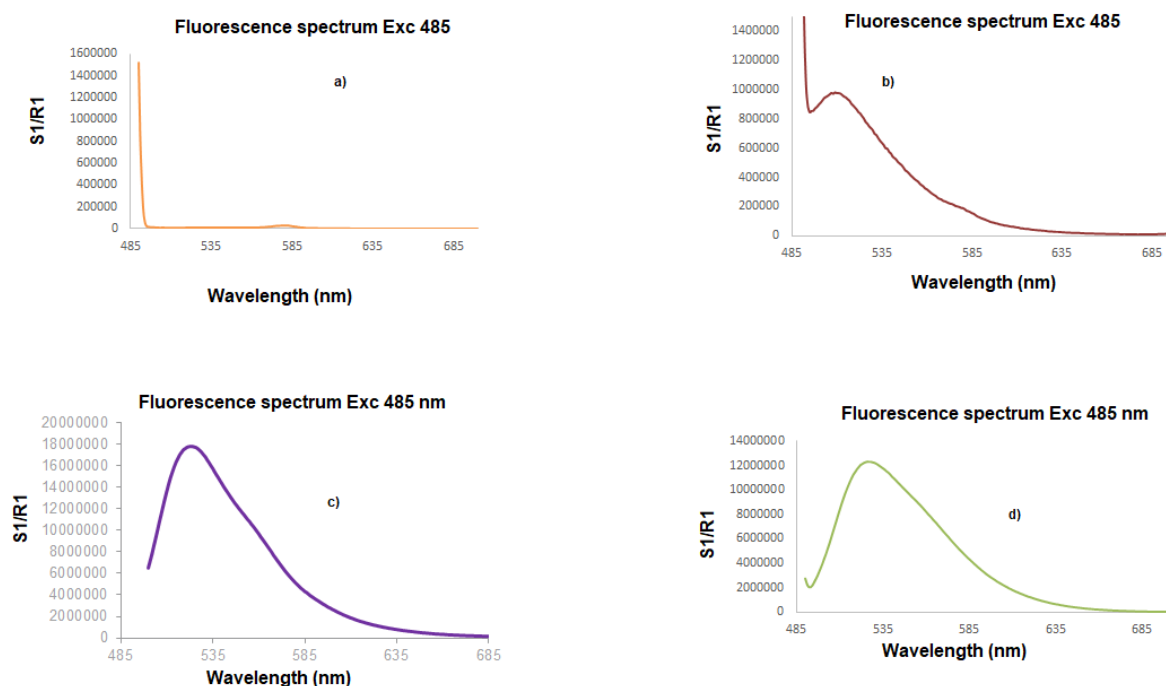


Figure 24. Fluorescence emission spectra of some representative compounds after excitation at λ_{exc} : 485 nm. a) Fluorescence emission spectrum of re-synthesized compound **1**. b) Fluorescence emission spectrum of compound **2**. c) Fluorescence emission spectrum of compound **3**. d) Fluorescence emission spectrum of compound **6**.

The proven compounds interference made the search of alternative assay conditions needed. In particular, it was thought to substitute the FITC probe with AlexCy3, a red-shifted fluorophore, able to emit fluorescence at 580 nm after excitation at 535 nm. Therefore, the capability of compounds **1-9** to interfere with AlexCy3 at the assay conditions was also investigated (λ_{exc} : 535, λ_{em} : 580 nm). Fluorescence spectra of compounds **1**, **2**, **4-9** (only representative examples have been reported in Figure 25 a, b, d) revealed a lack of interference of all compounds with the assay readout. On the contrary, compound **3** (Figure 25 c) showed a low-intensity emission around 580 nm, thus suggesting its minimal interference also with the assay conditions set for AlexaCy3 probe.

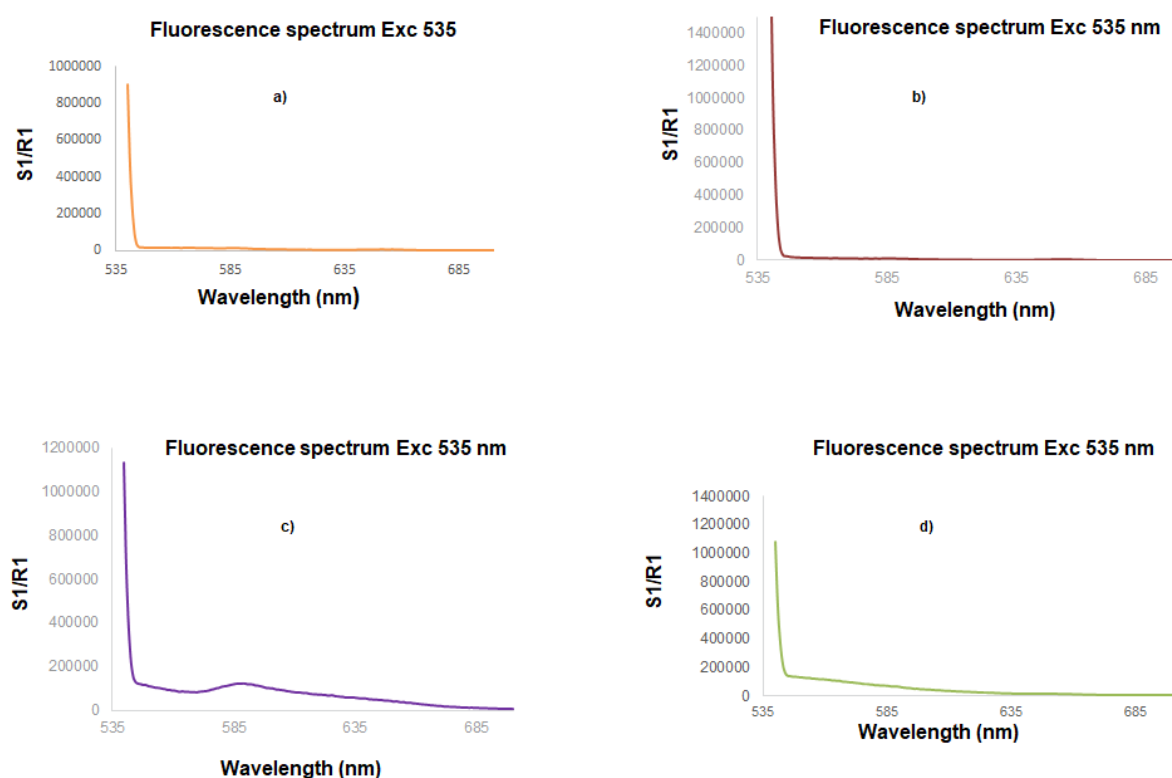


Figure 25. Representative fluorescence emission spectra of some representative compounds after excitation at λ_{exc} : 535 nm. a) Fluorescence emission spectrum of re-synthesized compound **1**. b) Fluorescence emission spectrum of compound **2**. c) Fluorescence emission spectrum of compound **3**. d) Fluorescence emission spectrum of compound **6**.

5. Conclusions

In this first research project, the lack of reproducibility of preliminary inhibition data of the ChD-competitive FP assay suggested compounds interference with the assay readout. A deep investigation of compounds spectroscopic properties confirmed compound **2-9** capability to give false positive results by emitting fluorescence in the FITC-labeled peptide emission region (λ_{em} : 535 nm), thus explaining the abnormal decrease of FP signal observed in their presence. Only re-synthesized compound **1**, which did not display any inhibition in the FP assay, did not show fluorescent properties when excited at the FITC probe's excitation wavelength (λ_{exc} : 485 nm). Since a significant FP signal change was instead observed in the presence of the less pure commercial compound **1**, we concluded that the main impurity, perhaps based on same 5,6,7,8-tetrahydro-1,6-naphthyridine scaffold of compound **2** and analogs of series 1 (**4-9**), could be responsible for interference with FP assay readout.

In an attempt to overcome the compounds interference, the possibility to employ AlexaCy3 probe in the FP assay was taken into account. However, the minimal compound **3** fluorescent emission in the AlexaCy3 probe emission region (λ_{em} : 580 nm) after excitation at 535 nm did not confirm the suitability of AlexaCy3 as an alternative probe for FP assay.

Not being able to use the FP assay to evaluate the synthesized compounds as potential binders of the selected ChD-containing protein, synthetic activities were stopped. Currently, various cell- and non-cell-based assays are being evaluated to test all the developed compounds.

Overall, the obtained results underlay the importance of hit compounds validation at the initial phase of drug discovery. Indeed, to define a compound as a hit, it is fundamental to assess if the signal observed in the screening assay in the presence of the compound is due to a desirable mechanism. Frequently, medicinal chemistry teams have to deal with false-positive results in the primary screening assay and different mechanisms underlying these false-positives have been identified. Some of them are linked to specific chemical and physical compounds features, such as their low solubility in the assay buffer, their tendency to form aggregates, non-specific binding, interference with the assay readout or high chemical reactivity. In other cases, the signal responsible of a false-positive result is related to impurities present in the sample of the tested compound.⁵⁵

Therefore, to confirm that the compounds selected from primary screening are really active against the selected target, different strategies can be adopted, according to the specific compound and assay employed. For instance, if a commercial compound results active in the primary screening assay, it could be re-synthesized and re-tested in order to exclude the possibility that the observed signal is due to impurities in the commercial batch. Moreover, it

is possible to evaluate compounds interference through orthogonal assays, that, relying on a different detection methods, could allow to avoid compound interference. In other cases, the use of biophysical methods, such as X-ray crystallography or NMR, could be useful to confirm the activity of the identified hit compound against the selected target.

In this specific project, even three different strategies were employed at different stages to validate presumed hits: re-synthesis of commercial compounds that resulted positive in the primary screening, chemical characterization of impurities of commercial batches that resulted active and spectrofluorometric assessment of compounds interference with the assay readout. In particular, new batches of compounds **1** and **2** were synthesized and re-tested to validate the activity of the commercial ones. Since re-synthesized compound **1** did not confirm the activity of the commercial counterpart, the main impurity of the commercial batch was characterized by ¹H-NMR in order to identify a likely active scaffold. The spectrum revealed the presence of a small molecule with a structure similar to that of compound **2**, and it was selected as an interesting starting point for the identification of new ChD binders. Finally, being compounds **2-9** suspected to be false positives, their ability to emit fluorescence at the wavelength of the FP assay was evaluated. Data confirmed that compounds **2-9** were able to emit fluorescence in the region of the assay readout, interfering with it and causing a consistent signal change.

In summary, the project described in this part of the thesis provides clear evidence to support the idea that hit validation is crucial for a successful drug discovery campaign.

III. Part 2: Development of small-molecules as Tubulin Colchicine-site binders for cancer therapy

1. Introduction

1.1. Microtubules roles and dynamics

Microtubules are part of the cellular cytoskeleton and play fundamental roles in several biological functions like cell division, motility, intracellular trafficking and maintenance of cell structure. From a structural viewpoint, they consist of hollow cylinders of around 25 nm in diameter, composed of typically 13 protofilaments aligned in a parallel manner. Each protofilament results from the “head-to-tail” assembly of $\alpha\beta$ -tubulin dimers and this assembly explains the polarized nature of microtubules.⁵⁵

Microtubules structure undergoes continuous cycles of elongation and shrinkage, which are responsible of their called “dynamic instability”.⁵⁸ The sudden switch from growing to shrinkage is stochastic and is called “catastrophe”, while the reverse process is defined “rescue” (Figure 26).⁵⁷ GTP hydrolysis regulates dynamic instability process. In particular, GTP-bound $\alpha\beta$ -tubulin heterodimers, displaying a “curved” structure, are added to plus-ends of growing microtubules and hydrolysis of GTP bound to β -tubulin subunit triggers gradual “curved-to-straight” conformational change of dimers and stabilization of the growing protofilament. The hydrolysis is delayed with respect to dimers incorporation into microtubules, thus growing ends maintain a so-called “GTP cap”, whose loss causes a destabilization and switch from assembly to disassembly.⁵⁹ The process is completed with exchange of GDP bound to β -tubulin to GTP.⁵⁶

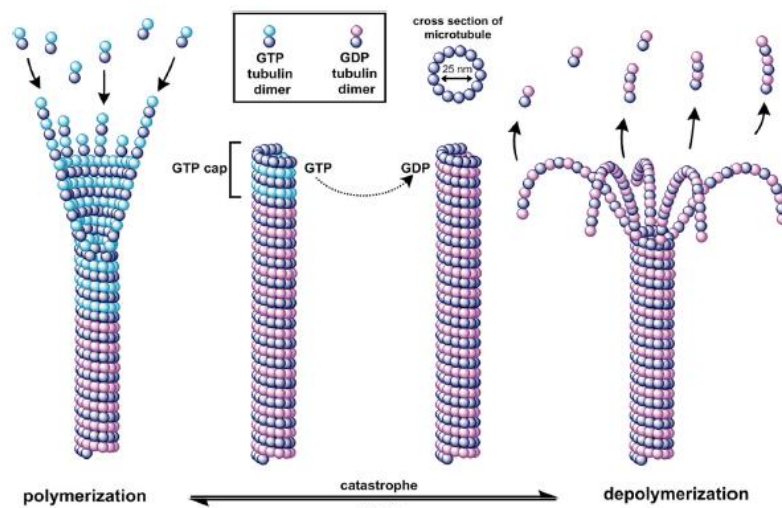


Figure 26. Dynamic instability of microtubules.⁵⁸

1.2. Altering microtubule dynamics and cancer therapy

Given the fundamental role played by microtubules in cell division, compounds targeting tubulin and, consequently, able to interfere with microtubules dynamics represent important tools in the anticancer therapy.⁶⁰ In this context, microtubule-targeting agents (MTAs), that are used in cancer therapy, act mainly by suppressing microtubule dynamics

during the mitotic cell division, thus interfering with mitotic spindle formation, causing mitotic arrest in the G2/M phase and leading in many cases to cell death.⁵⁶ Tumour cells are more susceptible to these agents than normal cells since they go through cell division much more frequently.⁶¹ MTAs are commonly classified in microtubule-stabilizing agents (MSAs) and microtubule-destabilizing agents (MDAs), according to their ability to promote microtubule polymerization or depolymerization, respectively.

There are several known tubulin-binding sites for MTAs. Taxane, Vinca and Colchicine binding sites were known since 2013, but, recently, X-ray crystallography and cryo-electron microscopy allowed the characterization of three additional sites: Maytansine, Laulimalide/Peloruside and Pironetin sites (Figure 27).⁵⁶ Compounds targeting one of these sites might lead to microtubule dynamics perturbation and, therefore, alter their biological function.⁵⁸

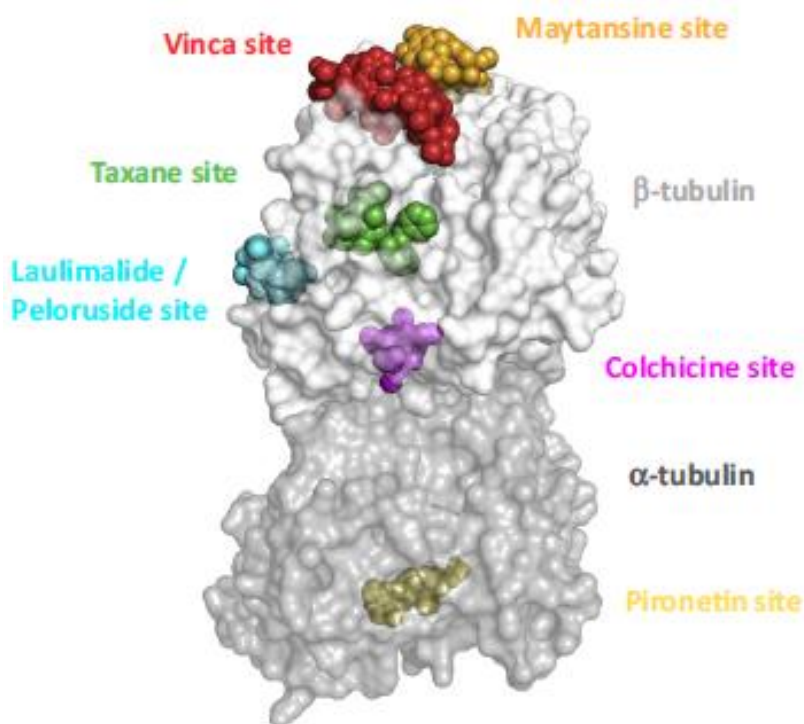


Figure 27. MTAs binding sites.⁵⁶

The most common classes of MTAs studied for cancer treatment include binding agents to Vinca, Taxane, Colchicine and Maytansine site domains. Vincristine and Vinblastine alkaloids, able to target the Vinca domain, together with Paclitaxel,⁶² paved the road to MTAs success in cancer therapy.⁵⁶ Despite the huge therapeutic advantages showed by these agents, their use in cancer treatment was partially hampered by “off-target” toxicity and resistance development. Thus, the need to address such issues has been promoting research until now.

Neurological toxicity is the most common side effect of MTAs, since microtubules are crucial for neuron functions. Peripheral neuropathy is different according to the dose, drug and schedule of administration with symptoms depending on the damaged fiber (sensory, motor, autonomic) and sometimes leads to significant sequelae.⁵⁹ To address toxicity, antibody drug conjugates (ADCs) of several of these chemotherapeutic agents have been studied and approved by FDA.⁵⁶ However, the problem is not completely solved and dose-limiting toxicity still causes suspension of these drugs.⁶³

Resistance development is another drawback of this class of anticancer agents and it can arise at different stages of MTAs pharmacodynamics, displaying impaired drug cellular transport, target engagement or abnormal apoptosis mechanisms. Mutations in β -tubulin, aberrant expression of some β -tubulin isotypes or microtubule-regulating proteins, membrane drug efflux pumps of the ATP binding cassette (ABC) family expression and changings in the actin cytoskeleton are the most common mechanism of resistance identified for MTAs.^{60,64}

In the light of this therapeutic limitations, new microtubule binding agents with improved safety profiles and less prone to develop resistance are still required.

1.3. Colchicine-binding site

Extensive literature suggests that MTAs targeting the Colchicine-site are less susceptible to certain types of resistance development and Colchicin-site binding agents research for cancer is a very fruitful field.^{58,65}

The Colchicine-binding site, first identified in 2004 by X-ray crystallography,⁶⁶ is a deep pocket allocated near the interface of α and β tubulin of the same heterodimer and Colchicine is the first recognized ligand.⁵⁸ Comparison of the very different binding mode of compounds that compete with Colchicine for tubulin binding, allowed Dorélan's group to define the Colchicine-binding site as a "binding domain",⁶⁷ later divided into three different zones: zone 2 (in the center), that accommodates Colchicine and other ligands, and two side pockets, zone 1 and zone 3, respectively (Figure 28).⁶⁸ Zone 1 faces α -tubulin and zone 3 is buried in β -tubulin subunit (Figure 28).⁶⁸

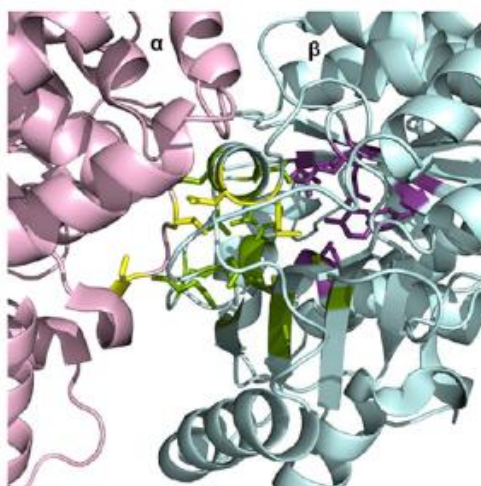
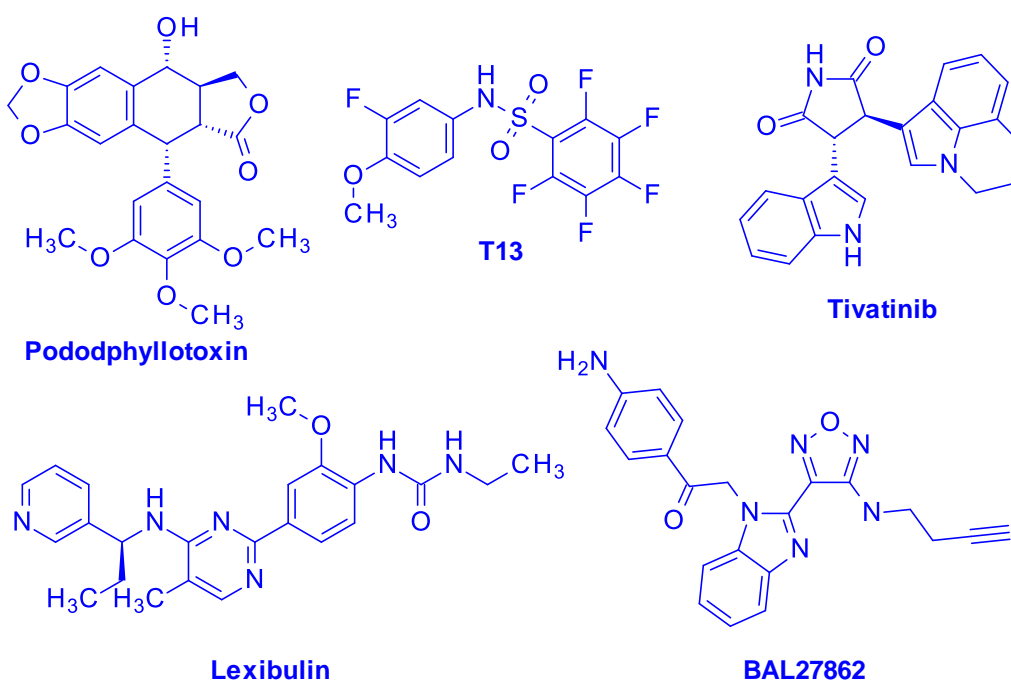


Figure 28. Colchicine-binding domain. Zone 1 (yellow), zone 2 (green) and zone 3 (violet) are highlighted with different colours. α -tubulin is in light pink and β -tubulin in cyan.⁶⁹

Colchicine-site binders are divided into two groups, according to the zones that they occupy. Some ligands (Figure 29, blue) are accommodated in zone 1 and 2 and bind tubulin similarly to Colchicine, while others (Figure 29, red) bind zone 2 and 3, accommodating deeper in β subunit. Curiously, no binder of the whole Colchicine-domain has been found so far.⁶⁹



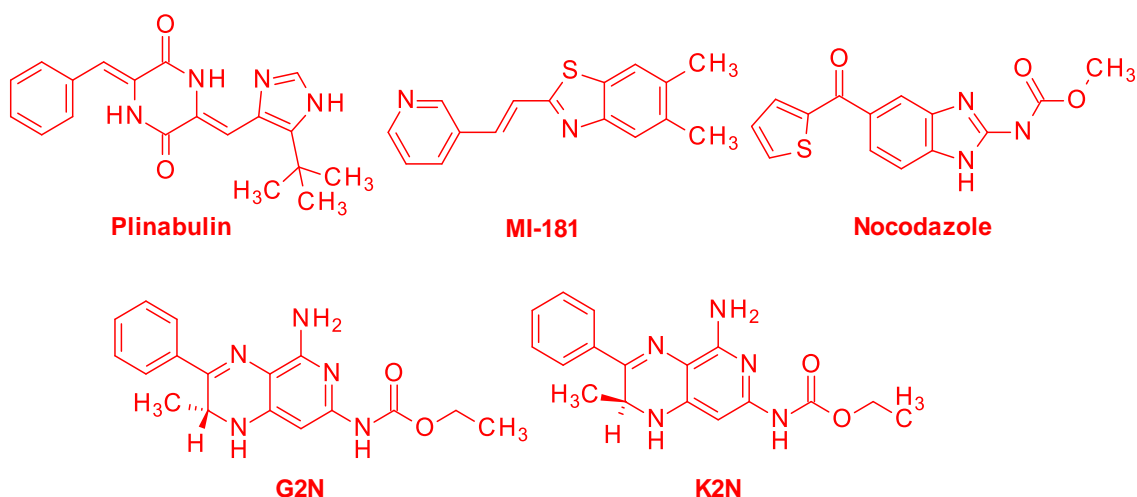


Figure 29. Ligands of the Colchicine domain. In blue, ligands that occupy zone 1 and 2 and in red ligands that occupy zones 2 and 3.⁶⁹

Colchicine-site binders act as MDAs, showing antimetabolic and vascular disrupting activity.⁵⁸ Their binding prevents tubulin structural rearrangements required for “curved-to-straight” conformational transition that is fundamental for microtubules assembly⁶⁷ (Figure 30). Since this mechanism of action differs from that of other tubulin binders without vascular disrupting properties, it is thought to rationalize Colchicine-site binders’ different biological activity⁶⁹ and explains their potential therapeutic value in cancer therapy.

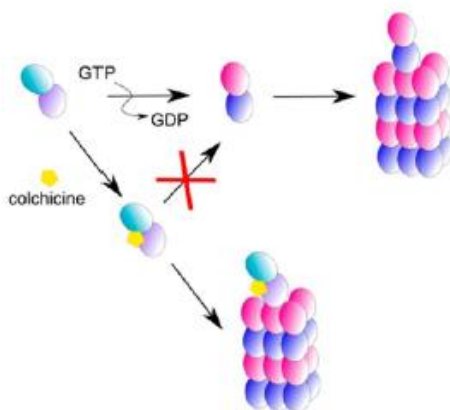


Figure 30. Curved-to-straight conformational change of tubulin dimer upon GTP binding (on top). Colchicine (represented in yellow) preventing the curved-to-straight transition of tubulin (below), required for microtubule assembly.⁶⁹

Indeed, this tubulin site is already validated for cancer treatment with several compounds in clinical trials for cancer.⁶⁵ However, currently there is no Colchicine-site binder approved in oncology.⁵⁸

1.4. Nocodazole

Nocodazole (Figure 31) is one of the most studied reversible Colchicine-site binders. It was identified in 1976 showing antifungal, anthelmintic and antineoplastic properties.⁷⁰ Its low solubility, modest activity in tumour animal models and toxicity limited its therapeutic use.⁷¹ However, it is currently used in pharmaceutical research.⁵⁸

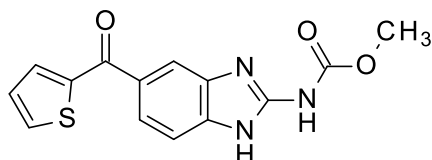


Figure 31. Nocodazole structure.

In 2016, Wang's group published the structure of tubulin in complex with Nocodazole (PDB code: 5CA1), together with other Colchicine-site binders complexes. It emerged that Nocodazole binds zone 2 and 3 and, in comparison with other binders like Colchicine, does not interact with α -tubulin and, specifically, contacts Asparagine (Asn)165 and Glu198 through H-bond interactions (Figure 32).⁷² This work represented a major breakthrough in tubulin research, since it provided essential structural information to define Colchicine-site binders interacting features that is required for rational and successful drug design.



Figure 32. Interactions between Nocodazole and tubulin (PDB code: 5CA1).⁷²

2. PhD project background

2.1. High-throughput X-ray crystallography for fragment screening in the identification of new tubulin binders

As previously described, the application of X-ray crystallography in the screening phase allows the assessment of compounds binding properties and provides structural information of interacting features contemporarily, thus reducing the time required to develop the identified active compounds into drug candidates. Moreover, this technique is particularly suitable for the screening of fragment-like libraries due to its high sensitivity. Therefore, a fragment-based campaign targeting tubulin assisted by X-ray crystallography offers promises for the fast identification of tubulin binders and their successful development into anticancer agents.

2.2. Identification of compound 29

The need to identify new tubulin binders and the promises offered by both FBDD and high-throughput X-ray crystallography in drug discovery strongly suggest the use of high-throughput X-ray crystallography for tubulin binding fragment screening in cancer research.

Taking into account this consideration, prof. Steinmetz's group from PSI (Paul Scherrer Institute) and prof. Cavalli's group from University of Bologna developed a specific workflow for a FBDD project targeting tubulin based on three main steps:

- 1) Identification of tubulin-binding fragments through X-ray crystallography based screening.
- 2) Exploration and elaboration of such fragments into new compounds.
- 3) Evaluation of synthesized compounds for tubulin binding and their capability of affecting cell viability.

Within this context, an X-ray crystallography based FBDD campaign was performed at PSI by prof. Steinmetz's group, allowing the identification of compound **29** (Figure 33) as a binder of the Colchicine-site, previously validated for tumour treatment. Compound **29** presents a 2-aminobenzimidazole core like Nocodazole (Figure 33), that also binds the Colchicine-site of tubulin.

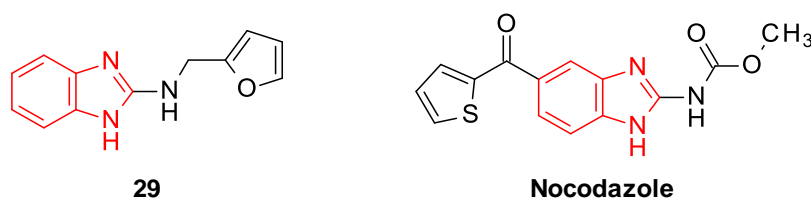


Figure 33. Structures of compound **29** (left) and Nocodazole (right).

The good matching superimposition of crystal structure of compound **29** with that of Nocodazole (PDB code: 5CA1)⁷² confirmed a similar binding mode, involving a network of hydrogen bond interactions with the target (Figure 34 and Figure 35). Specifically, the NH groups in 1 and 2-position of both molecules acted individually as hydrogen bond donors interacting both with E198, while the O atom of compound **29**'s furan ring and that of the carbamate moiety of Nocodazole were hydrogen bond acceptors contacting Asn165 (Figure 34 and Figure 35).

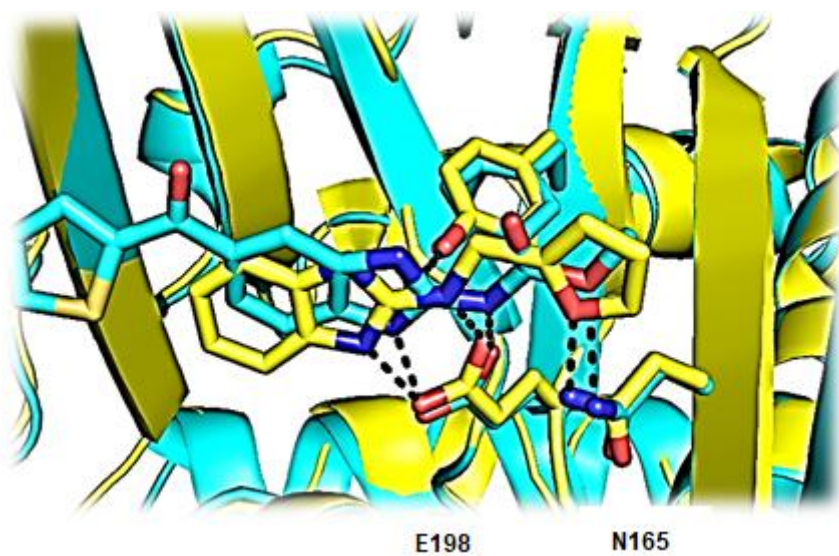


Figure 34. Superimposition of Nocodazole-tubulin (PDB code: 5CA1)⁷² and compound **29**-tubulin complex crystal structures.

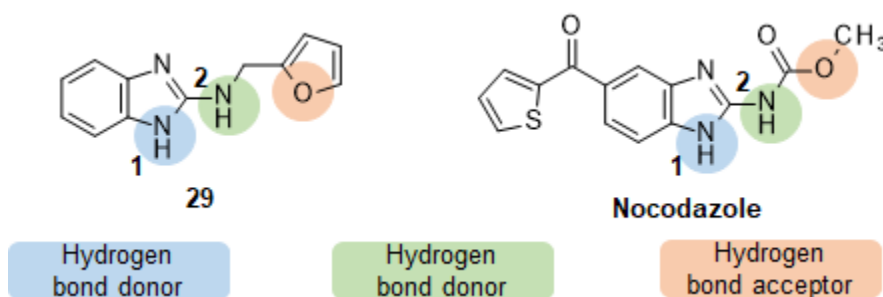


Figure 35. Compound **29** and Nocodazole's binding features. Groups that interact similarly with the target are highlighted with the same colour.

Since compound **29** targets a druggable site, whose binding notoriously alters microtubule dynamics,⁶⁶ it was selected for further development in order to validate the workflow strategy.

3. PhD project

3.1. Design of compounds

Two series of analogs of compound **29** were designed through a computer-aided drug approach to explore the fragment. Our aim was to identify the key binding features essential for target engagement and then rationally grow the fragment in order to access new binding interactions and increase the chance to improve the compound's affinity.

3.1.1. Design of series 1

Prior to fragment elaboration, we initially thought to resynthesize compound **29** in order to confirm the data obtained with its commercial counterpart. Then, we moved to analogs design. In this context, since crystal structure highlighted the importance of the hydrogen bond interactions for target binding (Figure 34), we focused on position 1 and 2 of the benzimidazole framework and the furan ring in order to confirm their role in establishing the essential network of H-bonds with the Colchicine-site of tubulin (Figure 36). Specifically, we thought to explore how the elimination of a hydrogen bond donor or its substitution with a hydrogen bond acceptor in 1-position could affect the binding; thus, we designed compounds **30** and **31**, respectively (Figure 36). In addition, we developed compound **34** in an effort to study how both a replacement of a hydrogen bond donor with a hydrogen bond acceptor and an increase of steric hindrance at the furan ring side could alter binding properties. We also considered to investigate binding properties of a derivative missing a hydrogen bond donor in 2-position (compound **32**, Figure 36). In a second step, we focused on modifications of the furan ring. In particular, we thought to design analogs **33**, **35** and **36** bearing heterocycles of different size (compounds **35**, **36**, Figure 36) to explore the shape of the target, and with different proton acceptor properties (compound **33** and **36**, Figure 36) to evaluate the contribution of such properties to the binding event. Moreover, in compounds **37** and **38**, we aimed at exploring the importance of aromaticity and conformational constraint of furan ring for target recognition (Figure 36).

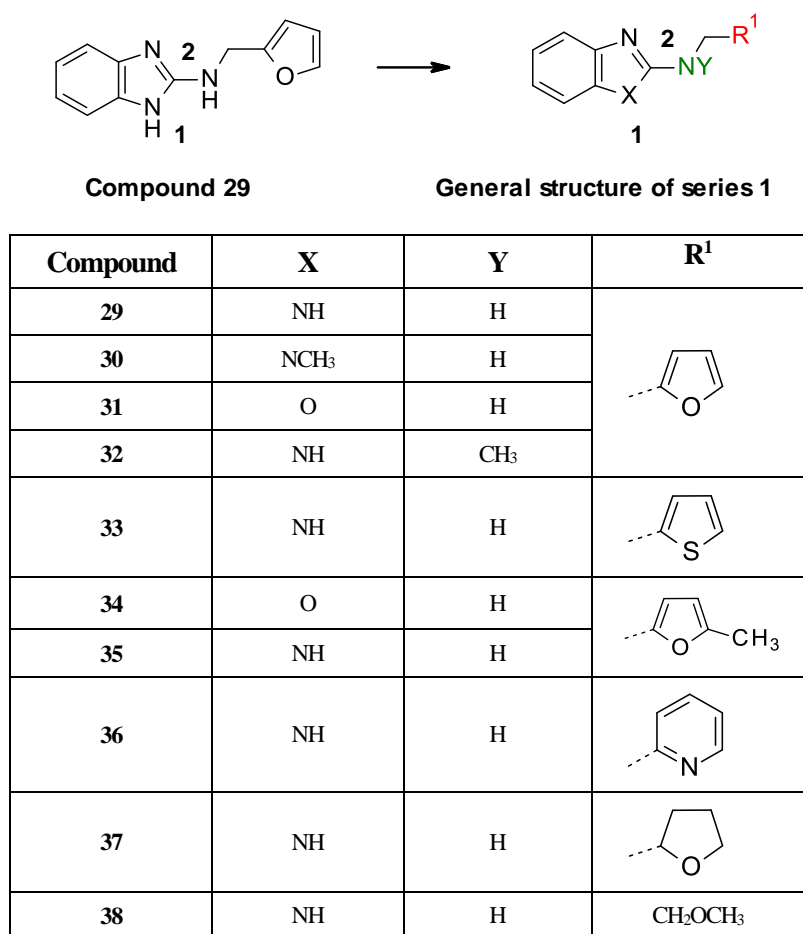


Figure 36. Design of series 1 compounds and their corresponding chemical structures.

In the analogs design framework, docking studies were performed, allowing the calculation for each compound of a score that approximately assess the binding affinity of the compound in a specific docking pose. The score was obtained taking into consideration positive and negative contributions to binding (Table 3).

For this first series of compounds, those bearing a *1H*-benzimidazole ring (compounds **29**, **32**, **33** and **35**) showed a better score than those containing a *N*-substituted benzimidazole (compound **30**) or a benzoxazole (**31**, **34**) core. Moreover, compounds with a bulky heterocycle, an aliphatic ring or an alkoxy-chain (compounds **36**, **37** and **38**, respectively) linked to the *1H*-benzimidazole the score was lower in comparison with those bearing a 5-term heterocycle (compounds **29**, **30**, **31**, **32**, **33**, **34**, **35**). Compound **37** presents a chiral center in the tetrahydrofuran ring and computational scores of both enantiomers of compound **37** were very similar (Table 3), suggesting that the target does not bind preferentially to a specific chiral form. Thus, it was decided to synthesize the racemic mixture in a first step.

Consistently with the above-mentioned results, computational studies had suggested that there should not be enough space to accommodate additional moieties in 1 and 2 positions

and that only small and hydrophilic groups could replace the furan ring, while maintaining target engagement. Moreover, it was reported that the protonation state of E198 at the Colchicine-site plays a crucial role in benzimidazole-based compounds binding, indicating that the amino-acid residue could be protonated in the protein environment.⁷³

Table 3. Docking scores of compounds of series 1.

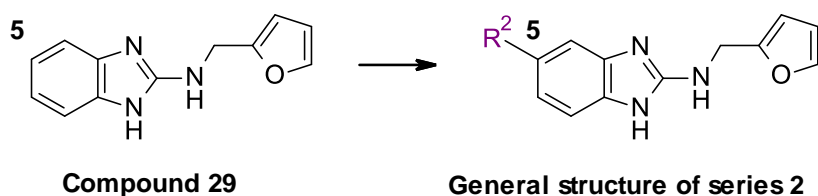
Compound	Score
29	-7.248
30	-5.283
31	-6.669
32	-7.142
33	-7.241
34	-6.036
35	-7.691
36	-6.42
37	-6.996/-6.529 (R/S)
38	-5.211

3.1.2. Design of series 2

With the aim to rationally grow compound **29**, we designed analogs of series 2. In this context, Nocodazole's structure and docking studies suggested an interesting growth vector from position 5 (Figure 37). Considering that, the insertion of a substituent at 5-position of the benzimidazole core generates two different tautomeric forms that could be both allocated at the binding site, tautomerism of the main scaffold was taken into consideration for docking studies (Figure 38 and Table 4). Interestingly, for almost all compounds very similar docking scores were obtained for tautomer 1 and 2, suggesting no preference for a specific form (Table 4, Figure 38).

Moreover, since computational studies suggested that there should be enough space to allocate very different hydrophobic and flexible moieties in 5-position, we designed compounds bearing flexible groups with a variety of electronic, steric and lipophilic properties (compounds **39-46**, Figure 37). Our aim was to explore the chemical space and the shape of the target in this specific environment. Specifically, we inserted different electron withdrawing groups, like -Cl, -COOCH₃, -CF₃, -CN (compounds **40**, **41**, **42** and **44**, respectively, Figure 37), electron-donating groups, as -CH₃ and -OCH₃ (compounds **39** and **45**, respectively, Figure 37) and bulky and lipophilic groups like -COPh and -OPh (compounds **43** and **46**, respectively, Figure 37). Since this set of compounds presents two different tautomeric forms (Figure 38)

that could allocate in a different way in the nocodazole binding site, both structures were taken in consideration for docking studies (Table 4). For each pair of tautomers evaluated, no significant difference in the docking scores was observed with the exception of that of compound **43** for which tautomer 1 seemed to have a higher affinity for the tubulin Colchicine-site than tautomer 2 (Table 4). Binding poses of some representative compounds are reported in Appendix, Figure A6-A11.



Compound	R ²	Compound	R ²
39	CH ₃	43	COPh
40	Cl	44	CN
41	COOCH ₃	45	OCH ₃
42	CF ₃	46	OPh

Figure 37. Design of series 2 and corresponding compounds.

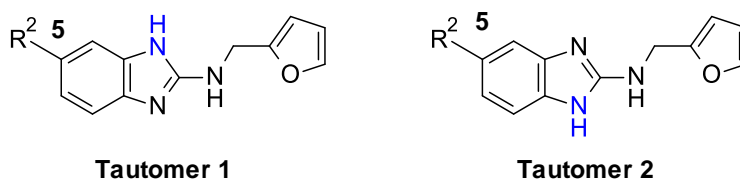


Figure 38. Tautomeric forms of general structure 2.

Table 4. Docking scores of compounds of series 2.

Compound	Score (tautomer 1)	Score (tautomer 2)
39	-6.376	-6.995
40	-6.995	-7.58
41	-7.696	-6.895
42	-8.065	-7.445
43	-8.903	-7.396
44	-7.398	-6.824
45	-7.842	-7.306
46	-7.991	-7.486

3.2. Synthesis of compounds

Compounds of series 1 and 2 were synthesized approaching two different strategies. One of them consisted in the heterocycle derivatization through a nucleophilic aromatic substitution reaction (S_NAr), while the other supposed the 2-amino benzimidazole heterocycle formation from an orto-dianiline (Figure 39). The specific strategic approach was selected depending on the commercial availability of the reagents to get the target compounds.

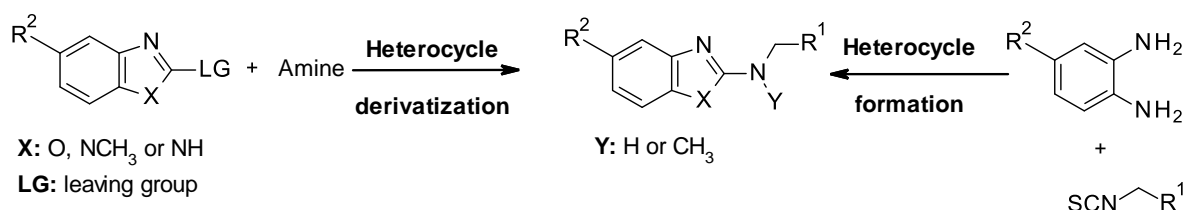
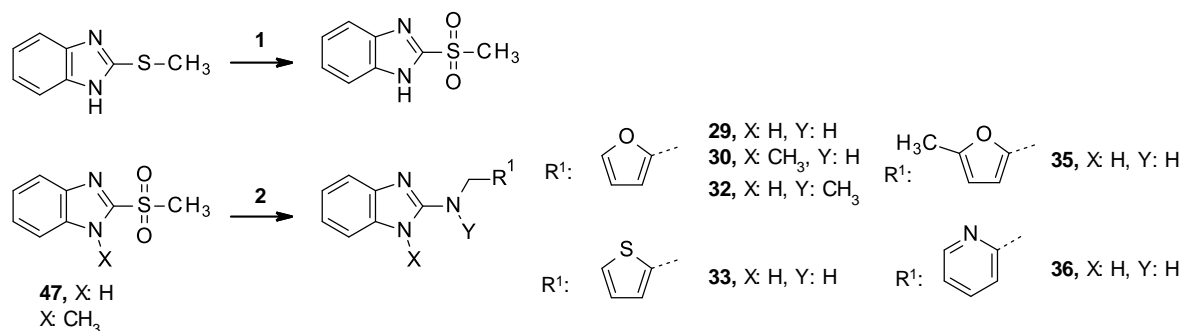


Figure 39. General strategies used for the synthesis of compounds 29-46.

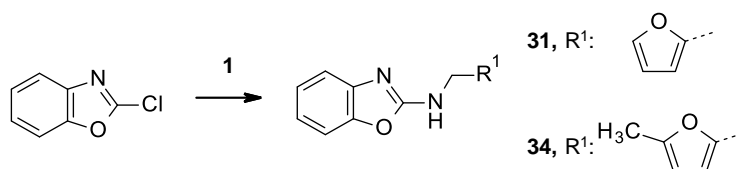
3.2.1. Nucleophilic aromatic substitution reaction (S_NAr) approach

Compounds **29**, **30**, **32**, **33**, **35** and **36** were obtained through a nucleophilic aromatic substitution (S_NAr) between the appropriate 2-methylsulfonylbenzimidazole and an appropriate amine in the presence of a weak base (Scheme 12).⁷⁴ This approach led in many cases to the complete consumption of benzimidazole starting material due to the large amount of amine (5 equivalents) and high-temperature reaction conditions. 2-methylsulfonyl-1H-benzimidazole precursor was in turn synthesized in-house from oxidation of the 2-methylsulfane counterpart,⁷⁵ while 1-methyl-2-methylsulfonyl-benzimidazole was commercially available (Scheme 12). Difficult purification of the crude residues was responsible of yields from moderate to low, as reported in Scheme 12.



Scheme 12. Reagents and conditions: 1. mCPBA (3 equiv.), DCM, 0 °C to rt, 1 h, yield: 85%. 2. NHYCH₂R¹ (5 equiv.), triethylamine (5 equiv), Ar, 120 or 130 °C, 24 h-3days, yield: 11-51 %.

Benzoxazole derivatives **31** and **34** were synthesized according to nucleophilic aromatic substitution (S_NAr) of commercial 2-chlorobenzoxazole with the appropriate amine in DMF (Scheme 13).⁷⁶ In comparison with the approach previously described for 2-amino benzyimidazole derivative, higher reactivity of benzoxazole allowed the application of milder conditions. Indeed, the reactions were carried out at room temperature.

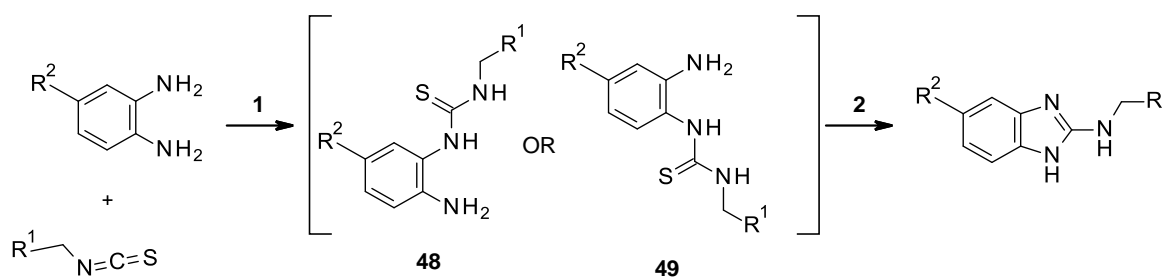


Scheme 13. Reagents and conditions: 1. $\text{NH}_2\text{CH}_2\text{R}^1$ (1 equiv.), DMF, rt, 16 h, yield: 26-38 %.

3.2.2. 2-amino benzimidazole formation approach

The cyclodesulfurization-based approach, consisting of a one-pot procedure, was adopted for compounds **37-46** synthesis (Scheme 14).⁷⁷ In this strategy, the appropriate isothiocyanate reacts with the corresponding *o*-phenylene-1,2-diamine to form the monothiourea intermediate (compounds **48** or **49**), which on phosphonium-mediated cyclization promoted by BOP and DBU, gives the desired 2-aminobenzimidazole (Scheme 14).⁷⁷ Final compounds were obtained in low to moderate yields due to both no complete formation of the monothiourea intermediate and difficult purification of the crude residues.

A presumed reaction mechanism is depicted in Figure 40. To simplify the description, only compound **48** is reported as the starting reagent, however the same mechanism can be proposed for intermediate **49**. In detail, compound **48** could follow two different pathways. In one case, compound **48** may be in equilibrium with intermediate **E**, which after activation by BOP, would lead to compound **50**. In the other case, BOP and compound **48** may react with elimination of 1 equiv. of HOBT to form intermediate **C**. This latter can undergo intramolecular cyclization with loss of 1 equiv of hexamethylthio-phosphonamide $[(\text{CH}_3)_2\text{N})_3\text{POS}]$ to afford compound **50** or it can form intermediate **D** after nucleophilic attack of HOBT. Eventually, intermediate **D** could lose 1 equiv. of HOBT leading to product **50**. Alternatively, both intermediates **C** and **D** could form intermediate **F**, whose intramolecular cyclization could afford the same product **50**.



Scheme 14. Reagents and conditions: 1. DIPEA (1 equiv.), CH_3CN , rt, 24 h-5 days. 2. BOP (1.5 equiv.), DBU (2 equiv.), rt to 80 °C, 1-27 h, yield: 8-47 %.

Table 5 Compounds obtained according to scheme 14.

Compound	R ¹	R ²	Compound	R ¹	R ²
37		H	42		CF ₃
38	CH ₂ OCH ₃	H	43		COPh
39		CH ₃	44		CN
40		Cl	45		OCH ₃
41		COOCH ₃	46		OPh

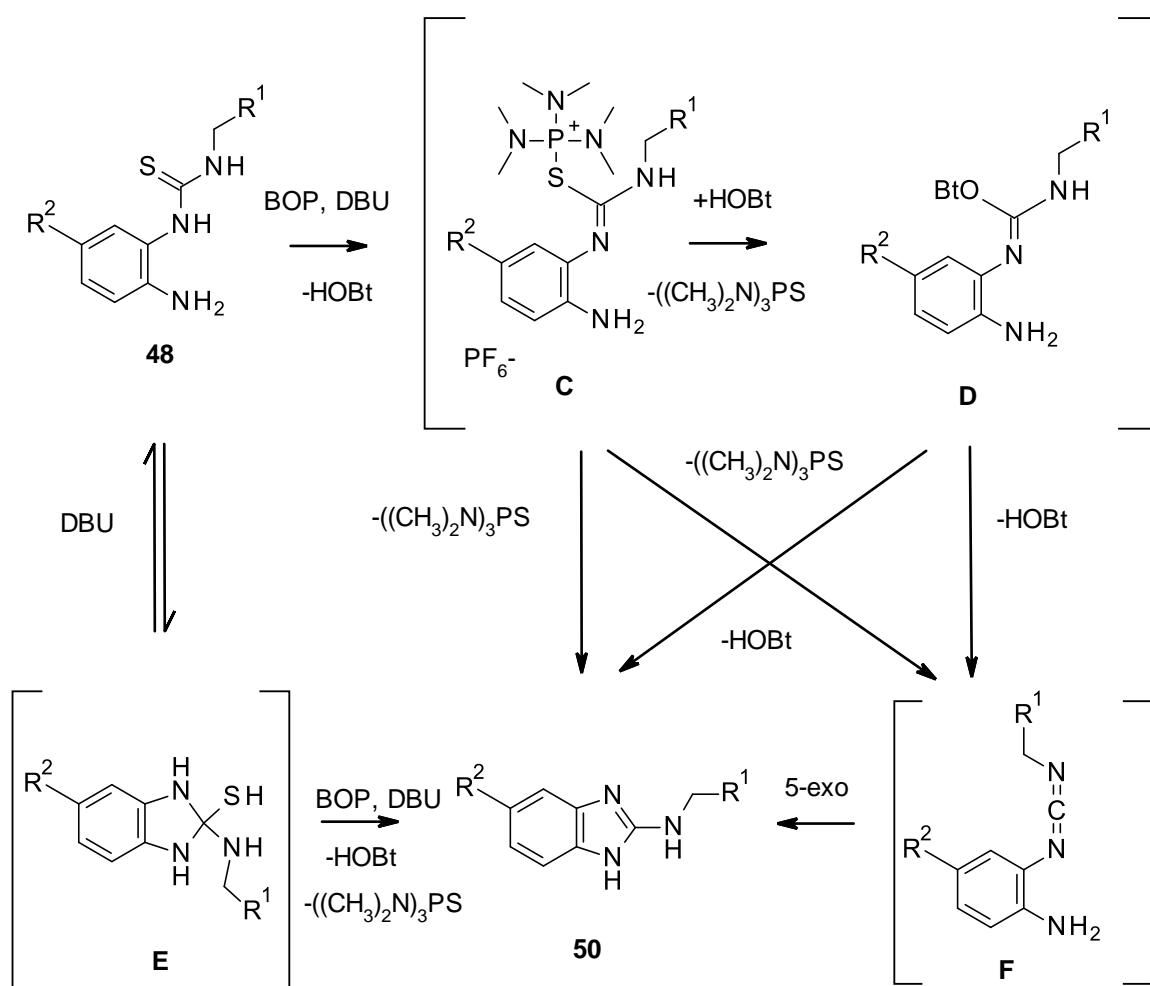


Figure 40. Proposed mechanism of cyclodesulfurization reaction.⁷⁷

The synthetic procedure was validated after the re-synthesis by cyclodesulfurization of compound **29** (Figure 36), previously obtained according to scheme 14. Indeed, ¹H-NMR

spectra of compounds afforded by both $\text{S}_{\text{N}}\text{Ar}$ or cyclodesulfurization were consistent with the same chemical structure.

2-Amino-benzimidazole nucleus formation was confirmed by COSY and ^{13}C -NMR experiments. A clear correlation between H_{a} and H_{b} peaks was observed in COSY spectrum when DMSO was used as solvent while, in ^{13}C -NMR spectra, a diagnostic C2 signal around 155 ppm was observed independently of the solvent employed (Figure 41).

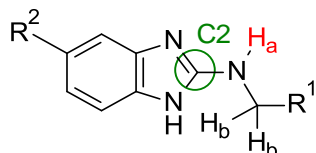


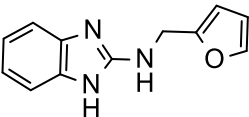
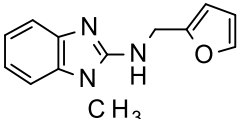
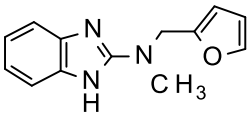
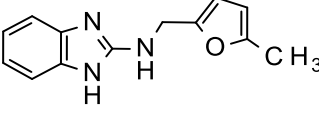
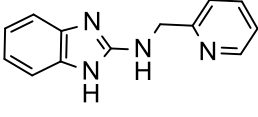
Figure 41. Product of cyclodesulfurization reaction. Diagnostic signals for structure determination are highlighted in colour.

4. Results and Discussion

4.1. Preliminary results

Compounds **29**, **30**, **32**, **35** and **36** of series 1 (Table 6) were preliminary evaluated for their ability of both tubulin binding and affecting cell viability. X-ray crystallography was used as a method to test ligand binding to tubulin, while the fluorescence-based test Resazurin reduction assay was selected for cell viability assessment on HeLa cell line (see IV. Experimental section, 2.3 Resazurin assay). Concerning the latter assay, each compound was tested in triplicate at three different concentrations (100, 10 and 1 μM), and Colchicine and DMSO were used as positive and negative control, respectively. Moreover, the fluorescence intensity of compounds without Resazurin was evaluated before the addition of the fluorogenic substrate at the same settings as used in the cell assay. It was proved that compounds alone did not emit fluorescence in that conditions and, therefore, they cannot act as potential source of false positives.

Table 6. Compounds evaluation for tubulin binding and ability to affect cell viability.

Compound	Structure	Tubulin binding	Cell viability reduction (100 μM)
29		Yes	60 %
30		No	No
32		No	No
35		Yes	60 %
36		No	No

X-ray studies revealed that only compounds **29** and **35** were able to interact with tubulin allocating at the Colchicine-site. On the contrary, compounds **30**, **32** and **36** did not show any tubulin binding properties (Table 6). Thus, re-synthesized compound **29** confirmed binding properties of the commercial counterpart. Compound **35**, with a methyl substituent in 5-position of the furan ring was able to engage the Colchicine-site, while compounds bearing

bigger heterocycles, like compound **36**, did not interact with tubulin. Interestingly, only compounds keeping the pattern of two hydrogen bond donors and one hydrogen bond acceptor, present in compound **29**, the starting point, were able to bind the Colchicine-site of tubulin.

Resazurin assay indicated that compounds **29** and **35** showed a similar effect and comparable to that of the reference compound Colchicine but only at a concentration of 100 micromolar (Figure 42). No effect was observed on cell viability for compounds **30**, **32** and **36** at all tested concentrations. Remarkably, an interesting effect on cell viability was only observed for compounds that also proved to bind to tubulin at the Colchicine-site.

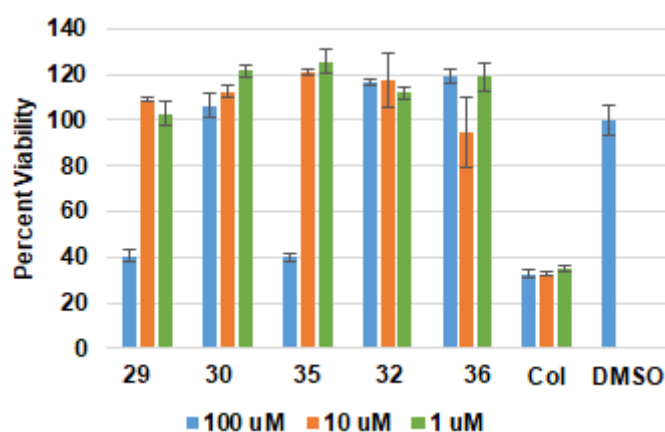


Figure 42. Effect of compounds **29**, **30**, **32**, **35** and **36** on HeLa cell viability after 72 h treatment. Each compound was tested in triplicate.

5. Conclusions

In the present part of the project, two series of analogs of compound **29**, identified in a fragment-based screening through X-ray crystallography, were designed and synthesized with the aim to define the role of the hydrogen bond network in target binding and to grow the fragment in order to add potential chemical interactions, respectively.

Preliminary assessment of compounds **29**, **30**, **32**, **35** and **36** for tubulin binding properties and ability to affect cell viability revealed interesting data for the project. Indeed, the only compounds that were able to bind tubulin at the Colchicine-site (**29** and **35**) showed also antiproliferative properties at 100 μ M on HeLa cells.

Further results from these studies are likely to offer an opportunity for identifying new Colchicine-site binders with effect on cell viability. Furthermore, our findings strongly suggest the application of this strategy for the identification and elaboration of compounds targeting other sites of tubulin for cancer therapy.

IV. Experimental section

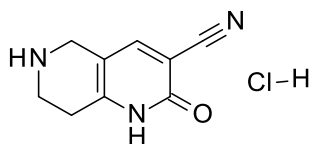
General conditions

All of the commercially available reagents and solvents were used as purchased from vendors without further purification. Automated column chromatography purifications were done using a Teledyne ISCO apparatus (*CombiFlash* Rf) with prepacked silica gel columns of different sizes and mixtures of increasing polarity of different solvents. NMR experiments were run on a Bruker Avance III 400 system, equipped with a BBI probe and Z-gradients and on a Bruker UltrashieldTM Plus FT-NMR 600 MHz Avance III, equipped with a CryoProbeTM QCI ¹H/¹⁹F/¹³C/¹⁵N and with a SampleJet autosampler and temperature control. Spectra were acquired at 300 K, using deuterated dimethyl sulfoxide (DMSO-*d*₆), deuterated chloroform (CDCl₃) or deuterated methanol (methanol-*d*₄) as solvents. For ¹H-NMR, standard abbreviations indicating spin multiplicity are given as follows: br = broad signal, s = singlet, d = doublet, dd = doublet of doublets, t = triplet, td = triplet of doublets, q = quartet, m = multiplet. The analyses by UPLC/MS were run on a Waters Acquity UPLC/MS system consisting of a SQD (single quadrupole detector) mass spectrometer equipped with an electrospray ionization interface and a photodiode array detector. The PDA range was 210-400 nm. Analyses were performed according to method 1, 2 or 3. In methods 1 and 3, a Waters Acquity UPLC BEH C₁₈ column (particle size 1.7 μm, 50 x 2.1 mm ID) with a Vanguard BEH C₁₈ pre-column (particle size 1.7 μm, 5 x 2.1 mm ID) was used. In method 2, the experiments were run on a Waters Acquity UPLC HSS T3 C₁₈ (particle size 1.8 μm, 50 x 2.1 mm ID) column with a VanGuard HSS T3 C₁₈ (particle size 1.8 μm, 5 x 2.1 mm ID) pre-column. The mobile phase was: 10 mM NH₄OAc in H₂O at pH 5 adjusted with AcOH (A) and 10 mM NH₄OAc in MeCN-H₂O (95:5) at pH 5 (B); depending on the analysis method used, different gradients were applied. In particular, in analysis method 1, the mobile-phase B proportion increased from 5 % to 95 % in 2.5 min. In analysis method 2, the mobile-phase B proportion increased from 0 % to 50 % in 2.5 min. In method 3, mobile-phase B proportion increased from 50 % to 100 % in 2.5 min. Electrospray ionization in positive and negative modes were applied. Microwave heating was performed using Explorer-48 positions instrument (CEM).

1. Section 1. Targeting Chromodomains (ChDs): a promising epigenetic approach for cancer treatment

1.1. Synthesis

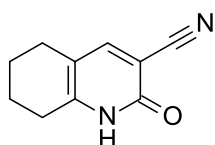
2-oxo-5,6,7,8-tetrahydro-1*H*-1,6-naphthyridine-3-carbonitrile hydrochloride (2)



2 was purchased from Enamine.

¹H-NMR (400 MHz, DMSO-*d*₆) δ 12.73 (br s, 1H, CONH), 9.69 (br s, 2H, protonated NH), 8.07 (s, 1H, CH), 3.96 (s, 2H, CH₂), 3.44-3.20 (m, 2H, CH₂), 2.89 (t, *J* = 6.0 Hz, 2H, CH₂). ¹³C-NMR (151 MHz, DMSO-*d*₆) δ 160.0 (C), 147.7 (CH), 146.7 (C), 116.1 (C), 106.5 (C), 101.4 (C), 40.9 (CH₂), 38.8 (CH₂), 23.4 (CH₂).

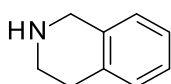
2-oxo-5,6,7,8-tetrahydro-1*H*-quinoline-3-carbonitrile (3)



3 was purchased from Enamine.

¹H-NMR (400 MHz, DMSO-*d*₆) δ 12.27 (br s, 1H, CONH), 7.88 (s, 1H, CH), 2.55 (t, *J* = 6.0 Hz, 2H, CH₂), 2.42 (t, *J* = 6.0 Hz, 2H, CH₂), 1.73-1.59 (m, 4H, 2CH₂).

1,2,3,4-tetrahydroisoquinoline (10)

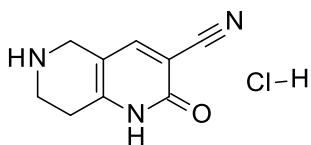


10 was purchased from Fluorochem.

¹H-NMR (400 MHz, DMSO-*d*₆) δ 7.12-7.01 (m, 3H, 3CH), 7.01-6.95 (m, 1H, CH), 3.83 (s, 2H, CH₂), 2.93 (t, *J* = 5.9 Hz, 2H, CH₂), 2.67 (t, *J* = 5.9 Hz, 2H, CH₂).

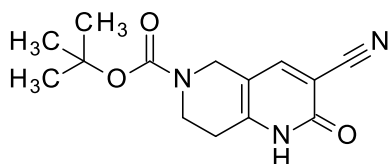
Synthesis of 2-oxo-1,5,7,8-tetrahydro-1*H*-1,6-naphthyridine-based derivatives (series 1)

Step 3. Synthesis of 2-oxo-5,6,7,8-tetrahydro-1*H*-1,6-naphthyridine-3-carbonitrile hydrochloride (2)



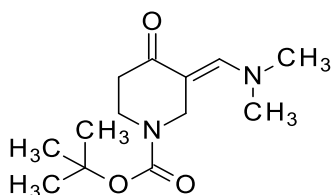
Compound **22** (0.058 g, 0.21 mmol) was treated with HCl (4 M) in 1,4-dioxane (1.58 ml, 6.32 mmol) in dry methanol (0.38 ml) at rt for 5 h. Then, the mixture was concentrated to dryness and sequentially triturated in diethyl ether (1 ml) and in methanol (1 ml) to afford **2** as a beige solid (18 mg, 40 % yield). Rt = 0.58 min (analysis method 2). MS (ESI) m/z: 176.3 [M-H]⁺, calculated: 176.08 [C₉H₁₀N₃O]⁺. ¹H-NMR (400 MHz, DMSO-*d*₆) δ 12.71 (br s, 1H, CONH), 9.65 (br s, 2H, protonated NH₂), 8.06 (s, 1H, CH), 3.97 (s, 2H, CH₂), 3.32 (signal overlapped with H₂O signal, 2H, CH₂), 2.89 (t, *J* = 6.2 Hz, 2H, CH₂). ¹³C-NMR (101 MHz, DMSO-*d*₆) δ 159.57 (C), 147.67 (CH), 146.86 (C), 116.16 (C), 106.66 (C), 101.33 (C), 40.92 (CH₂), 38.7 (CH₂), 23.47 (CH₂). ¹H-NMR and ¹³C-NMR were in agreement with commercial compound **2**.

Step 2. Synthesis of tert-butyl 3-cyano-2-oxo-1,5,7,8-tetrahydro-1,6-naphthyridine-6-carboxylate (22)



Sodium hydride 60 % dispersion in mineral oil (0.17 g, 4.28 mmol) was added to a stirred solution of 2-cyanoacetamide (0.19 g, 2.25 mmol) in dry DMF (7 ml) at 0 °C and under nitrogen atmosphere. The mixture was stirred at rt for 1 h followed by dropwise addition of a solution of compound **21** (0.545 g, 2.14 mmol) in dry DMF (8 ml) at 0 °C. Then, the reaction crude was stirred at rt for 3 h and at 80 °C for 12 h, cooled to rt and concentrated under reduced pressure. The obtained residue was diluted with water (100 ml) and extracted with ethyl acetate (3 x 100 ml). The organic layer was washed with water (100 ml), dried over Na₂SO₄ and concentrated to dryness at low pressure. Two sequential purifications by silica gel flash chromatography (DCM/DCM:MeOH (8:2) from 100/0 to 70/30 and then ethyl acetate 100 %, followed by trituration in water afforded **22** (58 mg, 10 % yield) as a pale yellow solid. Rt = 1.64 min (analysis method 1). MS (ESI) m/z: 276.5 [M-H]⁺, calculated: 276.13 [C₁₄H₁₈N₃O₃]⁺. ¹H-NMR (400 MHz, DMSO-*d*₆) δ 12.49 (br s, 1H, CONH), 8.00 (s, 1H, CH), 4.23 (s, 2H, CH₂), 3.54 (t, *J* = 5.8 Hz, 2H, CH₂), 2.63 (t, *J* = 5.8 Hz, 2H, CH₂), 1.41 (s, 9H, 3CH₃). ¹H-NMR was in agreement with data reported in the literature.⁴⁷

Step 1. Synthesis of (*E*)-tert-butyl-3-(dimethylaminomethylene)-4-oxo-piperidine-1-carboxylate (**21**)

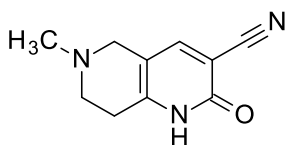


A mixture of 1-tert-butoxycarbonylpiperidin-4-one (1.0 g, 5.02 mmol) in DMF-DMA (7.4 ml, 54.2 mmol) was heated to 105 °C under nitrogen atmosphere for 21 h. The crude residue was cooled to rt and concentrated under reduced pressure. Purification by silica gel flash chromatography (ethyl acetate/ethyl acetate:ethanol (8:2) from 98/2 to 85/15) afforded **21** (849 mg, 66 % yield) as a yellow solid. Rt = 1.62 min (analysis method 1). MS (ESI) m/z: 255.5 [M-H]⁺, calculated: 255.17 [C₁₃H₂₃N₂O₃]⁺. ¹H-NMR (400 MHz, DMSO-*d*₆) δ 7.30 (s, 1H, CH), 4.47 (s, 2H, CH₂), 3.47 (t, *J* = 6.5 Hz, 2H, CH₂), 3.06 (s, 6H, N(CH₃)₂), 2.26 (t, *J* = 6.5 Hz, 2H, CH₂), 1.41 (s, 9H, 3CH₃).

Reductive amination: general procedure for the synthesis of compounds of series **1** (**4-7** and **9**)

Under nitrogen atmosphere, a mixture of corresponding aldehyde (from 5.0 to 33.5 molar equiv., according to the specific compound), commercial compound **2** (1.0 molar equiv.) and dry MeOH (amount specified for each compound) was then stirred at rt for 40 min. Then, STAB (from 2.4 to 4.88 molar equiv., according to the specific case) was added portionwise and the reaction mixture stirred at rt until total starting material conversion was observed. Afterwards, the mixture was concentrated to dryness at low pressure, the resulting crude purified by silica gel flash chromatography using mixtures of increasing polarity of DCM and DCM:MeOH (8:2) or chloroform and chloroform:ethanol (8:2), followed by trituration in diethyl ether only for some compounds.

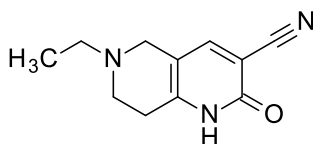
Synthesis of 6-methyl-2-oxo-1,5,7,8-tetrahydro-1,6-naphthyridine-3-carbonitrile (**4**)



Aqueous formaldehyde 36.5-38.0 % (5.2 ml, 63.24 mmol), **2** (0.42 g, 1.89 mmol) and STAB (1.42 g, 6.5 mmol) in dry MeOH (158 ml) were reacted following the general procedure previously described. After stirring for 18 h, addition of STAB (0.20 g, 0.94 mmol) was

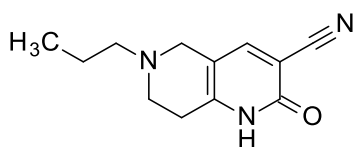
required to get total starting material conversion. Then, the mixture was stirred for further 2 h. Upon completion of the reaction, reaction mixture was concentrated to dryness and the crude residue was purified by silica gel flash chromatography (chloroform/chloroform:ethanol (8:2) from 70/30 to 0/100) to afford title compound (312 mg) as a solid. A batch of 200 mg was used in a next synthetic step without further purification to prepare compound **11**. The remaining 112 mg were triturated with diethyl ether (2 x 1 ml) to afford the pure compound **4** as a pink salmon solid (63 mg, 56 % yield after trituration). $R_t = 1.17$ min (analysis method 2). MS (ESI) m/z : 190.4 $[M-H]^+$, calculated: 190.10 $[C_{10}H_{12}N_3O]^+$. 1H -NMR (400 MHz, DMSO- d_6) δ 12.38 (br s, 1H, CONH), 7.90 (s, 1H, CH), 3.20 (s, 2H, CH₂), 2.69-2.61 (m, 2H, CH₂), 2.59-2.53 (m, 2H, CH₂), 2.30 (s, 3H, NCH₃). ^{13}C -NMR (101 MHz, DMSO- d_6) δ 159.96 (C), 148.76 (C), 147.52 (CH), 116.75 (C), 111.88 (C), 99.92 (C), 53.55 (CH₂), 49.95 (CH₂), 45.02 (CH₃), 27.11 (CH₂).

Synthesis of 6-ethyl-2-oxo-1,5,7,8-tetrahydro-1,6-naphthyridine-3-carbonitrile (**5**)



Compound **5** was obtained by reaction of acetaldehyde (0.07 ml, 1.2 mmol), **2** (0.05 g, 0.24 mmol) and STAB (0.13 g, 0.58 mmol) in dry MeOH (2.1 ml) following the general procedure previously described (15 h of reaction). Purification by silica gel flash chromatography (DCM/DCM:MeOH (8:2) from 95/5 to 40/60) afforded **5** as a light salmon solid (40 mg, 82 % yield). $R_t = 0.60$ min (analysis method 1). MS (ESI) m/z : 204.4 $[M-H]^+$, calculated: 204.11 $[C_{11}H_{14}N_3O]^+$. 1H -NMR (400 MHz, methanol- d_4) δ 7.87 (s, 1H, CH), 3.45 (s, 2H, CH₂), 2.80 (m, 4H, 2CH₂), 2.64 (q, $J = 7.2$ Hz, 2H, NCH₂), 1.18 (t, $J = 7.2$ Hz, 3H, CH₃). ^{13}C -NMR (101 MHz, DMSO- d_6) δ 159.86 (C), 148.96 (C), 147.65 (CH), 116.71 (C), 111.83 (C), 99.93 (C), 51.08 (CH₂), 50.80 (CH₂), 47.75 (CH₂), 27.07 (CH₂), 12.07 (CH₃).

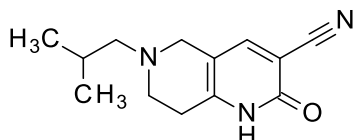
Synthesis of 2-oxo-6-propyl-1,5,7,8-tetrahydro-1,6-naphthyridine-3-carbonitrile (**6**)



2 (0.05 g, 0.24 mmol) in dry MeOH (3.2 ml) was treated with propionaldehyde (0.09 ml, 1.2 mmol) and STAB (0.13 g, 0.58 mmol) following the general procedure previously described (24 h of reaction). Purification by silica gel flash chromatography (DCM/DCM:MeOH (8:2) from 100/0 to 45/55) yielded **6** as an orange solid (30 mg, 58 %

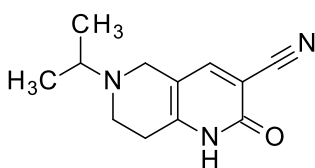
yield). $R_t = 0.95$ min (analysis method 1). MS (ESI) m/z : 218.4 $[M-H]^+$, calculated: 218.13 $[C_{12}H_{16}N_3O]^+$. 1H -NMR (400 MHz, DMSO- d_6) δ 12.41 (br s, 1H, CONH), 7.89 (s, 1H, CH), 3.26 (s, 2H, CH₂), 2.68-2.56 (m, 4H, 2CH₂), 2.38 (t, $J = 7.4$ Hz, 2H, NCH₂), 1.48 (m, 2H, CH₂), 0.86 (t, $J = 7.4$ Hz, 3H, CH₃). ^{13}C -NMR (101 MHz, DMSO- d_6) δ 159.97 (C), 149.07 (C), 147.74 (CH), 116.80 (C), 112.04 (C), 99.97 (C), 58.89 (CH₂), 51.62 (CH₂), 48.15 (CH₂), 27.13 (CH₂), 19.72 (CH₂), 11.79 (CH₃).

Synthesis of 6-isobutyl-2-oxo-1,5,7,8-tetrahydro-1,6-naphthyridine-3-carbonitrile (7)



7 was obtained following the general procedure previously described reacting isobutyraldehyde (0.22 ml, 2.4 mmol), **2** (0.11 g, 0.48 mmol) and STAB (0.26 g, 1.17 mmol) in dry MeOH (4.2 ml) (5 h of reaction). Purification by silica gel flash chromatography (DCM/DCM:MeOH (8:2) from 98/2 to 70/30) afforded **7** as a light yellow solid (44 mg, 40 % yield). $R_t = 1.25$ min (analysis method 1). MS (ESI) m/z : 232.4 $[M-H]^+$, calculated: 232.14 $[C_{13}H_{18}N_3]^+$. 1H -NMR (400 MHz, DMSO- d_6) δ 12.41 (s, 1H, CONH), 7.89 (s, 1H, CH), 3.25 (s, 2H, CH₂), 2.69-2.55 (m, 4H, 2CH₂), 2.18 (d, $J = 7.3$ Hz, 2H, NCH₂), 1.80 (m, 1H, CH), 0.86 (d, $J = 6.6$ Hz, 6H, 2CH₃). ^{13}C -NMR (101 MHz, DMSO- d_6) δ 159.89 (C), 149.01 (C), 147.67 (CH), 116.74 (C), 112.00 (C), 99.95 (C), 65.24 (CH₂), 52.08 (CH₂), 48.39 (CH₂), 27.09 (CH₂), 25.18 (CH), 20.69 (CH₃).

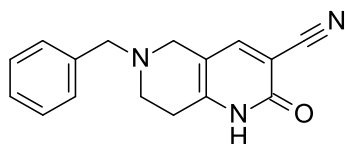
Synthesis of 6-isopropyl-2-oxo-1,5,7,8-tetrahydro-1,6-naphthyridine-3-carbonitrile (8)



Under nitrogen atmosphere, a mixture of **2** (0.11 g, 0.48 mmol) and acetone (0.53 ml, 7.2 mmol) in dry MeOH (4.2 ml) was stirred at 55 °C for 1 h. Then, was cooled to rt and STAB (4.88 molar equiv.) was added portionwise. The reaction mixture was heated to 55 °C and was allowed to stir at the same temperature for 1 h. Subsequent addition of acetone (15 molar equiv.) and STAB (4.88 molar equiv.) at rt, followed by stirring at 55 °C, was carried out 4 times every 1 h. Then the mixture was evaporated to dryness. Purification by silica gel flash chromatography (DCM/DCM:MeOH (8:2) from 100/0 to 60/40) yielded **8** as a pale yellow solid (42 mg, 40 % yield). $R_t = 0.77$ min (analysis method 1). MS (ESI) m/z : 218.4 $[M-H]^+$,

calculated: 218.13 [C₁₂H₁₆N₃O]⁺. ¹H-NMR (400 MHz, DMSO-*d*₆) δ 12.33 (br s, 1H, CONH), 7.89 (s, 1H, CH), 3.35 (signal overlapped with H₂O signal, 2H, CH₂), 2.83 (m, 1H, CH), 2.68-2.58 (m, 4H, 2CH₂), 1.01 (d, *J* = 6.6 Hz, 6H, 2CH₃). ¹³C-NMR (101 MHz, DMSO-*d*₆) δ 159.92 (C), 149.23 (C), 147.70 (CH), 116.80 (C), 112.52 (C), 99.76 (C), 53.21 (CH), 46.92 (CH₂), 43.69 (CH₂), 27.82 (CH₂), 18.05 (CH₃).

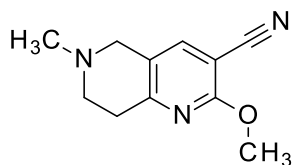
Synthesis of 6-benzyl-2-oxo-1,5,7,8-tetrahydro-1,6-naphthyridine-3-carbonitrile (**9**)



9 was synthesized following the general procedure previously described reacting **2** (0.05 g, 0.24 mmol) with benzaldehyde (0.24 ml, 2.4 mmol) and STAB (0.26 g, 1.17 mmol) in dry MeOH (2.1 ml) (17 h of reaction). Purification by silica gel flash chromatography (chloroform/chloroform:ethanol (8:2) from 100/0 to 70/30) afforded **9** as a yellow solid (19 mg, 30 % yield). Rt = 1.59 min (analysis method 1). MS (ESI) *m/z*: 266.4 [M-H]⁺, calculated: 266.32 [C₁₆H₁₆N₃O]⁺. ¹H-NMR (400 MHz, DMSO-*d*₆) δ 12.40 (br s, 1H, CONH), 7.84 (s, 1H, CH), 7.38-7.23 (m, 5H, 5CH), 3.63 (s, 2H, NCH₂), 3.26 (s, 2H, CH₂), 2.66 (br s, 4H, 2CH₂). ¹³C-NMR (101 MHz, DMSO-*d*₆) δ 160.42 (C), 149.43 (C), 147.26 (CH), 137.95 (C), 128.69 (CH), 128.28 (CH), 127.09 (CH), 116.97 (C), 111.70 (C), 99.55 (C), 61.05 (CH₂), 51.61 (CH₂), 47.99 (CH₂), 27.35 (CH₂).

Synthesis of compound **11** (series 2)

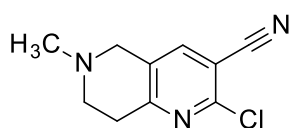
Step 2. Synthesis of 2-methoxy-6-methyl-7,8-dihydro-5H-1,6-naphthyridine-3-carbonitrile (**11**)



A mixture of palladium(II) acetate (10.8 mg, 0.048 mmol) and 2-di-*tert*-butylphosphino-2',4',6'-triisopropylbiphenyl (41.7 mg, 0.095 mmol) in dry toluene (8 ml) was stirred for 5 min under argon atmosphere at 80 °C. After cooling to rt, the previous mixture was added to a stirred solution of compound **23** (0.51 g, 1.59 mmol) and sodium methoxide (0.44 g, 7.95 mmol) in dry MeOH (8 ml) under argon atmosphere. Then, the reaction mixture was stirred for 15 h at 80 °C under argon atmosphere, cooled down to rt and evaporated to dryness at low pressure. Purification by silica gel flash chromatography (DCM/DCM:MeOH

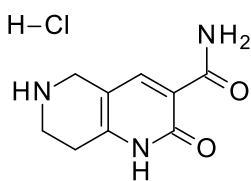
(8:2) from 98/2 to 75/25) afforded **11** as a beige solid (68 mg, 21 % yield). $R_t = 1.12$ min (analysis method 1). MS (ESI) m/z : 204.4 $[M-H]^+$, calculated: 204.11 $[C_{11}H_{14}N_3O]^+$. 1H -NMR (400 MHz, DMSO- d_6) δ 7.96 (s, 1H, CH), 3.93 (s, 3H, OCH₃), 3.42 (s, 2H, CH₂), 2.87 (t, $J = 5.9$ Hz, 2H, CH₂), 2.66 (t, $J = 5.9$ Hz, 2H, CH₂), 2.35 (s, 3H, NCH₃). ^{13}C -NMR (101 MHz, DMSO- d_6) δ 161.49 (C), 157.81 (C), 141.78 (CH), 123.60 (C), 115.58 (C), 92.46 (C), 55.01 (CH₂), 54.17 (OCH₃), 51.48 (CH₂), 45.26 (NCH₃), 32.30 (CH₂).

Step 1. Synthesis of 2-chloro-6-methyl-7,8-dihydro-5H-1,6-naphthyridine-3-carbonitrile (23)



A mixture of POCl₃ (2 ml, 21.14 mmol) and compound **4** (0.200 g, 1.06 mmol) under argon atmosphere was stirred at 0 °C for 5 min, at rt for 1 h and it was heated to 105 °C for 23 h. After cooling down to rt, the mixture was diluted with DCM (30 ml) and poured into a saturated solution of NaHCO₃ (120 ml) at 0 °C. The phases were separated and the aqueous phase was extracted with DCM (2 x 150 ml). The combined organic phases were dried over Na₂SO₄, filtered and concentrated under reduced pressure to give title compound **23** as a solid (336 mg) pure enough to be employed in the next synthetic step without further purification. $R_t = 1.94$ min (analysis method 2). MS (ESI) m/z : 208.4/210.4 $[M-H]^+$ (3/1), calculated: 208.06/210.06 $[C_{10}H_{11}ClN_3]^+$. 1H -NMR (600 MHz, DMSO- d_6) δ 8.42 (s, 1H, CH), 4.70-4.22 (m, 2H, CH₂), 3.83-3.05 (m, 4H, 2CH₂), 2.93 (s, 3H, NCH₃).

Synthesis of 2-oxo-5,6,7,8-tetrahydro-1H-1,6-naphthyridine-3-carboxamide hydrochloride (12, series 3)

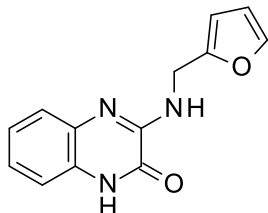


HCl solution (1.25 M) in MeOH (0.8 ml, 1.0 mmol) was added to commercial 2-oxo-5,6,7,8-tetrahydro-1H-1,6-naphthyridine-3-carboxamide (0.021 g, 0.10 mmol). The obtained mixture was stirred at rt for 3 h. Evaporation of the residual solvent yielded **12** as a white solid (22 mg, 93% yield). 1H -NMR (400 MHz, DMSO- d_6) δ 12.52 (br s, 1H, CONH), 9.25 (br s, 2H, protonated NH₂), 9.06-8.91 (m, 1H, CONH), 8.21 (s, 1H, CH), 7.62-7.51 (m, 1H, CONH), 4.11-4.05 (m, 2H, CH₂), 3.40-3.32 (m, 2H, CH₂), 2.87 (t, $J = 6.3$ Hz, 2H, CH₂). ^{13}C -NMR (101

MHz, DMSO-*d*₆) δ 164.32 (C), 161.85 (C), 144.02 (C), 143.00 (CH), 119.13(C), 107.03 (C), 41.29 (CH₂), 38.93 (CH₂), 23.00 (CH₂).

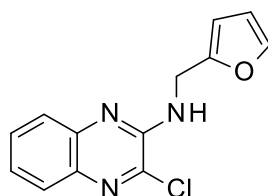
Synthesis of 2-hydroxyquinoxaline derivatives (series 4)

Step 3. Synthesis of 3-(2-furylmethylamino)-1*H*-quinoxalin-2-one (13)



A mixture of compound **25** (0.147 g, 0.56 mmol) and LiOH (0.068 g, 2.8 mmol) was stirred in a mixture of H₂O/1,4-dioxane (1/1, 3.9 ml) at 60 °C for 48 h. Then, the reaction mixture was cooled to rt, concentrated under reduced pressure, diluted with brine (120 ml) and extracted with ethyl acetate (3 x 120 ml). The combined organic phases were dried over Na₂SO₄ and evaporated to dryness. Purification of the crude product by silica gel flash chromatography (cyclohexane/ethyl acetate from 95/5 to 60/40) afforded **13** (94 mg, 70 % yield) as beige solid. Rt = 1.77 min (analysis method 1). MS (ESI) *m/z*: 242.4 [M-H]⁺, calculated: 242.09 [C₁₃H₁₂N₃O₂]⁺. ¹H-NMR (400 MHz, DMSO-*d*₆) δ 12.36 (s, 1H, CONH), 7.81 (t, *J* = 6.1 Hz, 1H, NH), 7.55 (s, 1H, CH), 7.40-7.33 (m, 1H, CH), 7.19-7.07 (m, 3H, 3CH), 6.40-6.35 (m, 1H, CH), 6.31-6.26 (m, 1H, CH), 4.59 (d, *J* = 6.1 Hz, 2H, CH₂). ¹³C-NMR (101 MHz, DMSO-*d*₆) δ 152.32 (C), 151.32 (C), 149.59 (C), 141.81 (CH), 133.06 (C), 128.06 (C), 124.67 (CH), 123.52 (CH), 123.25 (CH), 114.94 (CH), 110.47 (CH), 106.96 (CH), 36.90 (CH₂).

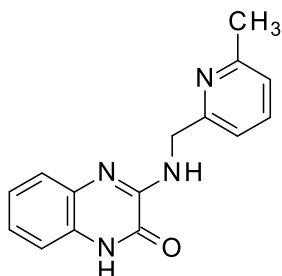
Step 2. Synthesis of 3-chloro-*N*-(2-furylmethyl)quinoxalin-2-amine (25)



Triethylamine (0.79 ml, 5.7 mmol), furfurylamine (0.17 ml, 1.9 mmol) and compound **24** (0.189 g, 0.95 mmol) were reacted under argon atmosphere in dry 1,4-dioxane (9.5 ml) at 100 °C for 24 h. Then, the mixture was cooled to rt and the volatiles were removed under reduced pressure. The obtained residue was partitioned between water (120 ml) and ethyl acetate (120 ml), and the combined organic phases were washed with brine (120 ml), dried over Na₂SO₄ and concentrated to dryness. Purification by silica gel chromatography (cyclohexane/ethyl acetate from 99.5/0.5 to 90/10) afforded compound **25** as a yellow oil (147

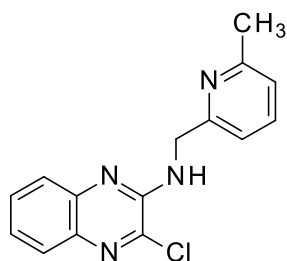
mg, 60 % yield). Rt = 2.35 min (analysis method 1). MS (ESI) m/z: 260.4/262.4 (3/1) [M-H]⁺, calculated: 260.06/262.06 [C₁₃H₁₁ClN₃O]⁺. ¹H-NMR (400 MHz, DMSO-*d*₆) δ 7.97 (t, *J* = 5.8 Hz, 1H, NH), 7.78-7.72 (m, 1H, CH), 7.69 -7.58 (m, 2H, 2CH), 7.57-7.53 (m, 1H, CH), 7.45-7.38 (m, 1H, CH), 6.39-6.31 (m, 2H, 2CH), 4.67 (d, *J* = 5.8 Hz, 2H, CH₂).

Step 3. Synthesis of 3-[(6-methyl-2-pyridyl)methylamino]-1*H*-quinoxalin-2-one (14)



Compound **26** (0.156 g, 0.55 mmol) was treated with LiOH (0.053 g, 2.2 mmol) in a mixture of H₂O/1,4-dioxane (1/1, 3.8 ml) at 70 °C for 48 h. The addition of DMA (1.25 ml) and 1,4-dioxane (1 ml) was required to promote the solubilization. The reaction mixture was cooled to rt, concentrated under reduced pressure, diluted with brine (120 ml) and extracted with ethyl acetate (3 x 120 ml). The combined organic phases were dried over Na₂SO₄ and evaporated to dryness. Purification of the crude product by silica gel flash chromatography (cyclohexane/ethyl acetate from 99/1 to 40/60) yielded **14** (23 mg, 16 % yield) as a white solid. Rt = 1.62 min (analysis method 1). MS (ESI) m/z: 267.5 [M-H]⁺, calculated: 267.12 [C₁₅H₁₅N₄O]⁺. ¹H-NMR (400 MHz, DMSO-*d*₆) δ 7.99 (t, *J* = 6.0 Hz, 1H, NH), 7.61 (t, *J* = 7.7 Hz, 1H, CH), 7.34-7.26 (m, 1H, CH), 7.20-7.05 (m, 5H, 5CH), 4.66 (d, *J* = 6.0 Hz, 2H, CH₂), 2.47 (s, 3H, CH₃). ¹³C-NMR (101 MHz, DMSO-*d*₆) δ 157.14 (C), 151.47 (C), 149.84 (C), 137.01 (CH), 133.25 (C), 128.14 (C), 124.64 (CH), 123.52 (CH), 123.30 (CH), 121.39 (CH), 118.04 (CH), 115.03 (CH), 45.18 (CH₂), 24.03 (CH₃).

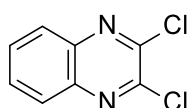
Step 2. Synthesis of 3-chloro-*N*-[(6-methyl-2-pyridyl)methyl]quinoxalin-2-amine (26)



Compound **26** was synthesized by treating triethylamine (0.6 ml, 4.28 mmol), 2-aminomethyl-6-methyl-pyridine (0.21 g, 1.62 mmol) and compound **24** (0.190 g, 0.95 mmol) in dry 1,4-dioxane (9.5 ml) at 100 °C for 24 h under argon atmosphere. The reaction mixture

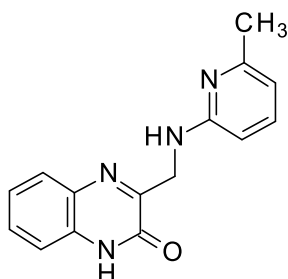
was then cooled to rt and the volatiles were removed under reduced pressure. The obtained residue was diluted with water (120 ml) and extracted with ethyl acetate (120 ml). The combined organic phases were washed with brine (120 ml), dried over Na₂SO₄ and concentrated under reduced pressure. Purification by silica gel chromatography (cyclohexane/ethyl acetate from 99.8/0.2 to 80/20) followed by trituration with diethyl ether (2 ml) afforded compound **26** as a white solid (156 mg, 58 % yield). Rt = 2.25 min (analysis method 1). MS (ESI) m/z: 285.4/287.4 (3/1) [M-H]⁺, calculated: 285.09/287.09 [C₁₅H₁₄ClN₄]⁺. ¹H-NMR (400 MHz, DMSO-*d*₆) δ 8.07 (t, *J* = 5.6 Hz, 1H, NH), 7.82-7.73 (m, 1H, CH), 7.66-7.54 (m, 3H, 3CH), 7.46-7.39 (m, 1H, CH), 7.21-7.08 (m, 2H, 2CH), 4.74 (d, *J* = 5.6 Hz, 2H, CH₂), 2.48 (s, 3H, CH₃).

Step 1. Synthesis of 2,3-dichloroquinoxaline (24)



A mixture of 1,4-dihydroquinoxaline-2,3-dione (0.316 g, 1.86 mmol) and phosphorous oxychloride (POCl₃) (1.74 ml, 18.6 mmol) was heated at 100 °C for 4 h, cooled down to rt and evaporated under *vacuum* to remove the excess of POCl₃. The resulting residue was dissolved in ethyl acetate (150 ml) and poured into a saturated solution of NaHCO₃ (120 ml) at 0 °C. After separation of the phases, the aqueous layer was extracted with ethyl acetate (3 x 120 ml), the combined organic layers were dried over Na₂SO₄ and concentrated to dryness at low pressure to afford title compound **24** (379 mg) that was pure enough to be used in the next synthetic step without further purification. Rt = 2.25 min (analysis method 1). No mass trace was observed. ¹H-NMR (400 MHz, DMSO-*d*₆) δ 8.14-8.05 (m, 2H, 2CH), 7.99-7.91 (m, 2H, 2CH).

Synthesis of 3-[[6-methyl-2-pyridyl] amino] methyl]-1H-quinoxalin-2-one (15)

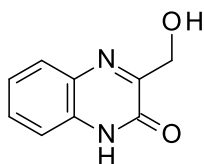


3-(bromomethyl) quinoxaline-2(1H)-one (0.34 g, 1.26 mmol) and 2-amino-6-methylpyridine (0.278 g, 2.52 mmol) were reacted in dry DMSO (15.75 ml) at rt for 14 h. Then, the solvent was partially evaporated under *vacuum*. The obtained concentrated solution was

diluted with water (150 ml) and extracted with ethyl acetate (3 x 150 ml). The combined organic phases were dried over Na₂SO₄ and concentrated to dryness. The crude product was purified twice by silica gel flash chromatography (DCM/DCM:MeOH (8:2) from 99/1 to 80/20) followed by semi-preparative HPLC-MS (Rt = 3.93 min). Semi-preparative HPLC-MS purification was run on a Waters Autopurification system consisting of a 3100 single quadrupole mass spectrometer equipped with an electrospray ionization interface and a 2998 photodiode array detector. The HPLC system included a 2747 Sample Manager, 2545 Binary Gradient Module, System Fluidic Organizer and 515 HPLC Pump. The PDA range was 210-400 nm. Electrospray ionization in positive and negative mode was used in the mass scan range 100-500 Da. The purification was performed on a XBridgeTM Prep C₁₈ OBD column (100 x 19 mm ID, particle size 5 μm) with a XBridgeTM Prep C₁₈ (10 x 19 mm ID, particle size 5 μm) Guard Cartridge. The mobile phase was 10 mM NH₄OAc in H₂O at pH 5 adjusted with AcOH (A) and 10 mM NH₄OAc in MeCN-H₂O (95:5) at pH 5 (B). A linear gradient was applied starting at 20 % B (initial hold for 0.5 min) to 50 % B in 7 min; 50-100 % B in 0.1 min; hold at 100 % B for 0.4 min; 100-20 % B in 0.1 min; hold at 20 % for 1.9 min. Flow rate was 20 ml/min.

The collected fractions were concentrated and basified with NaOH (2 N) to pH 10. Then, the aqueous phase was extracted with ethyl acetate (3 x 100 ml), the organic layer was dried over Na₂SO₄ and evaporated to dryness to afford **15** (26 mg, 8 % yield) as a white solid. Rt = 1.41 min (analysis method 1). MS (ESI) m/z: 267.4 [M-H]⁺, calculated: 267.12 [C₁₅H₁₅N₄O]⁺. ¹H-NMR (400 MHz, DMSO-*d*₆) δ 7.80-7.73 (m, 1H, CH), 7.50 (t, *J* = 7.7 Hz, 1H, CH), 7.36-7.25 (m, 3H, 3CH), 6.50-6.45 (m, 1H, NH), 6.42-6.35 (m, 1H, CH), 6.38 (d, *J* = 7.1 Hz, 1H, CH), 4.60 (d, *J* = 5.2 Hz, 2H, CH₂), 2.25 (s, 3H, CH₃). ¹³C-NMR (151 MHz, DMSO-*d*₆) δ 158.13 (C), 157.87 (C), 155.67 (C), 154.35 (C), 137.18 (CH), 131.92 (C), 131.33 (C), 129.73 (CH), 128.19 (CH), 123.24 (CH), 115.50 (CH), 111.07 (CH), 105.23 (CH), 42.62 (CH₂), 24.24 (CH₃).

Synthesis of 3-(hydroxymethyl)-1*H*-quinoxalin-2-one (16)

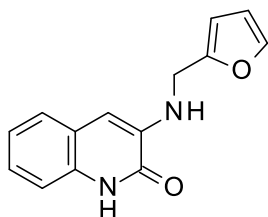


Under argon atmosphere, to a solution of ethyl 3-oxo-3,4-dihydro-2-quinoxalinecarboxylate (0.156 g, 0.69 mmol) in dry diethyl ether (5.1 ml) DIBAL-H solution

(1.0 M) in hexane (1.38 ml, 1.38 mmol) was added at 0 °C over a period of 2 h and 30 min. The resulting mixture was stirred at rt for additional 30 min. The mixture was cooled to 0 °C, and HCl (2 N, 3 ml) was dropwise added under magnetic stirring. Then, the pH was increased to 5 with NaOH (2 N), and the resulting mixture was extracted with ethyl acetate (3 x 20 ml). The combined organic phases were dried over Na₂SO₄ and concentrated to dryness. The crude product was purified by silica gel flash chromatography (chloroform/chloroform:ethanol (8:2) from 99.8/0.2 to 90/10), and triturated with diethyl ether (2 x 1 ml) to afford **16** (25 mg, 20 % yield) as white solid. Rt = 0.95 min (analysis method 1). MS (ESI) m/z: 177.3 [M-H]⁺, calculated: 177.07 [C₉H₉N₂O₂]⁺. ¹H-NMR (400 MHz, DMSO-*d*₆) δ 12.33 (br s, 1H, CONH), 7.78 (d, *J* = 8.4 Hz, 1H, CH), 7.50 (t, *J* = 7.8 Hz, 1H, CH), 7.35-7.26 (m, 2H, 2CH), 5.04 (br s, 1H, OH), 4.61 (s, 2H, CH₂). ¹³C-NMR (101 MHz, DMSO-*d*₆) 159.97 (C), 154.13 (C), 131.96 (C), 131.41 (C), 129.74 (CH), 128.20 (CH), 123.19 (CH), 115.47 (CH), 60.80 (CH₂).

Synthesis of a 2-quinolone derivative (series 5)

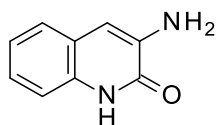
Step 2. Synthesis of 3-(2-furylmethylamino)-1*H*-quinolin-2-one (**17**)



Under argon atmosphere, a mixture of compound **27** (0.132 g, 0.82 mmol) and furaldehyde (0.14 ml, 1.64 mmol) in dry MeOH (8 ml) was stirred at 60 °C for 8 h. Then, the reaction mixture was cooled to rt, STAB was added (0.44 g, 2.00 mmol) and the mixture was stirred for 16 h at rt. Afterwards, the mixture was heated at 60 °C for 3 h, cooled down to rt, STAB (0.44 g, 2.00 mmol) was added and the reaction mixture stirred at rt for 20 h every day for a total of 4 days. Finally, the mixture was evaporated to dryness, purified by silica gel flash chromatography (cyclohexane/ethyl acetate from 95/5 to 70/30), and trituration with diethyl ether (2 ml) afforded compound **17** (25 mg, 13% yield) as a pink solid. Rt = 1.88 min (analysis method 1). MS (ESI) m/z: 241.4 [M-H]⁺, calculated: 241.10 [C₁₄H₁₃N₂O₂]⁺. ¹H-NMR (400 MHz, DMSO-*d*₆) δ 11.85 (s, 1H, CONH), 7.60-7.54 (m, 1H, CH), 7.39 (d, *J* = 7.8 Hz, 1H, CH), 7.23-7.18 (m, 1H, CH), 7.17-7.10 (m, 1H, CH), 7.09-7.02 (m, 1H, CH), 6.64 (s, 1H, CH), 6.41-6.31 (m, 2H, 2CH), 6.07 (t, *J* = 6.2 Hz, 1H, NH), 4.38 (d, *J* = 6.2 Hz, 2H, CH₂). ¹³C-NMR (101 MHz, DMSO-*d*₆) δ 157.88 (C), 152.15 (C), 142.15 (CH), 136.97 (C), 131.59 (C), 124.64

(CH), 124.25 (CH), 122.03 (CH), 121.66 (C), 114.61 (CH), 110.41 (CH), 107.21 (CH), 103.76 (CH), 39.13 (CH₂).

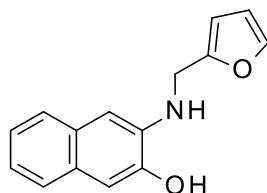
Step 1. Synthesis of 3-amino-1*H*-quinolin-2-one (27)



A reaction tube was charged with ethanol (12.2 ml), that was previously deoxygenated with a stream of argon, copper powder (0.014 g, 0.22 mmol), L-ascorbic acid (0.078 g, 0.44 mmol), pipercolinic acid (0.088 g, 0.68 mmol), NaN₃ (0.3 g, 4.48 mmol) and 3-bromo-2-quinolin-2-(1*H*)one (0.52 g, 2.242 mmol). The obtained mixture was stirred at 100 °C under argon atmosphere for 2 days and at rt for additional 2 days. During this time, the subsequent addition of extra copper powder (0.014 g, 0.22 mmol), L-ascorbic acid (0.078 g, 0.44 mmol), pipercolinic acid (0.088 g, 0.68 mmol), NaN₃ (0.3 g, 4.48 mmol) was carried out three times to force the reaction to proceed until the conditions stayed fixed according to UPLC-MS monitoring. Then, the mixture was cooled to rt and concentrated under reduced pressure. The obtained crude residue was diluted with ethyl acetate (150 ml) and some drops of ethanol, filtrated through celite and the resulting solid rinsed with ethyl acetate (100 ml). The collected filtrate was concentrated under vacuum to dryness and the resulting solid purified by silica gel flash chromatography (DCM/ethyl acetate from 90/10 to 40/60) to afford title compound **27** as a solid (100 mg), which was pure enough to be employed in the next synthetic step without further purification. Rt = 1.93 min (analysis method 2). MS (ESI) m/z: 161.3 [M-H]⁺, calculated: 161.07 [C₉H₉N₂O]⁺. ¹H-NMR (400 MHz, DMSO-*d*₆) δ 11.75 (s, 1H, CONH), 7.37-7.32 (m, 1H, CH), 7.21-7.16 (m, 1H, CH), 7.15-7.10 (m, 1H, CH), 7.07-7.00 (m, 1H, CH), 6.73 (s, 1H, CH), 5.41 (s, 2H, NH₂).

Synthesis of 2-naphtol derivatives (series 6)

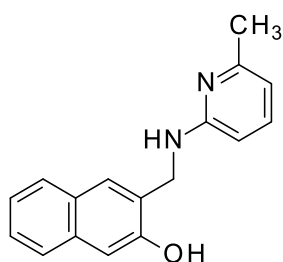
Synthesis of 3-(2-furylmethylamino) naphthalen-2-ol (18)



3-amino-2-naphthol (0.21 g, 1.26 mmol) was treated with 2-furaldehyde (0.21 ml, 2.52 mmol) in dry MeOH (13 ml), and the resulting suspension was stirred at 50 °C under argon atmosphere for 2 h. After cooling to rt, STAB was added (0.67 g, 3.07 mmol) and the mixture

was stirred at rt for additional 15 h. Afterwards, extra STAB (1.34 g, 6.14 mmol) was added in two equal 0.67 g portions while stirring, and the reaction was continued for additional 4 h. The mixture was concentrated under reduced pressure, diluted with water (50 ml), neutralized with a saturated solution of NaHCO₃ and extracted with ethyl acetate (3 x 100 ml). The combined organic phases were dried over Na₂SO₄ and evaporated to dryness at low pressure. Two sequential purifications by silica gel flash chromatography (cyclohexane/ethyl acetate from 99.9/0.1 to 92/8 and then chloroform 100 %) afforded compound **18** (65 mg, 22 % yield) as a white solid. Rt = 2.13 min (analysis method 1). MS (ESI) m/z: 240.3 [M-H]⁺, calculated: 240.10 [C₁₅H₁₄NO₂]⁺. ¹H-NMR (400 MHz, DMSO-*d*₆) δ 10.07 (br s, 1H, OH), 7.57 (s, 1H, CH), 7.53-7.43 (m, 2H, 2CH), 7.19-6.95 (m, 3H, 3CH), 6.81 (s, 1H, CH), 6.46- 6.27 (m, 2H, 2CH), 5.55 (t, *J* = 6.2 Hz, 1H, NH), 4.41 (d, *J* = 6.2 Hz, 2H, CH₂). ¹³C-NMR (101 MHz, DMSO-*d*₆) δ 153.04 (C), 145.77 (C), 141.95 (CH), 137.97 (C), 129.50 (C), 127.08 (C), 125.31 (CH), 125.05 (CH), 122.82 (CH), 121.49 (CH), 110.39 (CH), 107.45 (CH), 106.96 (CH), 103.16 (CH), 39.94 (CH₂).

Synthesis of 3-[[[(6-methyl-2-pyridyl)amino]methyl]naphthalen-2-ol (**19**)

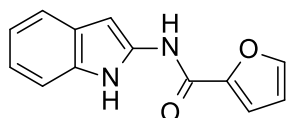


3-hydroxynaphthalene-2-carboxyaldehyde (0.053 g, 0.29 mmol) was added portionwise to a stirred mixture of 2-amino-3-methylpyridine (0.032 g, 0.29 mmol) in ethanol (2.9 ml) that was previously deoxygenated with nitrogen. The obtained mixture was stirred at reflux under nitrogen atmosphere for 4 h. After cooling to rt, sodium borohydride (0.027 g, 0.71 mmol) was added to the mixture and the reaction was continued for additional 1 h. Then, the solvent was evaporated, the crude residue was diluted with water (25 ml) and neutralized with a saturated solution of NH₄Cl. The aqueous phase was extracted with ethyl acetate (3 x 25 ml), the combined organic layers dried over Na₂SO₄ and concentrated to dryness at low pressure. Final purification by silica gel flash chromatography (cyclohexane/ethyl acetate from 99.5/0.5 to 88/12), afforded compound **19** (35 mg, 46 % yield) as a white solid. Rt = 2.20 min (analysis method 1). MS (ESI) m/z: 265.4 [M-H]⁺, calculated: 265.13 [C₁₇H₁₇N₂O]⁺. ¹H-NMR (400 MHz, DMSO-*d*₆) δ 10.89 (br s, 1H, OH), 7.73-7.67 (m, 2H, 2CH), 7.65 (d, *J* = 8.1 Hz, 1H, CH), 7.36-7.26 (m, 2H, 2CH), 7.25-7.19 (m, 1H, CH), 7.15 (s, 1H, CH), 7.06 (t, *J* = 6.2 Hz,

1H, NH), 6.40-6.32 (m, 2H, 2CH), 4.52 (d, $J = 6.2$ Hz, 2H, CH₂), 2.29 (s, 3H, CH₃). ¹³C-NMR (101 MHz, DMSO-*d*₆) δ 158.01 (C), 155.08 (C), 154.12 (C), 137.60 (CH), 133.79 (C), 129.61 (C), 127.83 (CH), 127.63 (C), 127.20 (CH), 125.58 (CH), 125.60 (CH), 122.71 (CH), 110.74 (CH), 109.39 (CH), 105.50 (CH), 40.42 (CH₂), 23.59 (CH₃).

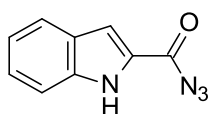
Synthesis of an indole-based derivative (series 7)

Step 2. Synthesis of *N*-(1*H*-indol-2-yl) furan-2-carboxamide (20)



Compound **28** (0.3 g, 1.62 mmol), 2-furoic acid (0.37 g, 3.24 mmol) and DMAP (20 mg, 0.162 mmol) were reacted for 5 h at 110 °C under argon atmosphere in dry toluene (3.24 ml). After cooling to rt and solvent evaporation at low pressure, the crude residue was diluted with DCM (150 ml), washed with a saturated NaHCO₃ solution (150 ml), dried over Na₂SO₄ and concentrated to dryness at low pressure. Purification by silica gel flash chromatography (cyclohexane/ethyl acetate from 95/5 to 0/100) and trituration with diethyl ether (2 ml) yielded compound **20** (20 mg, 5 % yield) as a brown solid. $R_t = 1.63$ min (analysis method 1). MS (ESI) m/z : 227.3 [M-H]⁺, calculated: 227.08 [C₁₃H₁₁N₂O₂]⁺. ¹H-NMR (400 MHz, DMSO-*d*₆) δ 10.90 (br s, 1H, NH), 7.89-7.88 (m, 1H, CH), 7.65 (br s, 2H, CH and NH), 7.40-7.36 (m, 1H, CH), 7.17-7.13 (m, 1H, CH), 7.03 (dd, $J = 3.4$ and 0.8 Hz, 1H, CH), 6.96-6.87 (m, 2H, 2CH), 6.69 (dd, $J = 3.4$ and 1.7 Hz, 1H, CH). ¹³C-NMR (101 MHz, DMSO-*d*₆) δ 175.13 (C), 156.29 (C), 153.81 (C), 144.34 (CH), 133.47 (C), 125.40 (C), 120.70 (CH), 120.55 (CH), 118.45 (CH), 113.91 (CH), 111.83 (CH), 110.20 (CH), 95.82 (CH).

Step 1. Synthesis of 1*H*-indole-2-carboxazide (28)



A mixture of 1*H*-indole-2-carboxylic acid (0.52 g, 3.2 mmol), triethylamine (0.8 ml, 6.4 mmol) and DPPA (0.6 ml, 2.88 mmol) in dry DCM (15 ml) was stirred under argon atmosphere for 7 h at room temperature. Then, the solvent was removed *in vacuo* and the crude residue was purified by silica gel flash chromatography (cyclohexane/chloroform from 99.5/0.5 to 80/20), affording compound **28** (495 mg, 83 % yield) as a white solid. $R_t = 2.06$ min (analysis method 1). MS (ESI) m/z : 185.2 [M-H]⁻, calculated: 185.05 [C₉H₅N₄O]⁻. ¹H-

NMR (400 MHz, CDCl₃) δ 8.92 (br s, 1H, NH), 7.73-7.67 (m, 1H, CH), 7.45-7.40 (m, 1H, CH), 7.40-7.34 (m, 1H, CH), 7.31-7.27 (m, 1H, CH), 7.20-7.14 (m, 1H, CH).

1.2. ChD-competition FP assay

N-terminal His6-tagged ChD was overexpressed in *Escherichia coli* and purified. Two different FITC-labeled peptide mimicking H3K27me3 were used (probe 1 or probe 2). In the experiments, the reference compound was a five-amino-acid peptide that corresponds to a truncated sequence of a specific methylated protein region able of interacting with ChD. The assay was performed in 384 well black plates, by employing a FP buffer 1x (according to the number of samples) obtained by diluting appropriately FP 11x (Table 8) in Tris/NaCl buffer (Table 7). Constant concentrations of ChD and FITC-peptide (probe 1 or 2) were 11 μ M and 11 nM, respectively. A DMSO tolerance experiment allowed to conclude that 0.5% final DMSO (in assay buffer) does not alter the affinity of the probe against ChD. Hence, samples of tested compounds were prepared diluting 20 mM DMSO stock solutions of compounds in the assay buffer to 6.25, 25 and 100 μ M, thus obtaining 0.5% DMSO solutions. The final well volume was 30 μ L. Plates were incubated for 15-30 min in darkness at rt prior to reading with a plate reader in FP reading mode with λ_{exc} : 485 nm, λ_{em} : 535 nm and λ_{exc} : 535, λ_{em} : 580 nm.

Table 7 Tris/NaCl buffer

REAGENT	[Stock]	Vol for 50ml	Dil factor	[Final]
Tris pH 8.0	1M	1 ml	1:50	20mM
NaCl	5M	3 ml	1:16.66	300mM
H2O		46ml		
		50ml		

Table 8 FP buffer 11x

REAGENT	[Stock]	Vol for 2ml	Vol for 5ml	[Final]
Tris/NaCl		1916	4790	
Tween 20	10%	22	55	0.11%
DTT	1M	22	55	11mM
Prot. Inh.	500X	40	100	10X
		2000	5000	

1.3. Fluorescence measurements

Samples were prepared diluting 20 mM DMSO stock solutions of the tested compounds in water to 100 μ M, thus obtaining 0.5% DMSO solutions.

Fluorescence experiments were performed in quartz cuvettes by using FluoroMax-4 Spectrofluorometer (Horiba Jobin Yvon). Samples were excited at 485 nm and 535 nm; bandwidth was 5. The fluorescence spectra were recorded in the 490-700 nm e 540-700 nm ranges, respectively.

2. Section 2. Development of small-molecules as Tubulin Colchicine-site binders for cancer therapy

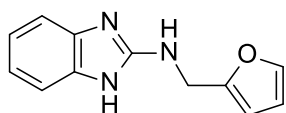
2.1. Synthesis

Synthesis of compounds *via* SNAr

Step 2. General procedure A for the synthesis of compounds **29**, **30**, **32**, **33**, **35**, **36**

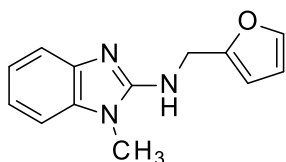
Unless otherwise specified, triethylamine (5.0 molar equiv.) was dropwise added to a mixture of the appropriate sulfone (1.0 molar equiv.) and amine (5.0 molar equiv.) under argon atmosphere. The obtained mixture was stirred at 120 °C by conventional heating for 24 h-3 days. If required, additional amine was added (amount specified for each compound) to get reaction completion. The reaction crude was cooled to rt and purified by silica gel flash phase chromatography. If required, final trituration was performed in a suitable solvent (specified for each compound) to afford pure compounds **29**, **30**, **32**, **33**, **35** and **36**.

Step 2. Synthesis of *N*-(2-furylmethyl)-1*H*-benzimidazol-2-amine (**29**)



Compound **29** was synthesized following the general procedure A previously described by reacting **47** (0.133 g, 0.68 mmol), and furfurylamine (0.31 ml, 3.4 mmol) for 24 h. Purification by silica gel flash chromatography (DCM/ethyl acetate from 100/0 to 40/60) afforded compound **29** as a beige solid (51 mg, 35 % yield). $R_t = 1.30$ min (analysis method 1). MS (ESI) m/z : 214.1 $[M-H]^+$, calculated: 214.10 $[C_{12}H_{12}N_3O]^+$. 1H -NMR (400 MHz, DMSO- d_6) δ 10.76 (br s, 1H, NH), 7.64-7.50 (m, 1H, CH), 7.22-7.06 (m, 2H, 2CH), 7.00 (t, $J = 6.0$ Hz, 1H, NH), 6.94-6.78 (m, 2H, 2CH), 6.44-6.33 (m, 1H, CH), 6.33-6.24 (m, 1H, CH), 4.49 (d, $J = 6.0$ Hz, 2H, CH₂). ^{13}C -NMR (101 MHz, DMSO- d_6) 155.08 (C), 153.24 (C), 141.92 (CH), 119.91 (CH), 118.33 (CH), 114.82 (CH), 110.41 (CH), 108.70 (CH), 106.66 (CH), 39.05 (CH₂).

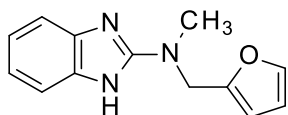
Step 2. Synthesis of *N*-(2-furylmethyl)-1-methyl-benzimidazol-2-amine (**30**)



Compound **30** was synthesized following the general procedure A previously described using commercial 1-methyl-2-(methylsulfonyl)benzimidazole (0.135 g, 0.63 mmol) and

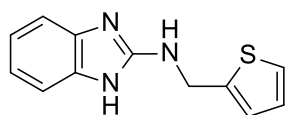
furfurylamine (0.28 ml, 3.15 mmol). The reaction was performed using conventional heating for 48 h. Then, additional amine (0.11 ml, 1.26 mmol) was added and the mixture was stirred under microwave irradiation for 6 h (120 °C, power 200 W). The crude mixture was purified by silica gel flash chromatography (DCM/ethyl acetate from 100/0 to 90/10). Final sequential trituration in petroleum ether (2 ml) and diethyl ether (2 ml) afforded compound **30** as a white solid (60 mg, 42 % yield). $R_t = 1.40$ min (analysis method 1). MS (ESI) m/z : 228.1 $[M-H]^+$, calculated: 228.11: $[C_{13}H_{14}N_3O]^+$. 1H -NMR (400 MHz, DMSO- d_6) δ 7.63-7.52 (m, 1H, CH), 7.25-7.06 (m, 3H, 2CH and 1NH), 7.00-6.88 (m, 2H, 2CH), 6.43-6.35 (m, 1H, CH), 6.35-6.28 (m, 1H, CH), 4.56 (d, $J = 5.7$ Hz, 2H, CH_2), 3.50 (s, 3H, NCH_3). ^{13}C -NMR (101 MHz, DMSO- d_6) 154.80 (C), 153.17 (C), 142.30 (C), 141.91 (CH), 135.35 (C), 120.27 (CH), 118.46 (CH), 115.11 (CH), 110.46 (CH), 107.35 (CH), 106.92 (CH), 39.15 (CH_2), 28.25 (NCH_3).

Step 2. Synthesis of *N*-(2-furylmethyl)-*N*-methyl-1*H*-benzimidazol-2-amine (**32**)



Compound **32** was afforded by reacting **47** (0.133 g, 0.68 mmol) and 1-(furan-2-yl)-*N*-methylmethanamine (0.4 ml, 3.4 mmol) according to the general procedure A for 48 h, then the mixture was heated to 130 °C for additional 3 days. The crude mixture was purified by silica gel flash chromatography (chloroform/chloroform:MeOH (8:2) from 99.5/0.5 to 90/10). Trituration in petroleum ether (2 ml), followed by additional trituration in diethyl ether (2 ml) and ethyl acetate (2 ml) afforded compound **32** as a beige solid (27 mg, 17 % yield). $R_t = 1.37$ min (analysis method 1). MS (ESI) m/z : 228.1 $[M-H]^+$, calculated: 228.11 $[C_{13}H_{14}N_3O]^+$. 1H -NMR (400 MHz, DMSO- d_6) δ 7.58 (br s, 1H, CH), 7.25-7.06 (m, 2H, 2CH), 6.99-6.78 (m, 2H, 2CH), 6.39 (br s, 1H, CH), 6.36-6.26 (m, 1H, CH), 4.68 (s, 2H, CH_2), 3.01 (s, 3H, NCH_3). ^{13}C -NMR (101 MHz, DMSO- d_6) δ 155.99 (C), 151.27 (C), 142.62 (CH), 119.34 (CH), 112.17 (CH), 110.42 (CH), 108.15 (CH), 46.40 (CH_2), 35.55 (NCH_3).

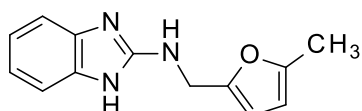
Step 2. Synthesis of *N*-(2-thienylmethyl)-1*H*-benzimidazol-2-amine (**33**)



Compound **33** was afforded by reacting **47** (0.133 g, 0.68 mmol) and 2-thiophenemethylamine (0.37 ml, 3.4 mmol) for 3 days according to the general procedure A. The crude mixture was purified by silica gel flash chromatography (DCM/ethyl acetate from 99/1 to 70/30). Sequential trituration in petroleum ether (2 ml) and diethyl ether (2 ml),

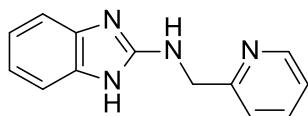
followed by freeze-drying afforded compound **33** as a white solid (17 mg, 11 % yield). Rt = 1.38 min (analysis method 1). MS (ESI) m/z: 230.0 [M-H]⁺, calculated: 230.08 [C₁₂H₁₂N₃S]⁺. ¹H-NMR (600 MHz, DMSO-*d*₆) δ 10.81 (s, 1H, NH), 7.38-7.34 (m, 1H, CH), 7.22-7.09 (m, 3H, 2CH and NH), 7.07-7.03 (m, 1H, CH), 6.98-6.93 (m, 1H, CH), 6.92-6.84 (m, 2H, 2CH), 4.67 (d, *J* = 6.0 Hz, 2H, CH₂). ¹³C NMR (151 MHz, DMSO-*d*₆) δ 154.89 (C), 143.45 (C), 126.61 (CH), 125.16 (CH), 124.68 (CH), 119.27(CH), 119.29 (CH), 114.79 (CH), 108.87 (CH), 40.93 (CH₂).

Step 2. Synthesis of *N*-[(5-methyl-2-furyl)methyl]-1*H*-benzimidazol-2-amine (**35**)



Compound **35** was obtained according to the general procedure A previously reported using **47** (0.133 g, 0.68 mmol) and (5-methylfuran-2-yl)methanamine (0.39 ml, 3.4 mmol). The reaction was performed for 24 h. Purification by silica gel column chromatography (first column: DCM/ ethyl acetate from 100/0 to 60/40; second column: chloroform/chloroform:MeOH (8:2) from 99.9/0.1 to 85/15) followed by trituration in petroleum ether (2 ml) and then diethyl ether (2 ml) afforded compound **35** as a white solid (60 mg, 39 % yield). Rt = 1.38 min (analysis method 1). MS (ESI) m/z: 228.1 [M-H]⁺, calculated: 228.11 [C₁₃H₁₄N₃O]⁺. ¹H-NMR (400 MHz, DMSO-*d*₆) δ 10.74 (br s, 1H, NH), 7.13 (s, 2H, 2CH), 7.02-6.75 (m, 3H, 2CH and NH), 6.20-6.12 (m, 1H, CH), 6.02-5.92 (m, 1H, CH), 4.43 (d, *J* = 5.3 Hz, 2H, CH₂), 2.23 (s, 3H, CH₃). ¹³C-NMR (101 MHz, DMSO-*d*₆) 155.10 (C), 151.33 (C), 150.53 (C), 133.77 (C), 119.95 (CH), 118.37 (CH), 114.78 (CH), 108.75 (CH), 107.55 (CH), 106.34 (CH), 38.95 (CH₂), 13.31 (CH₃).

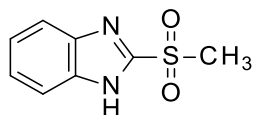
Step 2. Synthesis of *N*-(2-pyridylmethyl)-1*H*-benzimidazol-2-amine (**36**)



Compound **36** was afforded by reacting **47** (0.133 g, 0.68 mmol) and 2-picolylamine (0.35 ml, 3.4 mmol) for 48 h, following the general procedure A. The crude mixture was purified by silica gel flash chromatography (DCM/DCM:MeOH (8:2) from 90/10 to 30/70). Final sequential trituration in petroleum ether (2 ml) and diethyl ether (2 ml) afforded compound **36** as a beige solid (78 mg, 51 % yield). Rt = 1.21 min (analysis method 1). MS (ESI) m/z: 225.0 [M-H]⁺, calculated: 225.11 [C₁₃H₁₃N₄]⁺. ¹H-NMR (600 MHz, DMSO-*d*₆) δ 10.89 (br s, 1H, NH), 8.55-8.49 (m, 1H, CH), 7.74 (td, *J* = 7.7 and 1.8 Hz, 1H, CH), 7.38 (d, *J*

= 7.8 Hz, 1H, CH), 7.27-7.22 (m, 1H, CH), 7.18-7.08 (m, 3H, 2CH and NH), 6.86 (br s, 2H, 2CH), 4.61 (d, $J = 6.0$ Hz, 2H, CH₂). ¹³C-NMR (101 MHz, DMSO-*d*₆) 159.32 (C), 155.39 (C), 148.74 (CH), 136.62 (CH), 122.00 (CH), 120.93 (CH), 120.03 (CH), 117.91 (CH), 114.57 (CH), 108.63 (CH), 47.42 (CH₂).

Step 1. Synthesis of 2-methylsulfonyl-1*H*-benzimidazole (**47**)

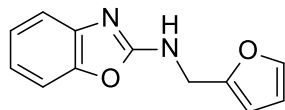


3-chloroperbenzoic acid (1.7 g, 7.8 mmol) was added to a stirred mixture of 2-methylsulfonyl-1*H*-benzimidazole (0.45 g, 2.6 mmol) in dry DCM (52 ml) at 0 °C. The obtained mixture was stirred at 0 °C for 10 minutes and at rt for additional 1 h. Saturated aqueous sodium sulfite solution (130 ml) was added at 0 °C and the obtained mixture was stirred at rt for extra 1 h. After separation of the phases, the organic phase was washed with brine (50 ml), dried over Na₂SO₄ and concentrated to dryness at low pressure to afford the title compound **47** as a white solid (435 mg, 85 % yield). Rt = 1.22 min (analysis method 1). MS (ESI) m/z : 197.0 [M-H]⁺, calculated: 197.04 [C₈H₉N₂O₂S]⁺. ¹H-NMR (400 MHz, DMSO-*d*₆) δ 7.78-7.66 (m, 2H, 2CH), 7.45-7.35 (m, 2H, 2CH), 3.49 (s, 3H, CH₃).

General procedure B for the synthesis of compounds **31** and **34**

A mixture of commercial 2-chlorobenzoxazole (1.0 molar equiv.) and the appropriate amine (1.0 molar equiv.) in dry DMF (1 ml) was stirred at rt for 16 h. The reaction crude was poured into water (10 ml) and filtrated under *vacuum* to afford a crude residue. The filtrate was then extracted with DCM (2 x 10 ml), dried over Na₂SO₄, concentrated to dryness and combined with the residue. Purification by silica gel flash phase chromatography, using mixtures of increasing polarity of cyclohexane and ethyl acetate, afforded compounds **31** and **34**.

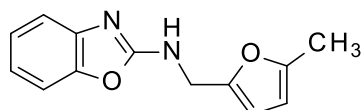
Synthesis of *N*-(2-furylmethyl)-1,3-benzoxazol-2-amine (**31**)



Compound **31** was synthesized following the general procedure B previously described by reacting commercial 2-chlorobenzoxazole (0.076 ml, 0.65 mmol) and furfurylamine (0.06 ml, 0.65 mmol). Purification by silica gel flash chromatography (cyclohexane/ethyl acetate from 95/5 to 40/60) afforded compound **31** as a white solid (53 mg, 38 % yield). Rt = 1.85 min (analysis method 1). MS (ESI) m/z : 215.0 [M-H]⁺, calculated: 215.08 [C₁₂H₁₁N₂O₂]⁺. ¹H-NMR

(400 MHz, DMSO-*d*₆) δ 8.50-8.33 (m, 1H, NH), 7.63-7.57 (m, 1H, CH), 7.38-7.32 (m, 1H, CH), 7.26 (d, *J* = 7.9 Hz, 1H, CH), 7.15-7.08 (m, 1H, CH), 7.03-6.94 (m, 1H, CH), 6.42-6.38 (m, 1H, CH), 6.37-6.33 (m, 1H, CH), 4.51 (d, *J* = 6.3 Hz, 2H, CH₂). ¹³C-NMR (101 MHz, DMSO-*d*₆) 162.16 (C), 151.86 (C), 148.12 (C), 143.01 (C), 142.35 (CH), 123.67 (CH), 120.35 (CH), 115.65 (CH), 110.51 (CH), 108.64 (CH), 107.30 (CH), 39.62 (CH₂).

Synthesis of *N*-[(5-methyl-2-furyl)methyl]-1,3-benzoxazol-2-amine (**34**)



Compound **34** was synthesized following the general procedure B previously described using commercial 2-chlorobenzoxazole (0.076 ml, 0.65 mmol) and (5-methylfuran-2-yl)methanamine (0.078 ml, 0.65 mmol). Purification by silica gel flash chromatography (cyclohexane/ethyl acetate from 100/0 to 60/40) gave compound **34** as a beige solid (38 mg, 26 % yield). *R*_t = 1.99 min (analysis method 1). MS (ESI) *m/z*: 229.0 [M-H]⁺, calculated: 229.10 [C₁₃H₁₃N₂O₂]⁺. ¹H-NMR (400 MHz, DMSO-*d*₆) δ 8.36 (br s, 1H, NH), 7.34 (d, *J* = 8.0 Hz, 1H, CH), 7.26 (d, *J* = 7.7 Hz, 1H, CH), 7.11 (m, 1H, CH), 6.98 (m, 1H, CH), 6.23-6.18 (m, 1H, CH), 6.02-5.96 (m, 1H, CH), 4.47-4.39 (m, 2H, CH₂), 2.23 (s, 3H, CH₃). ¹³C-NMR (101 MHz, DMSO-*d*₆) δ 162.13 (C), 150.94 (C), 149.99 (C), 148.10 (C), 143.04 (C), 123.64 (CH), 120.30 (CH), 115.61 (CH), 108.61 (CH), 108.15 (CH), 106.42 (CH), 39.18 (CH₂), 13.27 (CH₃).

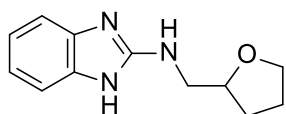
Synthesis of compounds *via* cyclodesulfurization

General procedure C for the synthesis of compounds **37-46**

Unless otherwise stated, the appropriate diamine (1.0 molar equiv.), DIPEA (1.0 mmol) and the corresponding isothiocyanate (1.0 molar equiv.) in dry MeCN (5 ml) were allowed to react at rt. Formation of monothiourea intermediate was monitored by UPLC-MS (the reaction time is specified for each compound). If required, further isothiocyanate was added during the course of the reaction (amount specified for each compound). Then, BOP (1.5 molar equiv.) and DBU (2 molar equiv.) were sequentially added and the mixture was allowed to stir at rt, for a specific time depending on the starting compounds used. In some specific cases, the mixture was heated to 80 °C to drive the reaction to completion. The mixture was concentrated to dryness, diluted with DCM (10 ml) and washed with a saturated NaHCO₃ solution (3 x 10 ml). The organic phase was dried over Na₂SO₄ and concentrated under *vacuum*. The crude residue was purified by gel flash chromatography using mixtures of increasing polarity of

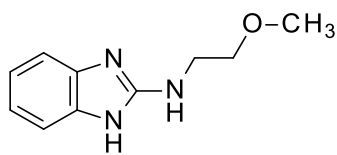
cyclohexane and ethyl acetate or DCM and DCM:NH₃ (1 N) solution in MeOH (8:2). The isolated product was treated differently depending on the case.

***N*-(tetrahydrofuran-2-ylmethyl)-1*H*-benzimidazol-2-amine (37)**



Compound **37** was synthesized following the general procedure C previously described by reacting commercial 1,2-diaminobenzene (0.387 g, 3.5 mmol) and 2-tetrahydrofurfuryl isothiocyanate (0.45 ml, 3.5 mmol) for 24 h. BOP (2.37 g, 5.25 mmol) and DBU (1.07 ml, 7 mmol) were added and the mixture was stirred at rt for additional 1 h. The crude was purified by two subsequent silica gel flash chromatography columns (cyclohexane/ethyl acetate from 50/50 to 0/100 and DCM/DCM:NH₃ (1 N) solution in MeOH (8:2) from 100/0 to 87/13, respectively). The obtained solid was dissolved in ethyl acetate (50 ml) and washed with a saturated NaHCO₃ solution (50 ml). The organic phase was dried over Na₂SO₄ and concentrated to dryness to afford a solid that, after trituration in ethyl acetate (2 x 2 ml), gave pure compound **37** (63 mg, 8 % yield). Rt = 1.17 min (analysis method 1). MS (ESI) m/z: 218.2 [M-H]⁺, calculated: 218.13 [C₁₂H₁₆N₃O]⁺. ¹H-NMR (400 MHz, methanol-*d*₄) δ 7.25-7.09 (m, 2H, 2CH), 7.00-6.89 (m, 2H, 2CH), 4.19-4.01 (m, 1H, CH), 3.96-3.83 (m, 1H, CH), 3.83-3.69 (m, 1H, CH), 3.60-3.47 (m, 1H, CH), 3.41-3.33 (m, 1H, CH), 2.13-1.99 (m, 1H, CH), 1.99-1.83 (m, 2H, CH₂), 1.65-1.72 (m, 1H, CH). ¹³C-NMR (101 MHz, methanol-*d*₄) δ 157.02 (C), 121.32 (CH), 112.77 (CH), 79.35 (CH), 69.12 (CH₂), 47.83 (CH₂), 29.64 (CH₂), 26.71 (CH₂).

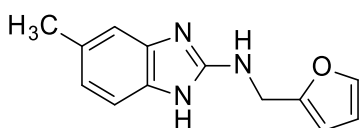
***N*-(2-methoxyethyl)-1*H*-benzimidazol-2-amine (38)**



Compound **38** was synthesized following the general procedure C previously described by reacting commercial 1,2-diaminobenzene (0.12 g, 1.05 mmol) and 2-methoxyethyl isothiocyanate (0.12 ml, 1.05 mmol) for 24 h. BOP (0.71 g, 1.6 mmol) and DBU (0.32 ml, 2.1 mmol) were added and the mixture was stirred at rt for additional 24 h and at 80 °C for extra 3 h. The crude residue was purified by two subsequent silica gel flash chromatography columns (cyclohexane/ethyl acetate from 50/50 to 0/100 and DCM/DCM:NH₃ (1 N) solution in MeOH (8:2) from 97/3 to 87/13, respectively). The obtained solid was dissolved in ethyl acetate (25 ml), washed with a saturated NaHCO₃ solution (25 ml). The aqueous phase was extracted with

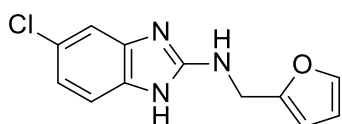
fresh ethyl acetate (3 x 20 ml) and the combined organic layers were dried over Na₂SO₄ and concentrated to dryness to afford pure compound **38** as a white solid (29 mg, 14 % yield). Rt = 1.08 min (analysis method 1). MS (ESI) m/z: 192.2 [M-H]⁺, calculated: 192.11 [C₁₀H₁₄N₃O]⁺. ¹H-NMR (400 MHz, DMSO-*d*₆) δ 10.65 (br s, 1H, NH), 7.20-7.00 (m, 2H, 2CH), 6.94-6.73 (m, 2H, 2CH), 6.60-6.45 (m, 1H, NH), 3.56-3.39 (m, 4H, 2CH₂), 3.28 (s, 3H, OCH₃). ¹³C-NMR (101 MHz, DMSO-*d*₆) δ 155.43 (C), 120.36 (CH), 118.30 (CH), 114.94 (CH), 109.08 (CH), 70.93 (CH₂), 57.96 (OCH₃), 41.80 (CH₂).

***N*-(2-furylmethyl)-5-methyl-1*H*-benzimidazol-2-amine (39)**



Compound **39** was synthesized following the general procedure C previously described by reacting 3,4-diaminotoluene (0.18 g, 1.47 mmol) and furfuryl isothiocyanate (0.15 ml, 1.47 mmol) for 16 h. Additional furfuryl isothiocyanate (0.5 ml, 5.16 mmol) was added to force the reaction to proceed and the mixture was stirred for additional 8 h. Then, BOP (1.00 g, 2.21 mmol) and DBU (0.45 ml, 2.94 mmol) were added and the mixture was stirred for further 18 h. Purification by silica gel flash chromatography (cyclohexane/ethyl acetate from 95/5 to 10/90), followed by trituration in DCM (2 ml) afforded compound **39** as a light pink solid (149 mg, 45 % yield). Rt = 1.47 min (analysis method 1). MS (ESI) m/z: 228.0 [M-H]⁺, calculated: 228.11 [C₁₃H₁₄N₃O]⁺. ¹H-NMR (400 MHz, DMSO-*d*₆) δ 10.63 (br s, 1H, NH), 7.57 (s, 1H, CH), 7.01 (d, *J* = 7.7 Hz, 1H, CH), 6.95 (s, 1H, CH), 6.93-6.85 (m, 1H, NH), 6.69 (d, *J* = 7.7, 1H, CH), 6.41-6.34 (m, 1H, CH), 6.31-6.25 (m, 1H, CH), 4.53-4.40 (m, 2H, CH₂), 2.30 (s, 3H, CH₃). ¹³C NMR (101 MHz, DMSO-*d*₆) 154.99 (C), 153.28 (C), 141.92 (CH), 119.98 (CH), 111.92 (CH), 111.39 (CH), 110.42 (CH), 106.66 (CH), 39.01 (CH₂), 21.26 (CH₃).

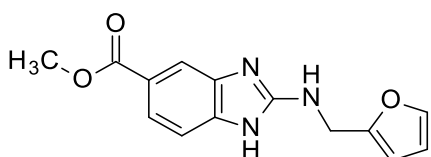
Synthesis of 5-chloro-*N*-(2-furylmethyl)-1*H*-benzimidazol-2-amine (40)



Compound **40** was synthesized following the general procedure C previously described by reacting commercial 4-chloro-1,2-diaminobenzene (0.2 g, 1.35 mmol) and furfuryl isothiocyanate (0.14 ml, 1.35 mmol) for 17 h. Then, additional furfuryl isothiocyanate (0.21 ml, 2.03 mmol) was added and the mixture was stirred for further 16 h. After the addition of BOP (0.91 g, 2.03 mmol) and DBU (0.41 ml, 2.7 mmol), the mixture was stirred for additional

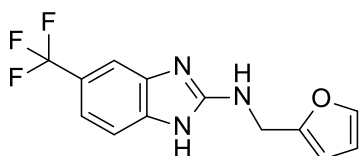
1 h. Purification by silica gel flash chromatography (cyclohexane/ethyl acetate from 80/20 to 40/60), followed by trituration in DCM (2 x 2 ml) afforded compound **40** as a yellow solid (93 mg, 28 % yield). Rt = 1.64 min (analysis method 1). MS (ESI) m/z: 248.0/250.0 [M-H]⁺ (3/1), calculated: 248.06/250.06 [C₁₂H₁₁ClN₃O]⁺. ¹H-NMR (400 MHz, DMSO-*d*₆) δ 10.91 (br s, 1H, NH), 7.58 (s, 1H, CH), 7.29-7.18 (m, 1H, NH), 7.18-7.06 (m, 2H, 2CH), 6.95-6.79 (m, 1H, CH), 6.42-6.35 (m, 1H, CH), 6.32-6.27 (m, 1H, CH), 4.49 (d, *J* = 5.8 Hz, 2H, CH₂). ¹³C NMR (101 MHz, DMSO-*d*₆) δ 156.07 (C), 152.93 (C), 142.04 (CH), 118.49 (CH), 114.81 (CH), 110.55 (CH), 110.45 (CH), 106.81 (CH), 39.62 (CH₂).

Methyl 2-(2-furylmethylamino)-1H-benzimidazole-5-carboxylate (41)



Compound **41** was synthesized following the general procedure C previously described by reacting commercial methyl-3,4-diaminobenzoate (0.21 g, 1.23 mmol) and furfuryl isothiocyanate (0.13 ml, 1.23 mmol) for 2 h. Additional furfuryl isothiocyanate (0.065 ml, 0.62 mmol) was added and the mixture was stirred for 16 h; then, extra furfuryl isothiocyanate (0.065 ml, 0.62 mmol) was added. The mixture was stirred for further 24 h; then, BOP (0.83 g, 1.85 mmol) and DBU (0.38 ml, 2.46 mmol) were added and the reaction was continued for 1 h. Purification by silica gel flash chromatography (cyclohexane/ethyl acetate from 90/10 to 10/90), followed by trituration in ethyl acetate (2 x 2 ml) afforded compound **41** as a pink solid (36 mg, 11 % yield). Rt = 1.48 min (analysis method 1). MS (ESI) m/z: 272.0 [M-H]⁺, calculated: 272.10 [C₁₄H₁₄N₃O₃]⁺. ¹H-NMR (400 MHz, methanol-*d*₄) δ 7.89-7.84 (m, 1H, CH), 7.73 (dd, *J* = 8.3 and 1.6 Hz, 1H, CH), 7.44-7.41 (m, 1H, CH), 7.23 (d, *J* = 8.3 Hz, 1H, CH), 6.37-6.29 (m, 2H, 2CH), 4.56 (s, 2H, CH₂), 3.87 (s, 3H, OCH₃). ¹³C NMR (101 MHz, methanol-*d*₄) δ 169.65 (C), 158.27 (C), 153.48 (C), 143.41 (CH), 123.93 (CH), 122.92 (C), 113.88 (CH), 112.76 (CH), 111.35 (CH), 108.08 (CH), 52.32 (OCH₃), 40.56 (CH₂).

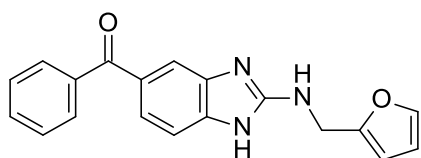
N-(2-furylmethyl)-5-(trifluoromethyl)-1H-benzimidazol-2-amine (42)



Compound **42** was synthesized following the general procedure C previously described by reacting commercial 3,4-diaminobenzotrifluoride (0.22 g, 1.19 mmol) and furfuryl

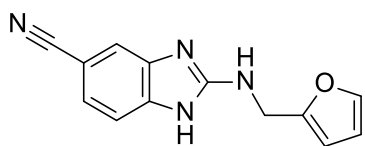
isothiocyanate (0.13 ml, 1.19 mmol) for 18 h, then extra furfuryl isothiocyanate (0.065 ml, 0.6 mmol) was added and the reaction was continued for further 30 h. Then, BOP (0.81 g, 1.79 mmol) and DBU (0.36 ml, 2.38 mmol) were added to the mixture and the reaction was continued for additional 1 h. Purification by silica gel flash chromatography (cyclohexane/ethyl acetate from 100/0 to 30/70), followed by trituration in DCM (2 ml) afforded compound **42** as a white solid (42 mg, 13 % yield). $R_t = 1.90$ min (analysis method 1). MS (ESI) m/z : 282.1 $[M-H]^+$, calculated: 282.09 $[C_{13}H_{11}F_3N_3O]^+$. 1H -NMR (400 MHz, methanol- d_4) δ 7.50-7.40 (m, 2H, 2CH), 7.34-7.22 (m, 2H, 2CH), 6.39-6.30 (m, 2H, 2CH), 4.57 (s, 2H, CH₂). ^{13}C NMR (101 MHz, methanol- d_4) δ 158.18 (C) 153.49 (C), 143.40 (CH), 118.44 (CH), 111.35 (CH), 110.55 (CH), 108.08 (CH), 40.56 (CH₂).

[2-(2-furylmethylamino)-1H-benzimidazol-5-yl]-phenyl-methanone (43)



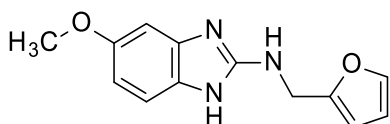
Compound **43** was synthesized following the general procedure C previously described by reacting commercial (3,4-diaminophenyl)-(phenyl)-methanone (0.23 g, 1.05 mmol) and furfuryl isothiocyanate (0.11 ml, 1.05 mmol) for 21 h. Then, extra furfuryl isothiocyanate (0.055 ml, 0.53 mmol) was added twice over a period of 5 h and the mixture was allowed to stir for extra 4 days. BOP (0.71 g, 1.58 mmol) and DBU (0.32 ml, 2.1 mmol) were added and the reaction was continued for additional 1 h. Purification by silica gel flash chromatography (cyclohexane/ethyl acetate from 95/5 to 0/100), followed by trituration with diethyl ether (2 ml), afforded compound **43** as a yellow solid (83 mg, 25 % yield). $R_t = 1.78$ min (analysis method 1). MS (ESI) m/z : 318.1.0 $[M-H]^+$, calculated: 318.12 $[C_{19}H_{16}N_3O]^+$. 1H -NMR (400 MHz, methanol- d_4) δ 7.78-7.65 (m, 3H, 3CH), 7.63-7.57 (m, 1H, CH), 7.56-7.47 (m, 3H, 3CH), 7.47-7.42 (m, 1H, CH), 7.29 (d, $J = 8.3$ Hz, 1H, CH), 6.38-6.28 (m, 2H, 2CH), 4.58 (s, 2H, CH₂). ^{13}C NMR (101 MHz, methanol- d_4) δ 198.96 (C), 158.51 (C), 153.39 (C), 143.45 (CH), 140.21 (C), 132.95 (CH), 130.73 (CH), 129.26 (CH), 125.66 (CH), 114.73 (CH), 112.82 (CH), 111.37 (CH), 108.14 (CH), 40.55 (CH₂).

(2-furylmethylamino)-1H-benzimidazole-5-carbonitrile (44)



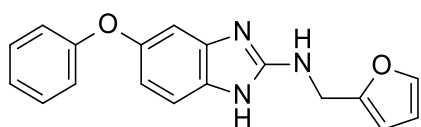
Compound **44** was synthesized following the general procedure C previously described by reacting 3,4-diaminobenzonitrile (0.19 g, 1.4 mmol) and furfuryl isothiocyanate (0.15 ml, 1.4 mmol) for 24 h. Extra furfuryl isothiocyanate (0.075 ml, 0.7 mmol) was added three times over a period of 2 days while stirring. Afterwards, BOP (0.95 g, 2.1 mmol) and DBU (0.43 ml, 2.8 mmol) were added and the reaction was continued for additional 1 h. Purification by silica gel flash chromatography (cyclohexane/ethyl acetate from 95/5 to 0/100), followed by trituration in diethyl ether (2 ml) and DCM (3 x 2 ml) afforded compound **44** as a beige solid (59 mg, 18 % yield). $R_t = 1.51$ min (analysis method 1). MS (ESI) m/z : 239.0 $[M-H]^+$, calculated: 239.09 $[C_{13}H_{11}N_4O]^+$. 1H -NMR (400 MHz, methanol- d_4) δ 7.61-7.40 (m, 2H, 2CH), 7.40-7.23 (m, 2H, 2CH), 6.42-6.20 (m, 2H, 2CH), 4.57 (s, 2H, CH_2). ^{13}C NMR (101 MHz, methanol- d_4) δ 158.58 (C), 153.29 (C), 143.45 (CH), 126.01 (CH), 121.50 (C), 116.10 (CH), 113.71 (CH), 111.36 (CH), 108.15 (CH), 40.50 (CH_2).

***N*-(2-furylmethyl)-5-methoxy-1*H*-benzimidazol-2-amine (45)**



Compound **45** was synthesized following the general procedure C previously described by reacting commercial 3,4-diaminoanisole (0.19 g, 1.37 mmol) and furfuryl isothiocyanate (0.14 ml, 1.37 mmol) for 3 h. Extra furfuryl isothiocyanate (0.07 ml, 0.69 mmol) was added five times while stirring over a period of 21 h. Then, BOP (0.93 g, 2.06 mmol) and DBU (0.42 ml, 2.74 mmol) were added and the mixture was stirred for additional 1 h. Purification by silica gel flash chromatography (cyclohexane/ethyl acetate from 60/40 to 0/100), followed by trituration in DCM (2 ml) afforded compound **45** as a beige solid (46 mg, 14 % yield). $R_t = 1.37$ min (analysis method 1). MS (ESI) m/z : 244.1 $[M-H]^+$, calculated: 244.11 $[C_{13}H_{14}N_3O_2]^+$. 1H -NMR (400 MHz, methanol- d_4) δ 7.44-7.40 (m, 1H, CH), 7.07 (d, $J = 8.5$ Hz, 1H, CH), 6.82 (d, $J = 2.4$ Hz, 1H, CH), 6.61 (dd, $J = 8.5, 2.4$ Hz, 1H, CH), 6.36-6.28 (m, 2H, 2CH), 4.52 (s, 2H, CH_2), 3.77 (s, 3H, OCH_3). ^{13}C -NMR (101 MHz, methanol- d_4) δ 156.64 (C), 156.50 (C), 153.82 (C), 143.27 (CH), 112.68 (CH), 111.31 (CH), 108.70 (CH), 107.91 (CH), 98.74 (CH), 56.34 (OCH_3), 40.71 (CH_2).

***N*-(2-furylmethyl)-5-phenoxy-1*H*-benzimidazol-2-amine (46)**



Compound **46** was synthesized following the general procedure C previously described by reacting commercial 4-phenoxybenzene-1,2-diamine (0.23 g, 1.09 mmol) and furfuryl isothiocyanate (0.11 ml, 1.09 mmol) for 2 h. Extra furfuryl isothiocyanate (0.06 ml, 0.55 mmol) was added seven times during the following 46 h while stirring. After that, BOP (0.74 g, 1.64 mmol) and DBU (0.33 ml, 2.18 mmol) were added and the mixture was stirred for additional 1 h. Purification by silica gel flash chromatography (cyclohexane/ethyl acetate from 95/5 to 0/100), followed by trituration with DCM (2 x 2 ml), afforded compound **46** as a white solid (158 mg, 47 % yield). Rt = 1.97 min (analysis method 1). MS (ESI) m/z: 306.1 [M-H]⁺, calculated: 306.12 [C₁₈H₁₆N₃O₂]⁺. ¹H-NMR (400 MHz, DMSO-*d*₆) δ 10.80 (br s, 1H, NH), 7.61-7.55 (m, 1H, CH), 7.35-7.26 (m, 2H, 2CH), 7.15-7.07 (m, 2H, CH and NH), 7.05-6.98 (m, 1H, CH), 6.92-6.87 (m, 2H, 2CH), 6.83 (d, *J* = 2.3 Hz, 1H, CH), 6.60 (dd, *J* = 8.3 and 2.3 Hz, 1H, CH), 6.41-6.35 (m, 1H, CH), 6.33-6.27 (m, 1H, CH), 4.49 (d, *J* = 5.6 Hz, 2H, CH₂). ¹³C-NMR (DMSO-*d*₆) δ 158.94 (C), 155.89 (C), 153.11 (C), 149.33(C), 141.98 (CH), 129.67 (CH), 121.93 (CH), 116.90 (CH), 111.31 (CH), 111.35 (CH), 110.44 (CH), 106.74 (CH), 104.17 (CH), 39.08 (CH₂).

2.2. Docking studies

Protein preparation

The protein structural model for the simulations was taken from the experimental crystallographic structure resolved by Steinmetz and his collaborators according to their standard protocol.⁷⁸ Simulations were performed on a single α/β-tubulin heterodimer, the one were the identified compound **29** binds. Therefore, the other chains corresponding to the additional heterodimer, stathmin, and tubulin tyrosine ligase (TTL), were removed along with calcium and chloride ions. The GTP and GDP molecules and the Mg²⁺ ions found in the X-ray structure were retained. Water molecules involved in the interaction with the Mg²⁺ ions were also kept.

An initial guess for missing hydrogens and ambiguous protonation states have been evaluated through Schrödinger 2018-3 Protein Preparation Wizard⁷⁹ and examined by visual inspection. Finally, the protein structure was refined to relieve steric clashes with a restrained minimization with the OPLS3a using Schrödinger default settings.

Ligands Preparation

All ligand structures were optimized by means of LigPrep tool of the Schrödinger 2018-3 Suite. After the generation of the 3D conformation, the molecules were submitted to Epik and all the tautomers and ionization states at pH 7.0 ± 2.0 were calculated.

Docking

The compounds were docked with Glide⁸⁰ by centering the grid on the co-crystallized fragment. To evaluate the impact of the introduced groups to the original fragment binding mode, a number of constraints have been employed. However, to avoid any bias to the docking process, the satisfaction of the constraints has been evaluated only after docking, so that only the poses similar to crystallographic one were retained. Two constraints were set (hydrogen bond to Glu198 and hydrogen bond to Val236) but the final poses had to match at least one of them (so as to evaluate correctly the tautomeric status of the neutral form). Docking were run with Glide SP (standard precision) protocol with a 2 times enhanced conformational sampling.

2.3. Resazurin assay ⁸¹⁻⁸³

To quantify the amount of live cells in the presence of tested compounds, the Resazurin assay was employed. The protocol is based on the reduction of the non-fluorescent blue Resazurin to a red fluorescent dye by the mitochondrion of live cells.

HeLa cells were seeded in Corning Costar 3603 plates at 5000 cells/well in 100 μ L DMEM (Dulbecco's Modified Eagle Medium) containing FCS (fetal calf serum) and left to attach for 24 h. For initial screening, the cells were exposed to 1, 10 and 100 μ M compound for 72 h. All measurements were done in triplicate. Subsequently, Resazurin was added to the wells to a final concentration of 20 μ M and incubated for 2 h. The readout was obtained on a PHERAstar FSX instrument with a filter for excitation at 575 nm and emission at 620 nm. Data were normed to the DMSO control and fitted to a non-linear regression model with GraphPad Prism 7.00.

Cell culture medium without neither cells or compounds (both in the presence or not of Resazurin) was used as further control.

V. Appendix

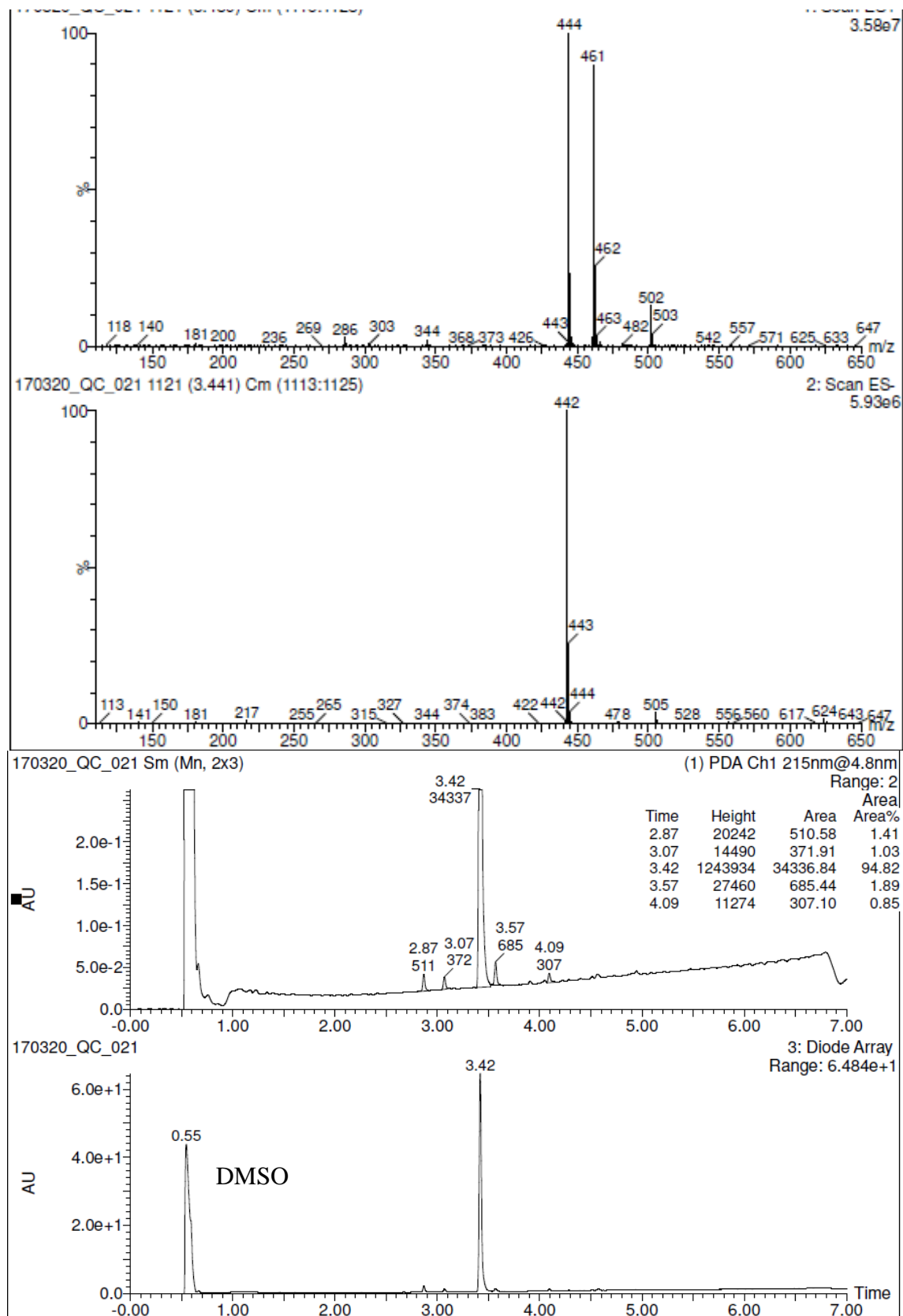


Figure A1. UPLC-MS chromatogram of commercial compound 1.

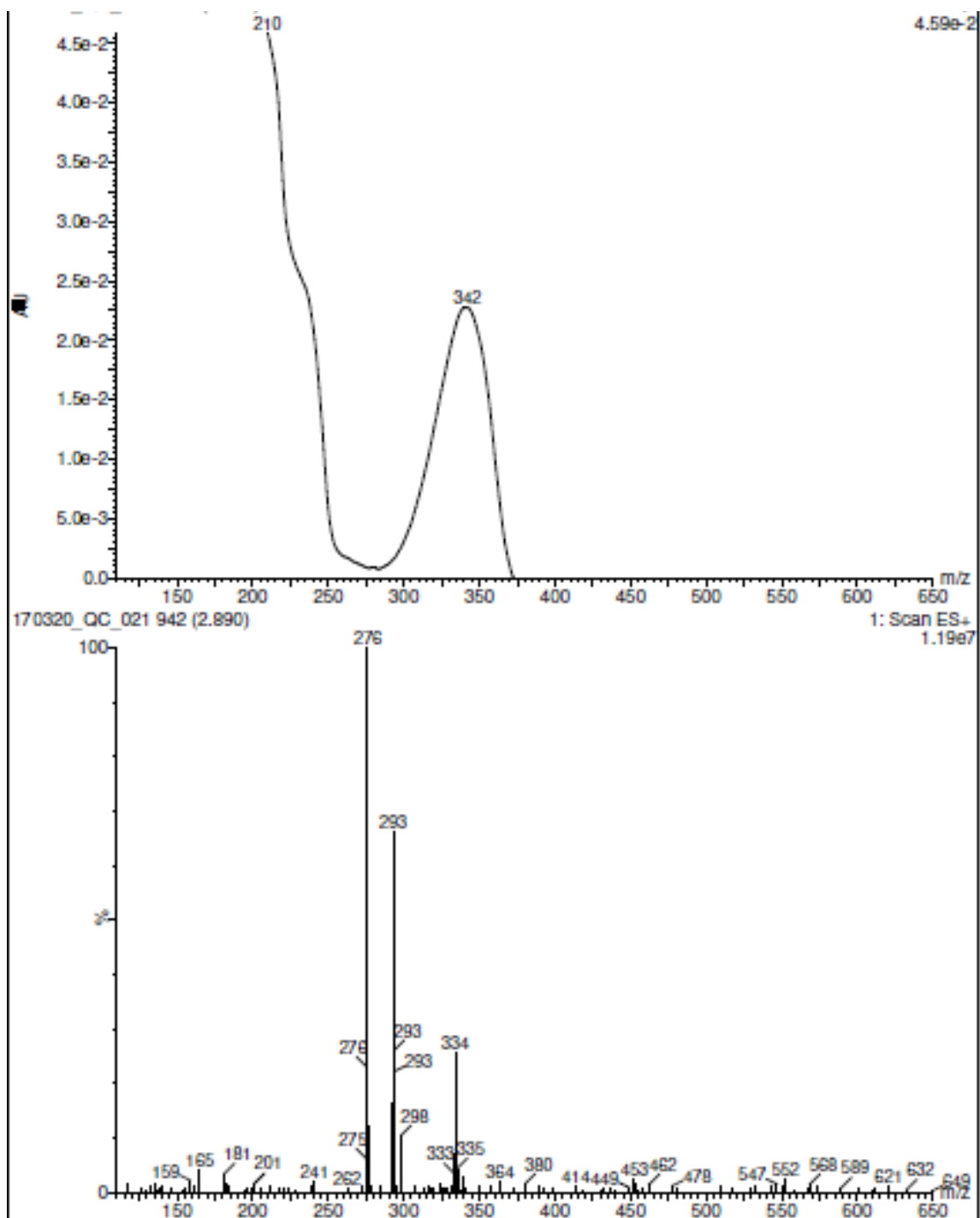


Figure A2. UV spectrum and UPLC-MS (Scan ES+) chromatogram of the impurity with Rt 2.87 min identified in commercial compound **1**.

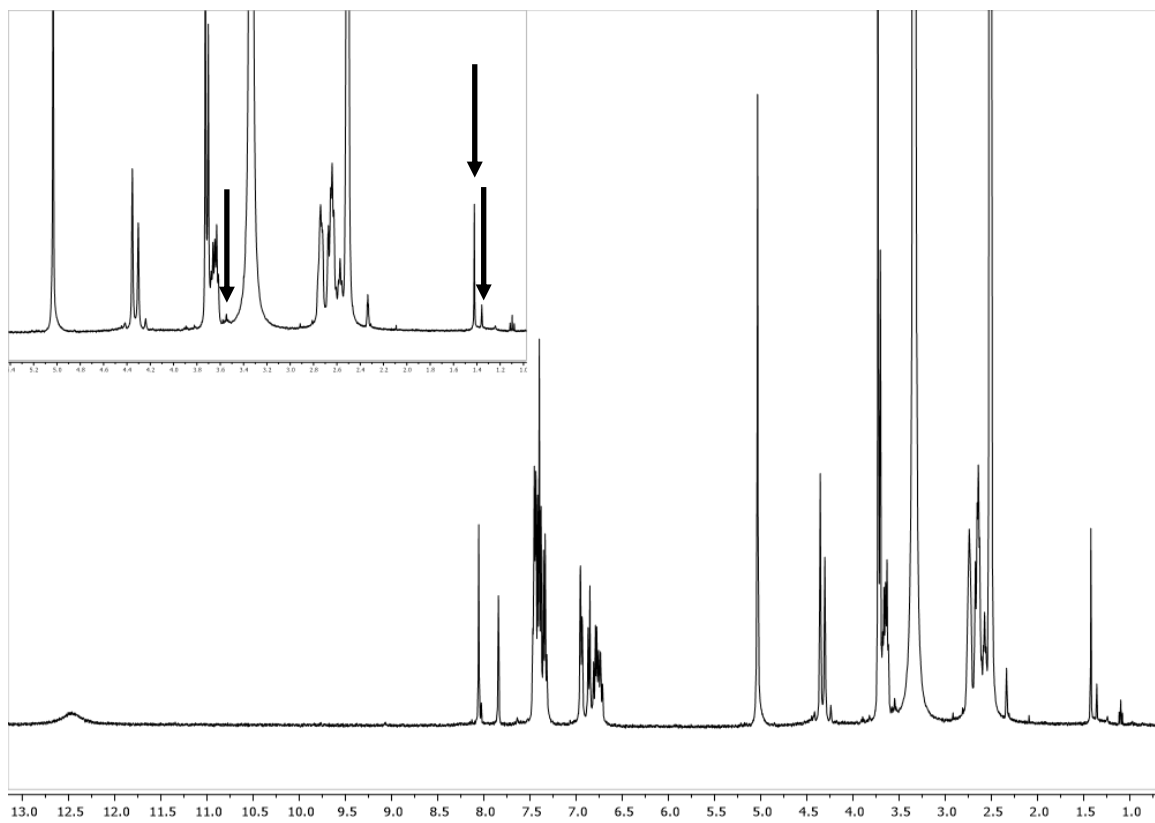


Figure A3. $^1\text{H-NMR}$ of commercial compound 1. The arrows point to the main impurities.

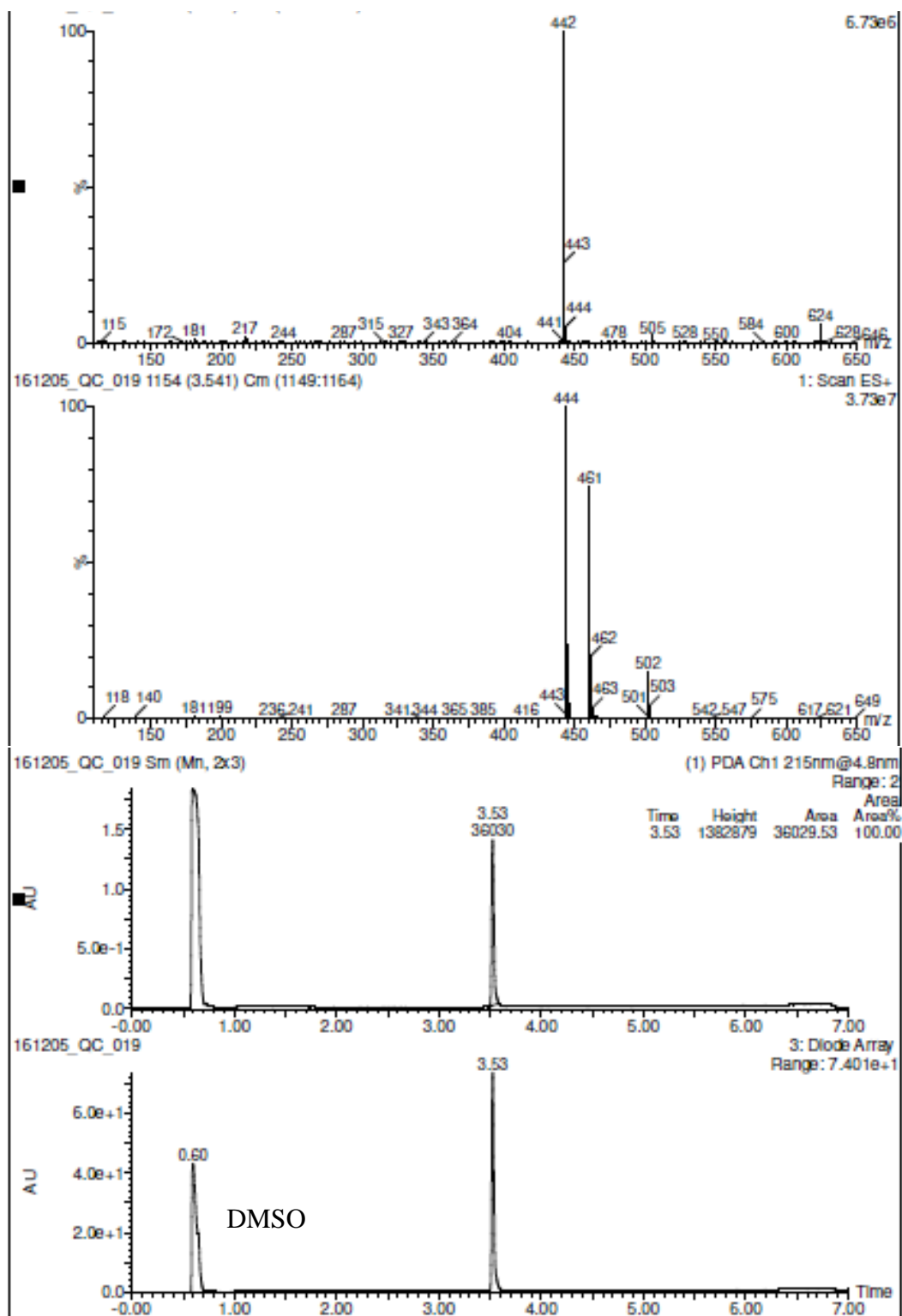


Figure A4. UPLC-MS chromatogram of re-synthesized compound 1.

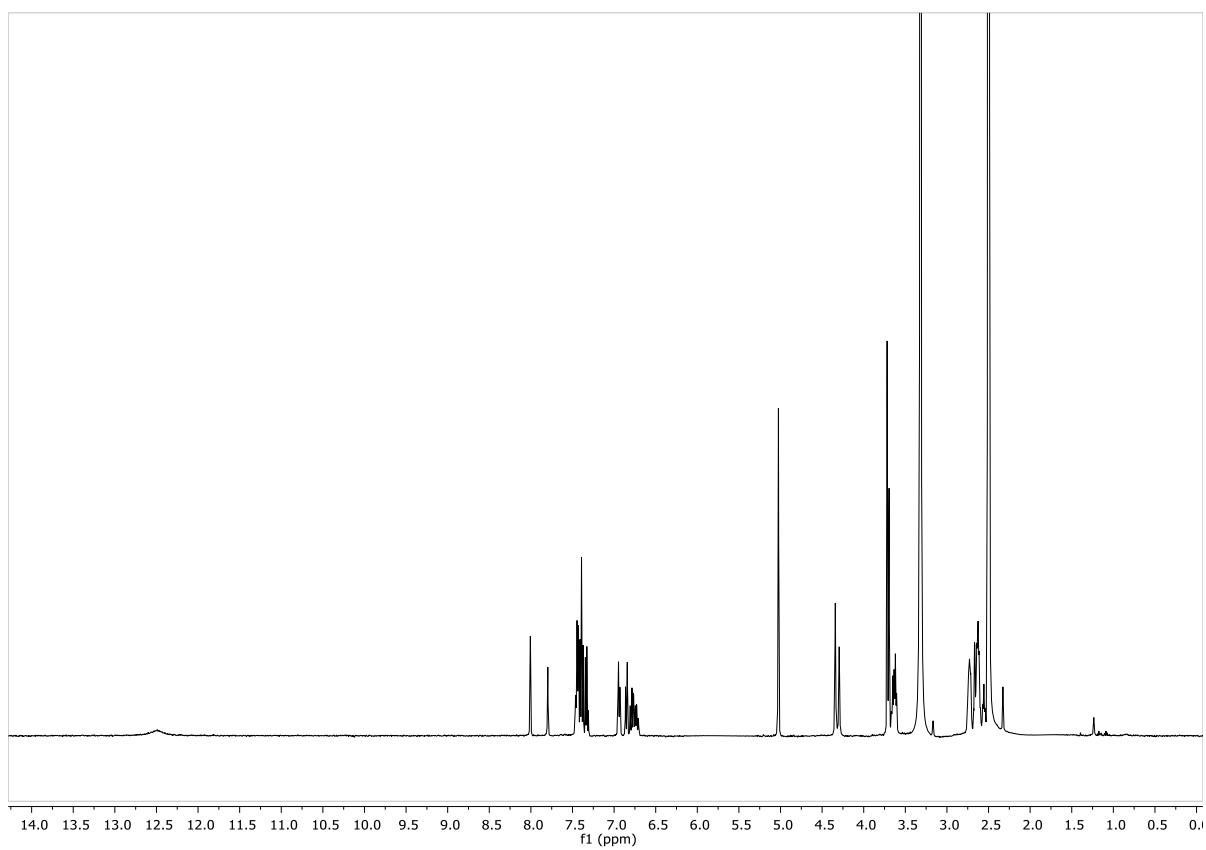


Figure A5. ¹H-NMR of re-synthesized compound **1**.

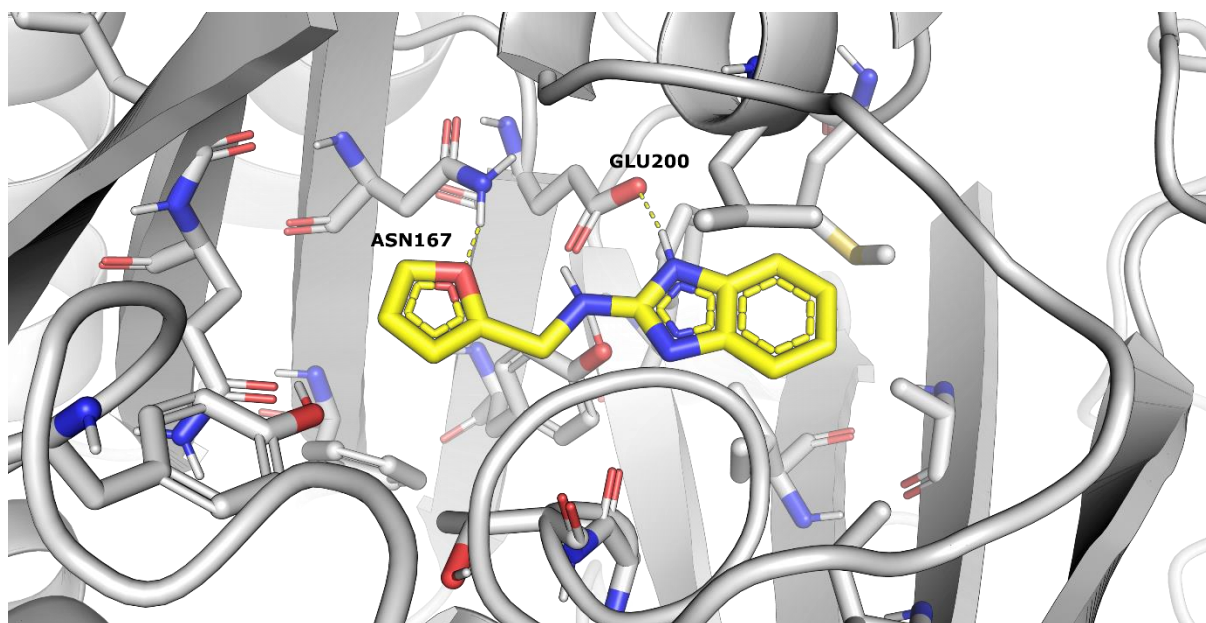


Figure A6. Binding pose of compound **29** according to docking studies.

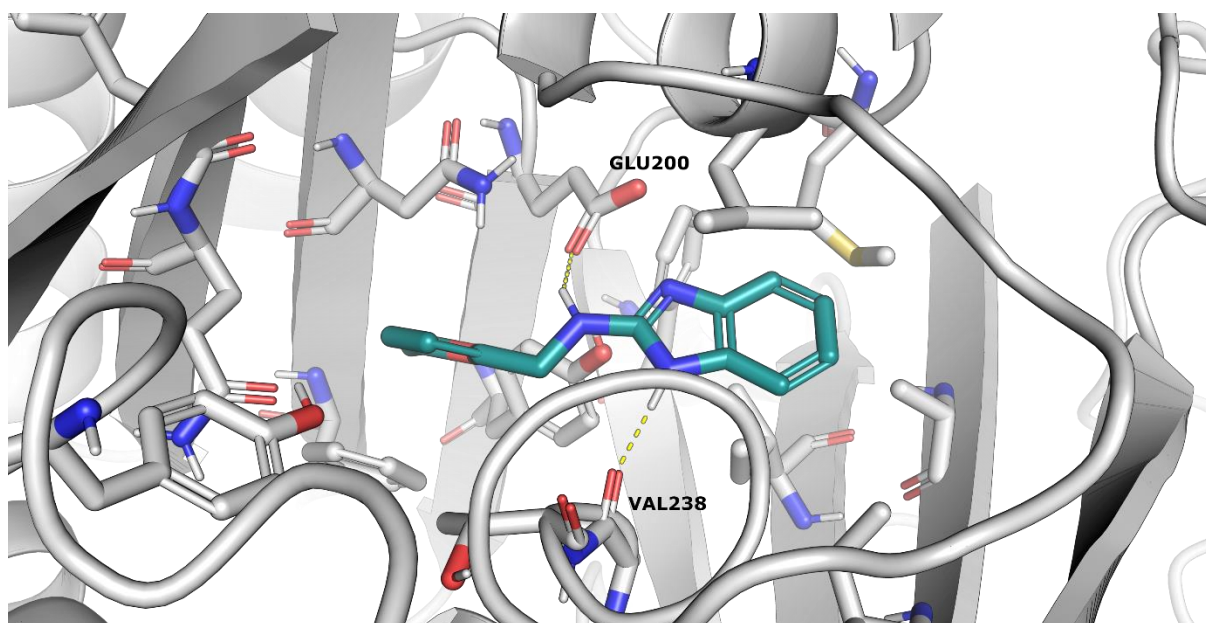


Figure A7. Binding pose of compound 35 according to docking studies.

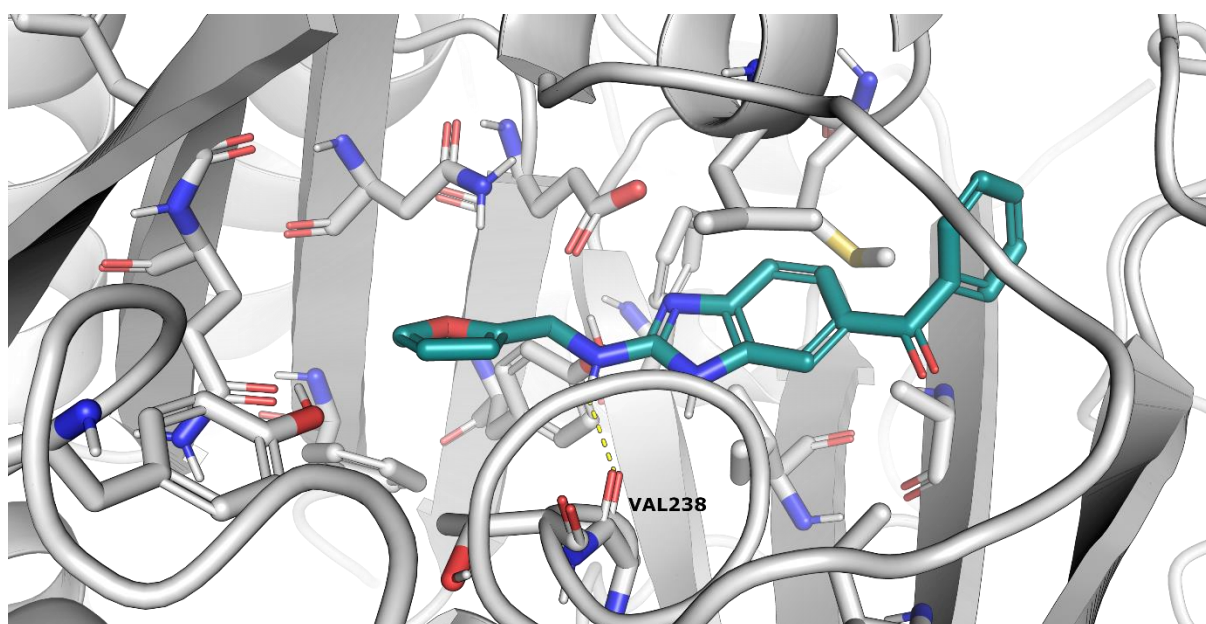


Figure A8. Binding pose of tautomer 1 of compound 43 according to docking studies.

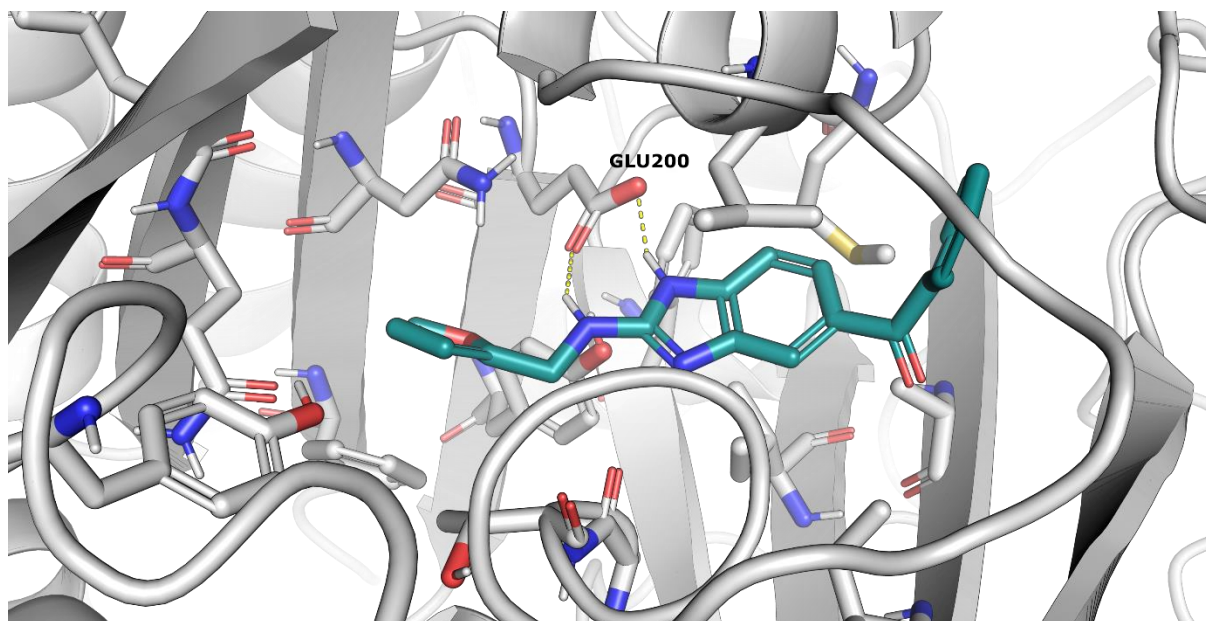


Figure A9. Binding pose of tautomer 2 of compound 43 according to docking studies.

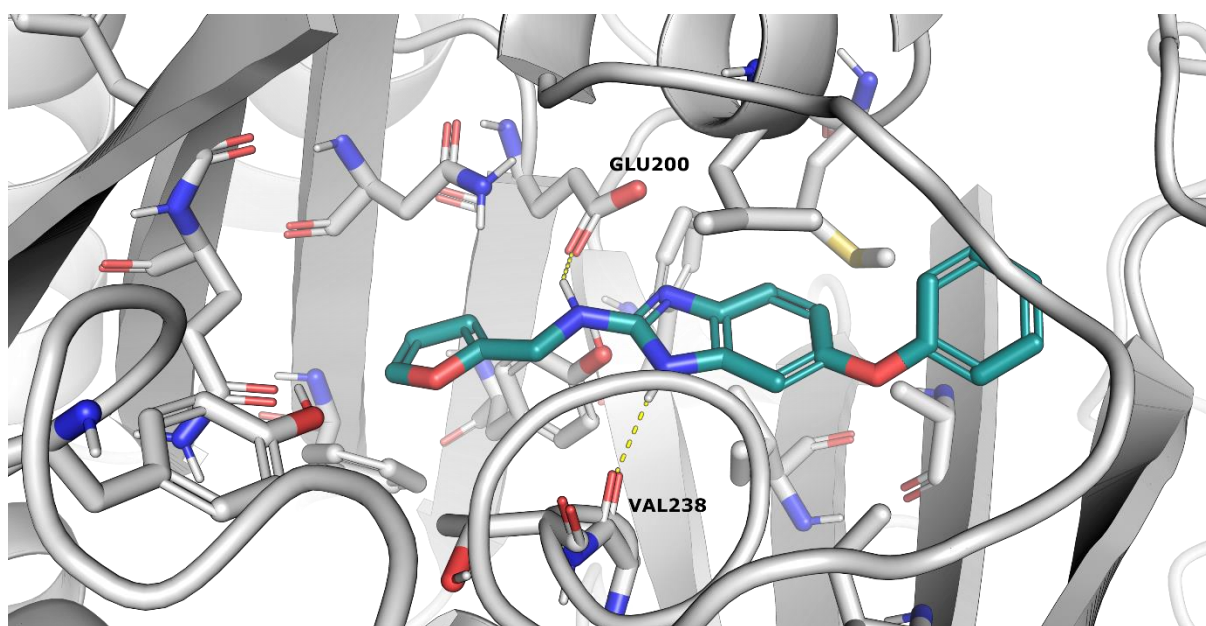


Figure A10. Binding pose of tautomer 1 of compound 46 according to docking studies.

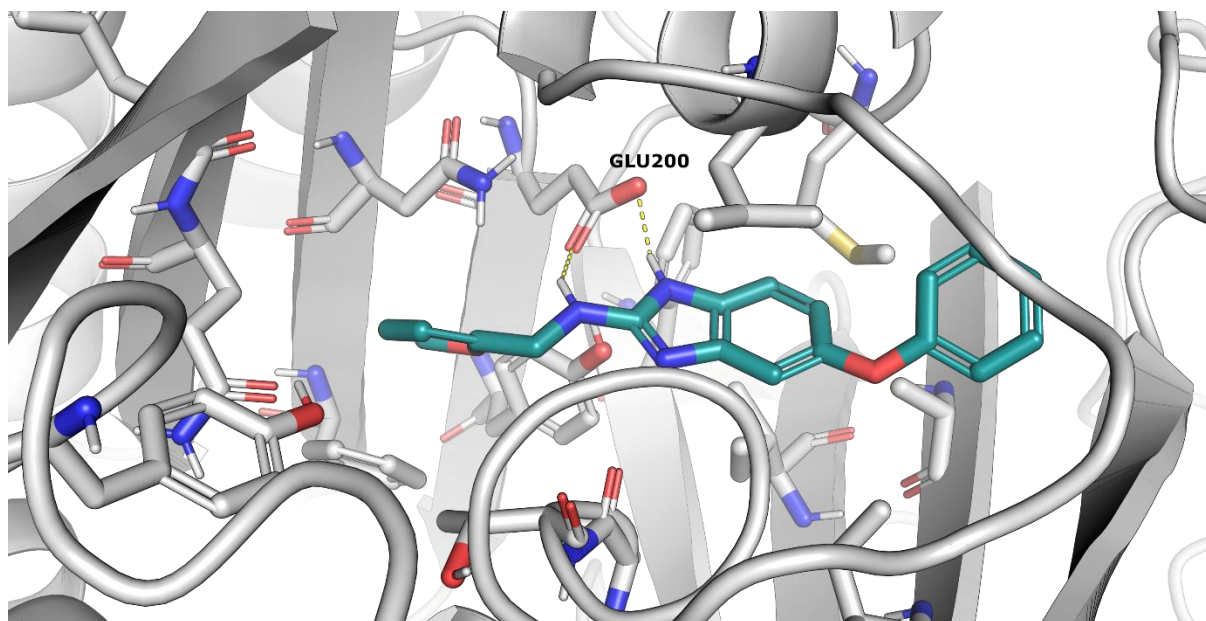


Figure A11. Binding pose of tautomer 2 of compound **46** according to docking studies.

VI. References

- (1) Hassanpour, S. H.; Dehghani, M. Review of Cancer from Perspective of Molecular. *J. Cancer Res. Pract.* **2017**, *4* (4), 127–129.
- (2) Seyfried, T. N.; Huysentruyt, L. C. On the Origin of Cancer Metastasis. *Crit. Rev. Oncog.* **2013**, *18* (1–2), 43–73.
- (3) Hanahan, D.; Weinberg, R. A. Hallmarks of Cancer: The Next Generation. *Cell* **2011**, *144* (5), 646–674.
- (4) Shen, L.; Shi, Q.; Wang, W. Double Agents: Genes with Both Oncogenic and Tumor-Suppressor Functions. *Oncogenesis* **2018**, *7* (3), 25.
- (5) Palumbo, M. O.; Kavan, P.; Miller, W. H.; Panasci, L.; Assouline, S.; Johnson, N.; Cohen, V.; Patenaude, F.; Pollak, M.; Jagoe, R. T.; et al. Systemic Cancer Therapy: Achievements and Challenges That Lie Ahead. *Front. Pharmacol.* **2013**, *4*.
- (6) Rebucci, M.; Michiels, C. Molecular Aspects of Cancer Cell Resistance to Chemotherapy. *Biochem. Pharmacol.* **2013**, *85* (9), 1219–1226.
- (7) Pucci, C.; Martinelli, C.; Ciofani, G. Innovative Approaches for Cancer Treatment: Current Perspectives and New Challenges. *ecancermedicalscience* **2019**, *13*.
- (8) Vanneman, M.; Dranoff, G. Combining Immunotherapy and Targeted Therapies in Cancer Treatment. *Nat. Rev. Cancer* **2012**, *12* (4), 237–251.
- (9) Hoos, A. Development of Immuno-Oncology Drugs — from CTLA4 to PD1 to the next Generations. *Nat. Rev. Drug Discov.* **2016**, *15* (4), 235–247.
- (10) Mohammad, H. P.; Barbash, O.; Creasy, C. L. Targeting Epigenetic Modifications in Cancer Therapy: Erasing the Roadmap to Cancer. *Nat. Med.* **2019**, *25* (3), 403–418.
- (11) Mai, A.; Altucci, L. Epi-Drugs to Fight Cancer: From Chemistry to Cancer Treatment, the Road Ahead. *Int. J. Biochem. Cell Biol.* **2009**, *41* (1), 199–213.
- (12) Wagner, T.; Robaa, D.; Sippl, W.; Jung, M. Mind the Methyl: Methyllysine Binding Proteins in Epigenetic Regulation. *ChemMedChem* **2014**, *9* (3), 466–483.
- (13) Helin, K.; Dhanak, D. Chromatin Proteins and Modifications as Drug Targets. *Nature* **2013**, *502* (7472), 480–488.
- (14) Arrowsmith, C. H.; Bountra, C.; Fish, P. V.; Lee, K.; Schapira, M. Epigenetic Protein Families: A New Frontier for Drug Discovery. *Nat. Rev. Drug Discov.* **2012**, *11* (5), 384–400.
- (15) Altucci, L.; Minucci, S. Epigenetic Therapies in Haematological Malignancies: Searching for True Targets. *Eur. J. Cancer* **2009**, *45* (7), 1137–1145.

- (16) Song, Y.; Wu, F.; Wu, J. Targeting Histone Methylation for Cancer Therapy: Enzymes, Inhibitors, Biological Activity and Perspectives. *J. Hematol. Oncol.* **2016**, *9* (1), 49.
- (17) Mio, C.; Bulotta, S.; Russo, D.; Damante, G. Reading Cancer: Chromatin Readers as Druggable Targets for Cancer Treatment. *Cancers* **2019**, *11* (1), 61.
- (18) Yap, K. L.; Zhou, M.-M. Structure and Mechanisms of Lysine Methylation Recognition by the Chromodomain in Gene Transcription. *Biochemistry* **2011**, *50* (12), 1966–1980.
- (19) Zaware, N.; Zhou, M.-M. Chemical Modulators for Epigenome Reader Domains as Emerging Epigenetic Therapies for Cancer and Inflammation. *Curr. Opin. Chem. Biol.* **2017**, *39*, 116–125.
- (20) Congreve, M.; Murray, C. W.; Blundell, T. L. Keynote Review: Structural Biology and Drug Discovery. *Drug Discov. Today* **2005**, *10* (13), 895–907.
- (21) Blundell, T. L.; Patel, S. High-Throughput X-Ray Crystallography for Drug Discovery. *Curr. Opin. Pharmacol.* **2004**, *4* (5), 490–496.
- (22) Lesley, S. A. High-Throughput Proteomics: Protein Expression and Purification in the Postgenomic World. *Protein Expr. Purif.* **2001**, *22* (2), 159–164.
- (23) Blundell, T. L.; Jhoti, H.; Abell, C. High-Throughput Crystallography for Lead Discovery in Drug Design. *Nat. Rev. Drug Discov.* **2002**, *1* (1), 45–54.
- (24) Erlanson, D. A.; Fesik, S. W.; Hubbard, R. E.; Jahnke, W.; Jhoti, H. Twenty Years on: The Impact of Fragments on Drug Discovery. *Nat. Rev. Drug Discov.* **2016**, *15* (9), 605–619.
- (25) Scott, D. E.; Coyne, A. G.; Hudson, S. A.; Abell, C. Fragment-Based Approaches in Drug Discovery and Chemical Biology. *Biochemistry* **2012**, *51* (25), 4990–5003.
- (26) Chilingaryan, Z.; Yin, Z.; Oakley, A. J. Fragment-Based Screening by Protein Crystallography: Successes and Pitfalls. *Int J Mol Sci* **2012**, *23*.
- (27) Milosevich, N.; Hof, F. Chemical Inhibitors of Epigenetic Methyllysine Reader Proteins. *Biochemistry* **2016**, *55* (11), 1570–1583.
- (28) Jenuwein, T. Translating the Histone Code. *Science* **2001**, *293* (5532), 1074–1080.
- (29) Helin, K.; Dhanak, D. Chromatin Proteins and Modifications as Drug Targets. *Nature* **2013**, *502* (7472), 480–488.

- (30) Taverna, S. D.; Li, H.; Ruthenburg, A. J.; Allis, C. D.; Patel, D. J. How Chromatin-Binding Modules Interpret Histone Modifications: Lessons from Professional Pocket Pickers. *Nat. Struct. Mol. Biol.* **2007**, *14* (11), 1025–1040.
- (31) Romero, F. A.; Taylor, A. M.; Crawford, T. D.; Tsui, V.; Côté, A.; Magnuson, S. Disrupting Acetyl-Lysine Recognition: Progress in the Development of Bromodomain Inhibitors. *J. Med. Chem.* **2016**, *59* (4), 1271–1298.
- (32) Igoe, N.; Bayle, E. D.; Fedorov, O.; Tallant, C.; Savitsky, P.; Rogers, C.; Owen, D. R.; Deb, G.; Somervaille, T. C. P.; Andrews, D. M.; et al. Design of a Biased Potent Small Molecule Inhibitor of the Bromodomain and PHD Finger-Containing (BRPF) Proteins Suitable for Cellular and in Vivo Studies. *J. Med. Chem.* **2017**, *60* (2), 668–680.
- (33) Herold, J. M.; Ingerman, L. A.; Gao, C.; Frye, S. V. Drug Discovery Toward Antagonists of Methyl-Lysine Binding Proteins. *Curr. Chem. Genomics* **2011**, *5* (Suppl 1), 51–61.
- (34) Milosevich, N.; Warmerdam, Z.; Hof, F. Structural Aspects of Small-Molecule Inhibition of Methyllysine Reader Proteins. *Future Med. Chem.* **2016**, *8* (13), 1681–1702.
- (35) Conway, S. J.; Woster, P. M.; Greenlee, W. J.; Georg, G.; Wang, S. Epigenetics: Novel Therapeutics Targeting Epigenetics. *J. Med. Chem.* **2016**, *59* (4), 1247–1248.
- (36) Pande, V. Understanding the Complexity of Epigenetic Target Space: Miniperspective. *J. Med. Chem.* **2016**, *59* (4), 1299–1307.
- (37) Filippakopoulos, P.; Qi, J.; Picaud, S.; Shen, Y.; Smith, W. B.; Fedorov, O.; Morse, E. M.; Keates, T.; Hickman, T. T.; Felletar, I.; et al. Selective Inhibition of BET Bromodomains. *Nature* **2010**, *468* (7327), 1067–1073.
- (38) Nicodeme, E.; Jeffrey, K. L.; Schaefer, U.; Beinke, S.; Dewell, S.; Chung, C.; Chandwani, R.; Marazzi, I.; Wilson, P.; Coste, H.; et al. Suppression of Inflammation by a Synthetic Histone Mimic. *Nature* **2010**, *468* (7327), 1119–1123.
- (39) Herold, J. M.; Wigle, T. J.; Norris, J. L.; Lam, R.; Korboukh, V. K.; Gao, C.; Ingerman, L. A.; Kireev, D. B.; Senisterra, G.; Vedadi, M.; et al. Small-Molecule Ligands of Methyl-Lysine Binding Proteins. *J. Med. Chem.* **2011**, *54* (7), 2504–2511.
- (40) Klauke, K.; Radulović, V.; Broekhuis, M.; Weersing, E.; Zwart, E.; Olthof, S.; Ritsema, M.; Bruggeman, S.; Wu, X.; Helin, K.; et al. Polycomb Cbx Family Members Mediate the Balance between Haematopoietic Stem Cell Self-Renewal and Differentiation. *Nat. Cell Biol.* **2013**, *15* (4), 353–362.

(41) Simhadri, C.; Daze, K. D.; Douglas, S. F.; Quon, T. T. H.; Dev, A.; Gignac, M. C.; Peng, F.; Heller, M.; Boulanger, M. J.; Wulff, J. E.; et al. Chromodomain Antagonists That Target the Polycomb-Group Methyllysine Reader Protein Chromobox Homolog 7 (CBX7). *J. Med. Chem.* **2014**, *57* (7), 2874–2883.

(42) Stuckey, J. I.; Dickson, B. M.; Cheng, N.; Liu, Y.; Norris, J. L.; Cholensky, S. H.; Tempel, W.; Qin, S.; Huber, K. G.; Sagum, C.; et al. A Cellular Chemical Probe Targeting the Chromodomains of Polycomb Repressive Complex 1. *Nat. Chem. Biol.* **2016**, *12* (3), 180–187.

(43) Ren, C.; Morohashi, K.; Plotnikov, A. N.; Jakoncic, J.; Smith, S. G.; Li, J.; Zeng, L.; Rodriguez, Y.; Stojanoff, V.; Walsh, M.; et al. Small-Molecule Modulators of Methyl-Lysine Binding for the CBX7 Chromodomain. *Chem. Biol.* **2015**, *22* (2), 161–168.

(44) Ren, C.; Smith, S. G.; Yap, K.; Li, S.; Li, J.; Mezei, M.; Rodriguez, Y.; Vincek, A.; Aguilo, F.; Walsh, M. J.; et al. Structure-Guided Discovery of Selective Antagonists for the Chromodomain of Polycomb Repressive Protein CBX7. *ACS Med. Chem. Lett.* **2016**, *7* (6), 601–605.

(45) Hall, M. D.; Yasgar, A.; Peryea, T.; Braisted, J. C.; Jadhav, A.; Simeonov, A.; Coussens, N. P. Fluorescence Polarization Assays in High-Throughput Screening and Drug Discovery: A Review. *Methods Appl. Fluoresc.* **2016**, *4* (2), 022001.

(46) Sun, H.-P.; Jia, J.-M.; Jiang, F.; Xu, X.-L.; Liu, F.; Guo, X.-K.; Cherfaoui, B.; Huang, H.-Z.; Pan, Y.; You, Q.-D. Identification and Optimization of Novel Hsp90 Inhibitors with Tetrahydropyrido[4,3-d]Pyrimidines Core through Shape-Based Screening. *Eur. J. Med. Chem.* **2014**, *79*, 399–412.

(47) WO2009121812A1.

(48) Dash, P.; Janni, M.; Peruncheralathan, S. Trideuteriomethoxylation of Aryl and Heteroaryl Halides. *Eur. J. Org. Chem.* **2012**, *2012* (26), 4914–4917.

(49) Xia, Q.-H.; Hu, W.; Li, C.; Wu, J.-F.; Yang, L.; Han, X.-M.; Shen, Y.-M.; Li, Z.-Y.; Li, X. Design, Synthesis, Biological Evaluation and Molecular Docking Study on Peptidomimetic Analogues of XK469. *Eur. J. Med. Chem.* **2016**, *124*, 311–325.

(50) Yang, Y.; Zhang, S.; Wu, B.; Ma, M.; Chen, X.; Qin, X.; He, M.; Hussain, S.; Jing, C.; Ma, B.; et al. An Efficient Synthesis of Quinoxalinone Derivatives as Potent Inhibitors of Aldose Reductase. *ChemMedChem* **2012**, *7* (5), 823–835.

(51) Mamedov, V. A.; Kalinin, A. A.; Gubaidullin, A. T.; Isaikina, O. G.; Litvinov, I. A. Synthesis and Functionalization of 3-Ethylquinoxalin-2(1H)-One. *Russ. J. Org. Chem.* **2005**, *41* (4), 599–606.

(52) Fjellström, O.; Akkaya, S.; Beisel, H.-G.; Eriksson, P.-O.; Erixon, K.; Gustafsson, D.; Jurva, U.; Kang, D.; Karis, D.; Knecht, W.; et al. Creating Novel Activated Factor XI Inhibitors through Fragment Based Lead Generation and Structure Aided Drug Design. *PLOS ONE* **2015**, *10* (1), e0113705.

(53) Messaoudi, S.; Brion, J.-D.; Alami, M. An Expeditious Copper-Catalyzed Access to 3-Aminoquinolinones, 3-Aminocoumarins and Anilines Using Sodium Azide. *Adv. Synth. Catal.* **2010**, *352* (10), 1677–1687.

(54) Reekie, T. A.; Wilkinson, S. M.; Law, V.; Hibbs, D. E.; Ong, J. A.; Kassiou, M. Rapid Access to N-(Indol-2-Yl)Amides and N-(Indol-3-Yl)Amides as Unexplored Pharmacophores. *Org. Biomol. Chem.* **2017**, *15* (3), 576–580.

(55) Keserü, G. M.; Makara, G. M. Hit Discovery and Hit-to-Lead Approaches. *Drug Discov. Today* **2006**, *11* (15–16), 741–748.

(56) Steinmetz, M. O.; Prota, A. E. Microtubule-Targeting Agents: Strategies To Hijack the Cytoskeleton. *Trends Cell Biol.* **2018**, *28* (10), 776–792.

(57) Margolin, G.; Gregoretti, I. V.; Cickovski, T. M.; Li, C.; Shi, W.; Alber, M. S.; Goodson, H. V. The Mechanisms of Microtubule Catastrophe and Rescue: Implications from Analysis of a Dimer-Scale Computational Model. *Mol. Biol. Cell* **2012**, *23* (4), 642–656.

(58) Arnst, K. E.; Banerjee, S.; Chen, H.; Deng, S.; Hwang, D.; Li, W.; Miller, D. D. Current Advances of Tubulin Inhibitors as Dual Acting Small Molecules for Cancer Therapy. *Med. Res. Rev.* **2019**, *39* (4), 1398–1426.

(59) Akhmanova, A.; Steinmetz, M. O. Control of Microtubule Organization and Dynamics: Two Ends in the Limelight. *Nat. Rev. Mol. Cell Biol.* **2015**, *16* (12), 711–726.

(60) Dumontet, C.; Jordan, M. A. Microtubule-Binding Agents: A Dynamic Field of Cancer Therapeutics. *Nat. Rev. Drug Discov.* **2010**, *9* (10), 790–803.

(61) Jordan, M. A.; Wilson, L. Microtubules as a Target for Anticancer Drugs. *Nat. Rev. Cancer* **2004**, *4* (4), 253–265.

(62) Yang, C.-P.; Horwitz, S. Taxol®: The First Microtubule Stabilizing Agent. *Int. J. Mol. Sci.* **2017**, *18* (8), 1733.

(63) Carlson, K.; Ocean, A. J. Peripheral Neuropathy with Microtubule-Targeting Agents: Occurrence and Management Approach. *Clin. Breast Cancer* **2011**, *11* (2), 73–81.

(64) Kavallaris, M. Microtubules and Resistance to Tubulin-Binding Agents. *Nat. Rev. Cancer* **2010**, *10* (3), 194–204.

(65) Arnst, K. E.; Wang, Y.; Hwang, D.-J.; Xue, Y.; Costello, T.; Hamilton, D.; Chen, Q.; Yang, J.; Park, F.; Dalton, J. T.; et al. A Potent, Metabolically Stable Tubulin Inhibitor Targets the Colchicine Binding Site and Overcomes Taxane Resistance. *Cancer Res.* **2018**, *78* (1), 265–277.

(66) Ravelli, R. B. G.; Gigant, B.; Curmi, P. A.; Jourdain, I.; Lachkar, S.; Sobel, A.; Knossow, M. Insight into Tubulin Regulation from a Complex with Colchicine and a Stathmin-like Domain. *Nature* **2004**, *428* (6979), 198–202.

(67) Dorleans, A.; Gigant, B.; Ravelli, R. B. G.; Mailliet, P.; Mikol, V.; Knossow, M. Variations in the Colchicine-Binding Domain Provide Insight into the Structural Switch of Tubulin. *Proc. Natl. Acad. Sci.* **2009**, *106* (33), 13775–13779.

(68) Massarotti, A.; Coluccia, A.; Silvestri, R.; Sorba, G.; Brancale, A. The Tubulin Colchicine Domain: A Molecular Modeling Perspective. *ChemMedChem* **2012**, *7* (1), 33–42.

(69) Pérez-Pérez, M.-J.; Priego, E.-M.; Bueno, O.; Martins, M. S.; Canela, M.-D.; Liekens, S. Blocking Blood Flow to Solid Tumors by Destabilizing Tubulin: An Approach to Targeting Tumor Growth. *J. Med. Chem.* **2016**, *59* (19), 8685–8711.

(70) De Brabander, M. J.; Van de Veire, R. M.; Aerts, F. E.; Borgers, M.; Janssen, P. A. The Effects of Methyl (5-(2-Thienylcarbonyl)-1H-Benzimidazol-2-Yl) Carbamate, (R 17934; NSC 238159), a New Synthetic Antitumoral Drug Interfering with Microtubules, on Mammalian Cells Cultured in Vitro. *Cancer Res.* **1976**, *36* (3), 905–916.

(71) Kruse, L. I.; Ladd, D. L.; Harrsch, P. B.; McCabe, F. L.; Mong, S. M.; Faucette, L.; Johnson, R. Synthesis, Tubulin Binding, Antineoplastic Evaluation, and Structure-Activity Relationship of Oncodazole Analogs. *J. Med. Chem.* **1989**, *32* (2), 409–417.

(72) Wang, Y.; Zhang, H.; Gigant, B.; Yu, Y.; Wu, Y.; Chen, X.; Lai, Q.; Yang, Z.; Chen, Q.; Yang, J. Structures of a Diverse Set of Colchicine Binding Site Inhibitors in Complex with Tubulin Provide a Rationale for Drug Discovery. *FEBS J.* **2016**, *283* (1), 102–111.

(73) Guzmán-Ocampo, D. C.; Aguayo-Ortiz, R.; Cano-González, L.; Castillo, R.; Hernández-Campos, A.; Dominguez, L. Effects of the Protonation State of Titratable Residues and the Presence of Water Molecules on Nocodazole Binding to β -Tubulin. *ChemMedChem* **2018**, *13* (1), 20–24.

(74) Lan, P.; Romero, F. A.; Malcolm, T. S.; Stevens, B. D.; Wodka, D.; Makara, G. M. An Efficient Method to Access 2-Substituted Benzimidazoles under Solvent-Free Conditions. *Tetrahedron Lett.* **2008**, *49* (12), 1910–1914.

(75) Loghmani-Khouzani, H.; Hajiheidari, D. Synthesis of Difluorinated β -Ketosulfones and Novel Gem-Difluoromethylsulfone-Containing Heterocycles as Fluorinated Building Blocks. *J. Fluor. Chem.* **2010**, *131* (5), 561–569.

(76) WO2000064876A1.

(77) Wan, Z.-K.; Ousman, E. F.; Papaioannou, N.; Saiah, E. Phosphonium-Mediated Cyclization of N-(2-Aminophenyl)Thioureas: Efficient Synthesis of 2-Aminobenzimidazoles. *Tetrahedron Lett.* **2011**, *52* (32), 4149–4152.

(78) Prota, A. E.; Bargsten, K.; Zurwerra, D.; Field, J. J.; Díaz, J. F.; Altmann, K.-H.; Steinmetz, M. O. Molecular Mechanism of Action of Microtubule-Stabilizing Anticancer Agents. *Science* **2013**, *339* (6119), 587–590.

(79) Madhavi Sastry, G.; Adzhigirey, M.; Day, T.; Annabhimoju, R.; Sherman, W. Protein and Ligand Preparation: Parameters, Protocols, and Influence on Virtual Screening Enrichments. *J. Comput. Aided Mol. Des.* **2013**, *27* (3), 221–234.

(80) Friesner, R. A.; Murphy, R. B.; Repasky, M. P.; Frye, L. L.; Greenwood, J. R.; Halgren, T. A.; Sanschagrin, P. C.; Mainz, D. T. Extra Precision Glide: Docking and Scoring Incorporating a Model of Hydrophobic Enclosure for Protein–Ligand Complexes. *J. Med. Chem.* **2006**, *49* (21), 6177–6196.

(81) Ansar Ahmed, S.; Gogal, R. M.; Walsh, J. E. A New Rapid and Simple Non-Radioactive Assay to Monitor and Determine the Proliferation of Lymphocytes: An Alternative to [3H]Thymidine Incorporation Assay. *J. Immunol. Methods* **1994**, *170* (2), 211–224.

(82) Hamid, R.; Rotshteyn, Y.; Rabadi, L.; Parikh, R.; Bullock, P. Comparison of Alamar Blue and MTT Assays for High Through-Put Screening. *Toxicol. In Vitro* **2004**, *18* (5), 703–710.

(83) *Assay Guidance Manual*; Sittampalam, G. S., Grossman, A., Brimacombe, K., Arkin, M., Auld, D., Austin, C. P., Baell, J., Bejcek, B., Caaveiro, J. M. M., Chung, T. D. Y., et al., Eds.; Eli Lilly & Company and the National Center for Advancing Translational Sciences: Bethesda (MD), **2004**.